Convection Heat Transfer from Cylinders in a Porous Medium using the Two-Equation Energy Model

by

Gazy Faissal Al-Sumaily

A Thesis submitted to Monash University
for the degree of
Doctor of Philosophy in Engineering Science

July 2012

Department of Mechanical & Aerospace Engineering
Monash University, Clayton Campus, Australia

For My Imam Ali ibn Abu Talib (a.s.)

Statement of Originality

This thesis contains no material that has been accepted for the award of a degree or diploma in this or any other university. To the best of the candidate's knowledge and belief, this thesis contains no material previously published or written by another person except where due reference is made in the text of this thesis.

Gazy Al-Sumaily

July 2012

Life is too short.

(Enjoy it while you can)

Anonymous

Abstract

This numerical study is directed at exploring the flow characteristics and thermal response for the flow over a circular cylinder(s) embedded in a horizontal packed bed under steady or unsteady forced convection. The analysis is made for an incompressible fluid flow through a two-dimensional bed, which consists of spherical particles that are packed randomly. The subproblems that are considered in the present study are: First, forced convective steady and pulsatile cross flows over a single cylinder placed in a porous bed. Second, forced convective steady cross flow over multiple cylinders arranged in two staggered or in-line configurations, embedded in a porous bed. The cylinder(s) is/are isothermally heated at a constant temperature and cooled by the incoming external flow. The confining horizontal walls of the bed have the same temperature as the flow at the inlet. Domain size is checked, and the results found to be domain independent to an accuracy of 0.1% for the important flow and thermal parameters.

Specifically, the generalised momentum model, i.e., the Darcy-Brinkmann-Forchheimer (*DBF*) model, is employed to model the flow field. This takes into consideration the non-Darcian terms, such as inertial and viscous effects. Moreover, the energy transport within the solid and fluid phases is modelled using separate energy equations for each phase. This is sometimes called the *Local Thermal Non-Equilibrium* (*LTNE*) model, in that it makes no assumptions about local thermal equilibrium between phases. The additional convective heat transfer term between the fluid and solid phases, which emerges when using the two-phase model, is formulated using a documented empirical correlation. Furthermore, the thermal dispersion phenomenon due to the complex path of local fluid elements through the solid matrix, causing mixing and recirculation in both the longitudinal and the transverse directions, is incorporated in the modelling of the fluid phase energy equation.

For generality, the governing equations are transformed into a non-dimensional vectorial form. This naturally leads to the appearance of a number of non-dimensional parameters, generally appearing as coefficients premultiplying the

terms in the equations, These govern the flow and heat transfer, and can be associated with a balance between various physical properties, forces or mechanisms. These parameters are the solid-to-fluid thermal diffusivity and conductivity ratios, cylinder-to-particle diameter ratio, porosity, and Reynolds, Prandtl, and Biot numbers. For the problems considered within this thesis, the ranges for these parameters are chosen based both on previous studies published in the literature and to include typical combinations for physical systems. The non-dimensional equations are discretised in space using a *spectral-element* method. They are then discretised in time using a second-order fractional step method. Meshes are constructed to model the problems of a single cylinder and multiple cylinders, confined by horizontal walls. Thorough spatial resolution studies verify that the meshes maintain a spatial accuracy in the order of 0.5% or better. Next, verification and validation of the implemented algorithm is achieved by comparing results from the code to previously published numerical and experimental results, in both the presence and absence of porous media.

For the first problem, the effect of the presence of porous media on the fluid flow and heat transfer from a cylinder is assessed at different steady and pulsatile flow conditions. Furthermore, for steady flow, the effects of the thermal and structural properties of the porous medium on the convective and conductive heat transfer to the fluid and solid phases, are also examined using the *LTNE* energy model. The results show that a considerable heat transfer enhancement can be achieved by packing the channel with porous media; however, this is at the expense of a several thousand fold increase in pressure drop. It is found that the conductivity ratio has a positive influence on the fluid Nusselt number, Nu_f, up to a certain value, beyond which the influence is totally governed by Biot number. It is also shown that the effects of particle diameter and porosity on Nu_f are non-linear. This means that their impacts can be positive or negative, or a combination of the two, depending on other parameters. Interestingly, it is found that the heat transfer enhancement can be considerably increased and the pressure drop generated in the packed bed can be greatly decreased by using spheres with larger diameter and/or a porous medium with high permeability. Furthermore, comparisons are made between results from the *LTE* and *LTNE* energy models for the effects of the above thermal and structural parameters on Nu_f, at different Reynolds numbers. These comparisons lead to the conclusion that the two models may predict completely different heat transfer trends; the differences in predicted heat transfer coefficients increases as the particle diameter decreases, or as the porosity decreases, or as Reynolds number, thermal conductivity, or interfacial

heat transfer coefficient increases.

The flow and heat transfer is also investigated subject to a sinusoidally varying inlet flow, for both a non-filled and porous material filled channels. The effects of pulsation frequency and amplitude on heat transfer are quantified. Steady and unsteady wakes that evolve for increasing Reynolds number are observed for the empty channel; however, in the porous channel, the increased damping of the porous medium produces much more stable flows. The results show that using porous media alone results in a much higher heat transfer enhancement than that promoted by using pulsating inlet flow. However, still a significant benefit can be achieved by using pulsatile flow through a porous channel.

The assessment of the local thermal equilibrium (LTE) condition is also performed using the $LTNE$ model with an evaluation parameter used in the literature. This study yields that the LTE assumption is true at lower Reynolds and Prandtl numbers, and for higher solid-to-fluid thermal conductivity ratio, Biot number, cylinder-to-particle diameter ratio, porosity, and Darcy number. Oscillatory inlet flow has little effect on the degree of thermal equilibrium between the phases.

Finally, the characteristics of flow and heat transfer are analysed for a bundle of cylinders embedded in a porous channel. A staggered and an in-line configuration are considered. The focus is directed on how the spacing parameter between the cylinders affects heat transfer from each, at different Reynolds numbers for both configurations. The variations of the local and average fluid and solid Nusselt numbers are shown to vary strongly with spacing parameter and the kind of cylinder configuration. The thermal performance of the staggered system is much higher than that of the in-line one, therefore, that type of arrangement is recommended to be used as a basis for manufacturing tubular heat exchangers.

Acknowledgments

Firstly, I would like to express my gratitude to my supervisors, Prof. Mark Thompson and Prof. John Sheridan. Prof. Mark Thompson's ability to explain complicated concepts in a simple way, and Prof. John Sheridan's sharp sense of logic and scientific method, have been integral in my development as a researcher and allowing me to write this thesis. Their collective guidance throughout the thesis has been crucial to its completion and their professionalism a fine role-model for a young researcher. For their guidance and teaching I am truly thankful.

I am grateful to the Department of Mechanical Engineering, Monash University, for providing the office space and resources necessary for the completion of this study. Furthermore, I wish to acknowledge the National Computational Infrastructure (NCI), and Monash Sun Grid (MSG), for granting access to their high performance computing facility. Financial support for this research has been gratefully received through an Iraqi Postgraduate scholarships.

During my candidature there have been several people who have always made themselves available to discuss ideas and offer moral support. For their personal and professional assistance during this time I would like to acknowledge Mr Wisam Al-Saadi, Dr. Joe Berry, Dr. Martin Griffith and Dr. Justin Leontini.

To my family, I would like to thank my parents, Abo-Ahmad and Om-Ahmad, my son Musstafa and my daughters Fatima and Zainab, for their patience, love and support that they have offered throughout this time. To my brothers, Mr. Qassem, Mr. Jassem and Mr. Fadel, my thanks for keeping my head high. Finally, to my wife Ruaa, you have encouraged and strengthened me during the ups and downs of the last few years. Thank you.

List of publications related to this research

Al-Sumaily, G.F., Leontini, J., Sheridan, J. & Thompson, M.C. 2010 Time-dependent fluid flow and heat transfer around a circular heated cylinder embedded in a horizontal packed bed of spheres. *AIP Conference Proceedings*, Montecatini, Italy, June 2010.

Al-Sumaily, G.F., Sheridan, J. & Thompson, M.C. 2011 Validation of Thermal Equilibrium Assumption in Forced Convection Flow over a Cylinder Embedded in a Porous Medium. *In the 9TH Australian Heat and Mass Transfer Conference - 9AHMTC*, Monash University, Melbourne, Victoria, Australia, November 2-4, 2011.

Al-Sumaily, G.F., Sheridan, J. & Thompson, M.C. 2012 Analysis of forced convection heat transfer from a circular cylinder embedded in a porous medium. *International Journal of Thermal Sciences* **51**, 121–131.

Al-Sumaily, G.F., Nakayama, A., Sheridan, J. & Thompson, M.C. 2012 The effect of porous media particle size on forced convection from a circular cylinder without assuming local thermal equilibrium between phases. *International Journal of Heat and Mass Transfer* **55**, 3366–3378.

Al-Sumaily, G.F., Leontini, J., Sheridan, J. & Thompson, M.C. 2012 Forced convection from a bank of cylinders immersed in a porous medium. *International Journal of Heat and Mass Transfer* **Under consideration for publication**.

Nomenclature

A list of nomenclature used throughout the thesis is included here. Greek alphabet nomenclature is presented, followed by English alphabet nomenclature.

Symbol	Description
α_f	Thermal fluid diffusivity
α_r	Solid/fluid thermal diffusivity ratio
α_s	Thermal solid diffusivity
γ	Porosity-scaled fluid/solid thermal conductivity ratio parameter, $\varepsilon k_f/(1-\varepsilon)k_s$
ε	Porosity
ε_{op}	Optimal porosity for obtaining maximum heat transfer
η	Coordinate axis in computational space
θ	Dimensionless temperature, $\theta = (\acute{T} - \acute{T}_o)/(\acute{T}_h - \acute{T}_o)$
θ_f	Dimensionless fluid phase temperature, $\theta_f = (\acute{T}_f - \acute{T}_o)/(\acute{T}_h - \acute{T}_o)$
θ_h	Dimensionless cylinder surface temperature, or heat source temperature
θ_o	Dimensionless inlet fluid temperature
θ_s	Dimensionless solid phase temperature, $\theta_s = (\acute{T}_s - \acute{T}_o)/(\acute{T}_h - \acute{T}_o)$
θ_w	Dimensionless wall temperature
μ_f	Fluid dynamic viscosity
ν_f	Fluid kinematic viscosity, μ_f/ρ_f
ξ	Coordinate axis in computational space
ρ_f	Fluid density
ρ_s	Solid density
τ	Non-dimensional time for one oscillating period

Continued on the next page.

Continued from previous page.

Symbol	Description
ϕ	Volume fraction
φ	Angular coordinate
ω	Angular velocity
Ψ	General quantity
Ω	Subscript referring to the computational domain
A	Pulsating amplitude of axial inlet velocity
A_o	Occupied area by multiple cylinders
a	Index in the ξ-direction used for the weighting coefficients for Gauss-Legendre-Lobatto quadrature
a_{sf}	Specific interfacial area
Bi	Biot number
b	Index in the η-direction used for the weighting coefficients for Gauss-Legendre-Lobatto quadrature
C_F	Coefficient of friction
c_p	Specific heat capacity
D_{cy}	Cylinder diameter
Da	Darcy number, K/D_{cy}^2
d	Jet opening width
d_p	Particle diameter
El	Subscript denoting integration over a single element
F	Geometric function
f	Pulsating frequency
H	Channel height
H_v	Volumetric convective heat transfer parameter, $h_{sf}a_{sf}H^2/k_f$
h_{cy}	Cylinder surface heat transfer coefficient
h_{sf}	Interfacial heat transfer coefficient
i	Index of the data point being considered during construction of the Lagrange polynomial in the ξ-direction

Continued on the next page.

Continued from previous page.

Symbol	Description
J	Jacobian operator for coordinate transformation
j	Index of the data point being considered during construction of the Lagrange polynomial in the η-direction
K	Permeability
k_d	Thermal dispersion conductivity
k_f	Fluid thermal conductivity
$k_{f.eff}$	Effective fluid thermal conductivity
k_r	Solid/fluid thermal conductivity ratio
k_s	Solid thermal conductivity
$k_{s.eff}$	Effective solid thermal conductivity
k_{st}	Stagnant thermal conductivity
L	Channel length
L_{Darcy}	The linear Darcy term in the *DBF* equation
L_d	Channel downstream length
L_u	Channel upstream length
$M1$	The first mesh used for the domain size study
$M2$	The second mesh used for the domain size study
$M3$	The third mesh used for the domain size study
$M4$	The fourth mesh used for the domain size study
$m\cdot$	Fluid mass flow rate
N	The total number of nodes in the domain
N_{adv}	The non-linear convection term in the *DBF* equation, $(\mathbf{u}.\nabla)\mathbf{u}$
N_{Forch}	The non-linear Forchheimer term in the *DBF* equation, $\lvert\mathbf{u}\rvert\,\mathbf{u}$
$N_{i,j}$	Two-dimensional tensor-product Lagrange polynomial component for point i, j
Nu_{empty}	Time-mean average Nusselt number in the empty channel
Nu_f	Time-mean average fluid Nusselt number
$Nu_{f\varphi}$	Time-mean local fluid Nusselt number

Continued on the next page.

Continued from previous page.

Symbol	Description
Nu_{porous}	Time-mean average total Nusselt number in the porous channel
Nu_s	Time-mean average solid Nusselt number
$Nu_{s\varphi}$	Time-mean local solid Nusselt number
Nu_t	Time-mean average total Nusselt number
Nu_t, all	Time-mean average total Nusselt number from multiple cylinders
n	Timestep count to the current timestep
$\mathbf{n}$	Unit vector in the normal direction to a boundary
P_f	Normalised fluid pressure, $\acute{P}_f/\rho_f u_o^2$
$\acute{P}_f$	Fluid pressure
$P_{f.empty}$	Normalised fluid pressure in the empty channel
$P_f^{(n)}$	Pressure filed at timestep n
$P_f^{(n+\frac{1}{2})}$	Pressure filed at the middle of the time-step $n + \frac{1}{2}$
$P_{f.o}$	Normalised fluid pressure at the inlet of the channel
$P_{f.out}$	Normalised fluid pressure at the outlet of the channel
$P_{f.porous}$	Normalised fluid pressure in the porous channel
Pe	Péclet number
ΔP_f	Pressure drop throughout the channel
Pr	Prandtl number, ν_f/α_f
p	Order of the Lagrange polynomials used as shape and weighting functions for the spectral-element method
p_l	Longitudinal pitch between cylinders' centres
p_t	Transverse pitch between cylinders' centres
q	Data point index in computational space in ξ-direction
R	Residual formed when substituting trial solution into governing equations
Ra	Rayleigh number
Re_D	Reynolds number, $u_o D_{cy}/\nu_f$
Re_{max}	Maximum Reynolds number, $u_{max} D_{cy}/\nu_f$

Continued on the next page.

Continued from previous page.

Symbol	Description
Re_p	Reynolds number in the pore scale, $\mathbf{u}d_p/\nu_f$
S	Circumference of the cylinder
SP	Spacing parameter, the space between cylinder centres
SP_{crt}	Critical spacing parameter
SP_{op}	Optimal spacing parameter
St	Normalised pulsating frequency, Strouhal number, fD_{cy}/u_o
s	Data point index in computational space in η-direction
$\mathbf{s}$	Unit vector in the tangential direction to a boundary
$\acute{T}$	Temperature
$\acute{T}_f$	Fluid phase temperature
$\acute{T}_h$	Cylinder surface temperature
$\acute{T}_o$	Inlet fluid temperature
$\acute{T}_s$	Solid phase temperature
$\acute{T}_w$	Channel wall temperature
t	Non-dimensional time, $\acute{t}u_o/D_{cy}$
$\acute{t}$	Time variable
Δt	The non-dimensional timestep
$\mathbf{u}$	Normalised vectorial fluid velocity, $\acute{\mathbf{u}}/u_o$
$\mathbf{u}^*$	Intermediate normalised velocity vector at the end of the advection sub-step
$\mathbf{u}^{**}$	Intermediate normalised velocity vector at the end of the pressure sub-step
$\mathbf{u}^{(n)}$	Normalised velocity vector at timestep n
$\mathbf{u}^{(n+1)}$	Normalised velocity vector at timestep n+1
$\acute{\mathbf{u}}$	Vectorial fluid velocity
$\mathbf{u}_{trial}$	Trial solution for velocity
$\widehat{\mathbf{u}^*}$	Vector of $\mathbf{u}^*$ at the node points
u	Dimensionless horizontal velocity component, $\acute{u}/u_o$

Continued on the next page.

Continued from previous page.

Symbol	Description
$\acute{u}$	Horizontal velocity component
$\acute{u}_{max}$	Horizontal maximum velocity, the average velocity at the minimum cross-sectional area
$\acute{u_o}$	Horizontal fluid velocity at the inlet of the channel
V	Volume of the Representative Elementary Volume (REV)
V_f	Fluid volume
V_s	Solid volume
V_{total}	Total volume
v	Dimensionless vertical velocity component, $\acute{v}/u_o$
$\acute{v}$	Vertical velocity component
$W_{a,b}$	Weighting coefficient associated with point a, b for Gauss-Legendre-Lobatto quadrature
x	Normalised cartesian horizontal coordinate, $\acute{x}/D_{cy}$
$\acute{x}$	Cartesian horizontal coordinate
y	Normalised cartesian vertical coordinate, $\acute{y}/D_{cy}$
$\acute{y}$	Cartesian vertical coordinate

Contents

1 Introduction **1**

1.1 Background 1

1.1.1 Fluid flow in porous media 1

1.1.2 Heat transfer in porous media 3

1.2 Fundamental Principles 6

1.2.1 What is a porous medium? 7

1.2.2 Porosity 7

1.2.3 Permeability 8

1.2.4 Volume-averaging method 9

1.3 Overview and aims of the study 11

1.4 Structure of the thesis 12

2 Methodology and validation **13**

2.1 Introduction 13

2.2 Mathematical formulation 13

2.2.1 Statement of the problem 13

2.2.2 Governing equations 14

2.2.3 Boundary conditions 21

2.3 Numerical method of solution 23

2.3.1 Temporal discretisation 23

2.3.2 Spatial discretisation 26

2.4 Resolution studies 29

2.4.1 Domain size study 29

2.4.2 Grid resolution study 32

2.5 Chapter summary 37

3 Validation of the numerical code **43**

3.1 Introduction 43

3.2 Mixed convection of a jet impingement 43

3.3 Forced convection over a single cylinder 49

3.4 Forced convection over a bundle of cylinders 52
3.4.1 With porous media 52
3.4.2 Without porous media 57
3.5 Validation summary 59

Chapter 1

Introduction

1.1 Background

In keeping up with advances in technology, considerable attention is being focused on the subject of convective heat transfer through porous media due to its various applications in contemporary technology. These applications include, but are not restricted to, packed and fluidized beds, chemical catalytic reactors, heat exchangers, solar collectors, energy storage units, nuclear waste repositories, and heat pipe technologies. Although the mechanics of fluid flow in porous media has been the subject of research for more than a century, convection heat transfer in porous media has been investigated only throughout the preceding few decades. The presence of a complicated solid structure in the path of a fluid extends the contact surface area, and thus enhances the ability of the overall system to transport energy. Thus, there is an intensive interest to study this problem due to the intricate and interesting phenomenon related to energy transport within a solid matrix.

1.1.1 Fluid flow in porous media

The dynamics of fluid flows through porous media is a relatively old and classical topic, Muskat (1937), Scheidegger (1960) and Bear (1972), and has been examined extensively for its practical importance in the management of groundwater table and irrigation systems. This branch of the fluid dynamics was first studied by Darcy (1856) in the nineteenth century. He undertook experimental work to investigate the flow of water through a vertical column packed with sand, and

correlated a linear relationship between the pressure drop and the flow velocity by defining a special constant property of the medium called permeability. This correlation is now well known as Darcy's law and has been utilised in the studies to describe the fluid motion in an unbounded porous medium by many researchers. However, Darcy's formulation, which exhibits the effect of linear frictional drag due to the presence of a solid matrix inside the porous medium and neglects the effects of the solid boundary and the inertial forces, is valid and reliable only when the representative Reynolds number is low, and when the viscous and pressure forces are dominant. Following that, the range of the applicability of the Darcy's law was extended by Forchheimer (1901), who added the effect of the non-linearity of the fluid motion, which is attributed to the appreciated increase in the inertial resistance offered by the solid matrix, and then by Brinkmann (1949), who introduced a term that superimposes the bulk and boundary effects together for flows with bounding walls.

The inertial and the solid boundary effects are known in the literature as non-Darcian effects. The inclusion of these effects has a significant influence on the predicted hydrodynamic and thermal behavior in porous media. For instance, the inertial effect, which is expected to be important in high-porosity media or lower fluid viscosity, retards the momentum transport, causing less energy to be carried away by convection compared to the case where the inertial effects are neglected Amiri & Vafai (1994). In addition, the impermeable boundary effect reduces the velocity in the momentum boundary layer, and thus decreases the convective heat transfer, which is typically a boundary phenomenon. However, an impermeable wall causes an irregular redistribution of porosity near the wall, which causes the velocity to reach its peak near the wall and not at the centreline, and thus leads to an important phenomenon known as the *channeling effect*, see Vafai (1984). It was found that the porosity of the bed exhibits sinusoidal damping decay especially close to a solid boundary (Roblee *et al.* 1958; Benenati & Brosilow 1962). Consequently, the overall effect of the rigid wall was found to enhance the energy transport due to the large velocity magnitude close to the wall. However, this enhancement is challenged by the magnitude of the inertia term Amiri &

Vafai (1998).

1.1.2 Heat transfer in porous media

The convective heat transfer of flows through porous media has emerged as a new interest due to its utilisation in the new thermal technologies. The pioneering studies of heat and mass transfer in porous media were reported by Horton & Rogers (1945) and Lapwood (1948), who established the criterion for the onset of free convection in a fluid-saturated porous medium surrounded by two infinite parallel horizontal surfaces heated from below. Afterwards, a large number of papers have been published by researchers in various fields of interest relating to natural convection, forced convection, and mixed convection. The topic of convection heat transfer from a body immersed in a fluid-saturated porous medium is an important one of these fields because of its several practical applications. The present document presents the results of a theoretical study of the problem of transient and steady forced convection heat transfer from a circular cylinder or multiple cylinders immersed in a packed bed of solid spherical particles. Packed beds are porous beds of granular material in which the particles are in constant contact with each other. A packed bed is generally considered to be a porous medium that is fluid-saturated, homogenous, non-deformable and isotropic. Distinguishing features of a packed bed are the packing material, porosity, permeability and effective thermal conductivity. The packing material, also referred to as the solid matrix, is considered to be made up of non-consolidated solid particles.

Regardless of the geometry of the problem at hand, proper analysis of the convective heat transfer process is necessary. In the context of energy transport, a fundamental approximation frequently used in modelling is that of local thermal equilibrium (LTE), which is also called the one-equation energy model, between the fluid and the solid phases. The LTE energy model assumes that both fluid and solid phases have locally similar temperatures at any location in the porous medium and at every instant of time. This produces an approximation that is identical to the standard advection-diffusion energy equation for energy transport

in a homogenous fluid. However, in the *LTE* approximation, heat capacity effects are associated with the two phases, whereas advection effects arise from the fluid velocity alone.

In reality, the phase temperatures may be significantly different. This depends on the nature of the transient performance and the thermo-physical properties of each phase. In several industrial applications, see Nield & Kuznetsov (1999), such as nuclear fuel rods placed in a coolant fluid bath and thermal energy storages in underground reservoirs, the temperature difference between the local fluid and solid phases is essential and the transport process is naturally time-dependent, hence, the performance of the system relies strongly on the degree of non-equilibrium between the two phases. More and more studies, for example by Vafai & Sözen (1990a) and Kaviany (1999), have found the *LTE* assumption invalid for a number of applications involving convection in porous media. They mentioned that when there is a significant difference between advection and conduction mechanisms in transferring heat, the deviation between the solid and fluid phase temperatures increases, and therefore the *LTE* model becomes progressively less valid. It was also noted by Pop & Cheng (1992) that this approach may be questionable when the particle size in the solid porous matrix is comparable to or exceeds the thermal boundary layer thickness. In addition, Quintard (1998) argued that assessing the validity of the assumption of *LTE* is not a simple task since the temperature difference between the two phases cannot be easily estimated. He suggested that the use of a two-energy equation model is a possible approach to solving the problem. Numerous other physical situations where *LTE* fails are cited by Quintard & Whitaker (1993). Therefore, a local thermal non-equilibrium (*LTNE*) model, which assigns individual local temperatures to the fluid and the solid, allowing heat transfer between them, is necessary and must be incorporated for accurate modeling.

The origin of the two-phase model is the classical model established by Schumann (1929) who proposed a simple two-equation formulation to account for the non-equilibrium condition for forced convective incompressible flow in a porous medium. The Schumann model is a simplified model which neglects the diffusion

terms in both phases, and predicts the mean fluid and solid thermal fields as a function of axial position and time. In recent years, more attention has been paid to the *LTNE* model and its use has considerably increased in numerical and theoretical research for convection heat transfer in porous media. Consequently, the use of the two-phase model requires information on additional modes of heat transfer that emerge to account for the energy interaction between the phases. These modes are of radiative and convective natures; however, the convective heat transfer mode is only considered in the present study since forced convection is the prime source of energy transport under consideration. The inter-phase convective heat transfer in the two-phase model also needs information about an important quantity, namely the interfacial heat transfer coefficient (h_{sf}), (Kuznetsov 1998) as well as the interfacial surface area, which are usually determined through experimental investigations. Although experimental data are available for heat transfer in packed beds, the interstitial heat transfer coefficient is not generally known a priori for other kinds of porous media. A considerable amount of work has been carried out, for example, experimentally by Gamson *et al.* (1943), Dixon & Cresswell (1979), Wakao *et al.* (1979) and Achenbach (1995), and numerically by Kuwahara *et al.* (2001), and Moghari (2008), for determining this quantity for packed beds using different size, shapes, and packing configurations of solid particles.

The energy convected by fluid flow in porous media is not as simple as that in the case of a pure fluid, as the fluid element in a porous medium takes on a tortuous path. The microscopic mixing of a fluid element due to the presence of the complex porous structure is referred to as mechanical dispersion. This is one important feature of the porous system which leads to an enhancement in the transport phenomenon. At high flow rates, dispersion overwhelms diffusion, thus dominating the transport process. It should be emphasized that dispersion occurs even at low Reynolds numbers when the flow is laminar. The dispersion in porous media is similar to turbulent eddy motion. However, their mechanisms are different in nature. Turbulent eddies arise from the instability of the flow, whereas dispersion is due to the existence of the solid matrix, which forces the flow to

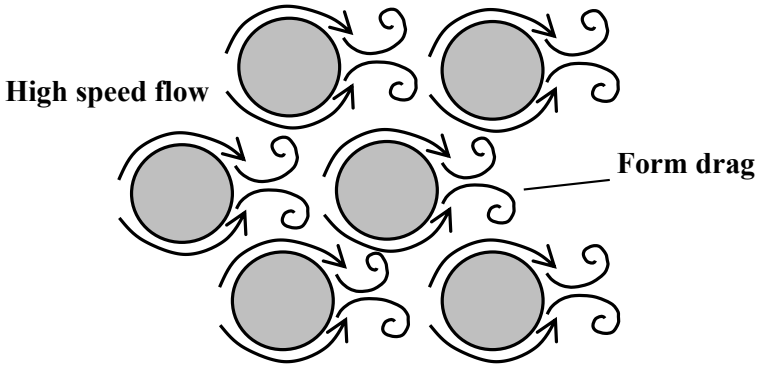

FIGURE 1.1: Fluid eddies formed due to the torturous path offered by the solid matrix of a porous medium.

undergo local transverse motion and produces laminar eddies behind it, as shown in figure 1.1. In other words, the dispersion represents the transport induced as the fluid is forced to follow a tortuous way around the solid matrix. The dispersion effect will influence thermal characteristics, both in the longitudinal and the transverse directions with respect to the bulk flow. Most of the existing models view the effect of thermal dispersion as a diffusive term added to the stagnant thermal conductivity of the fluid. Thus, the thermal dispersion conductivity depends on the fluid velocity and the size of the particles. The experimental works of Yagi & Kunii (1957), Yagi & Wakao (1959) and Yagi *et al.* (1960) established the pioneering empirical relations that represent the longitudinal and transverse thermal dispersion. These studies have received considerable attention in the literature in addition to other recent investigations reported by Cheng (1981), Wakao & Kaguei (1982), Levec & Carbonell (1985), Cheng & Vortmeyer (1988), Kuo & Tien (1988b) and Hsu & Cheng (1990).

1.2 Fundamental Principles

Transport phenomena in fluid-saturated porous media are based on basic special concepts and terminology that characterise a porous medium and are not found in pure fluid. Examples of such terminology are the porosity and the permeability of the porous medium, effective thermal conductivity and volume-averaging method.

1.2.1 What is a porous medium?

A simple rigorous definition of a porous medium is a region in space comprising solid structure usually called the matrix with voids called pores. Each pore in a porous system can be connected to more than one other pore (*inter-connected*), connected merely to one other pore (*dead-end*) or may not be connected at all (*isolated*). Flow of interstitial fluid is possible only if at least part of the pore space is inter-connected. The inter-connected part of the pore system is called the effective pore space of the porous medium, Scheidegger (1974). Also, the pores could be saturated by single fluid as in single-phase flow or they could share liquid and gas as in two-phase flow.

The matrix structure of porous media based on the structural characteristics are classified by Kaviany (1999). For example, porous media where the solid structure is not connected to each other are considered unconsolidated. If the solid structure is cemented together, such solid matrix is called consolidated porous media. Then, the major divisions are based on *ordered* against *disordered*, *isotropic* versus *anisotropic* and so on. In a porous medium, the solid matrix and the fluid flowing through voids could be stationary or mobile, or could one of them fixed and another is moving, see figure 1.2, which is the requirement of analysing transport phenomena in a porous medium.

1.2.2 Porosity

Porosity ε, or volumetric porosity, a macroscopic porous medium property, is defined as the volume fraction occupied by voids, i.e. the ratio of volume of the void space, or the volume which is taken by fluid V_f, to the total volume V_{total} of the medium (solid matrix and fluid), as follows:

$$\varepsilon = \frac{V_f}{V_{total}}. \tag{1.1}$$

Occasionally, volume fraction ϕ of the solid matrix is used instead of porosity for the description of the porous medium. With the volume taken by the solid matrix V_s, equation 1.1 can be defined as:

$$\phi = \frac{V_{total} - V_f}{V_{total}} = \frac{V_s}{V_{total}}. \tag{1.2}$$

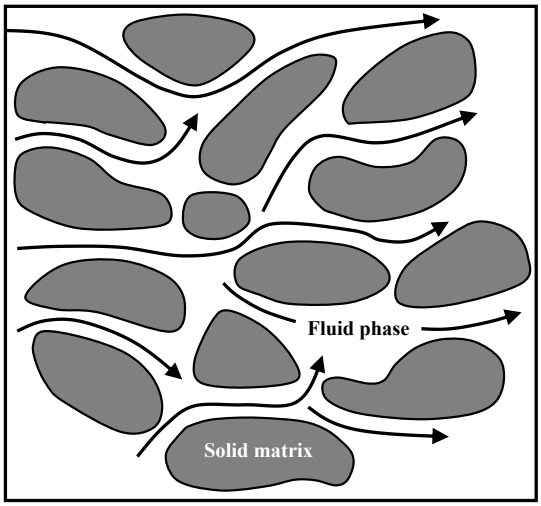

FIGURE 1.2: Flow in a rigid porous medium.

For natural media, the porosity does not exceed 0.6. For packed bed of spheres, it ranges from 0.245 to 0.476. For man-made materials such as metallic foam the porosity can approach the value 1.0. Other details about the measurement of porosity and its values can be found in Bear (1972).

1.2.3 Permeability

Permeability K is a measurable property of hydraulic conductance to the flow through the solid matrix of a porous medium. It is the proportionality factor in the simple Darcy's model which relates flow rate of the flowing fluid and its physical properties to a pressure gradient applied to the porous medium:

$$u = \frac{K}{\mu_f}\left(\frac{\Delta P_f}{\Delta x}\right), \tag{1.3}$$

where u is the superficial fluid flow velocity through the medium, μ is the dynamic viscosity of the fluid, ΔP_f is the pressure difference applied within a thickness Δx of the porous medium used. The units of the permeability are m^2 or ft^2, but the traditional unit for it is the Darcy (D). Kaviany (1999) provides examples of the magnitude of the permeability for some matrices, and further details can be aslo found in Scheidegger (1974).

Various attempts have been made to correlate permeability to easily measur-

able structural variables such as porosity, pore diameter, etc. Among the many models such as capillary tube models, fissure models, hydraulic radius models, and so forth, see Kaviany (1999), the hydraulic radius model is used widely for a packed bed of spheres. The semi-heuristic Carman-Kozeny equation for permeability is given by:

$$K = \frac{1}{180}\frac{\varepsilon^3}{(1-\varepsilon^2)}d_p^2, \tag{1.4}$$

where, d_p is the particle diameter and the constant $1/180$ is used to fit the experimental data.

1.2.4 Volume-averaging method

Practically, a more rigorous approach for investigating transport through porous media is through the use of the volume-averaging technique. The complexity associated with the geometric structure of a porous medium and flow pattern such as fluid eddies hinders and limits investigations of a detailed microscopic transport phenomena. Direct simulation of a simple geometry would be feasible, but it is not a practical engineering application. Instead, it is a general practice in porous media studies to integrate the point transport equations over volumes or areas containing many pores and accommodating the fluid and solid phases. This practice is commonly regarded in developing the transport processes in porous media to smooth out the local complexity of the actual phenomena, and focus on the conservation of the overall aspects of mass, momentum and energy.

The mathematical application of the volume-averaging method has been originated with Anderson & Jackson (1967) who derived the macroscopic equations of motion for fluidized beds, with Slattery (1967) who studied the problem of viscoelastic flow in porous media, and with Whitaker (1967) who used the method to derive a dispersion equation for mass transport in porous media and to outline a method of closure. The key mathematical theorem used in those studies is known as the averaging theorem and it was presented independently by the above workers in 1967.

The method of volume-averaging is based on the idea that with every point in space there is associated an averaging volume or a representative elementary

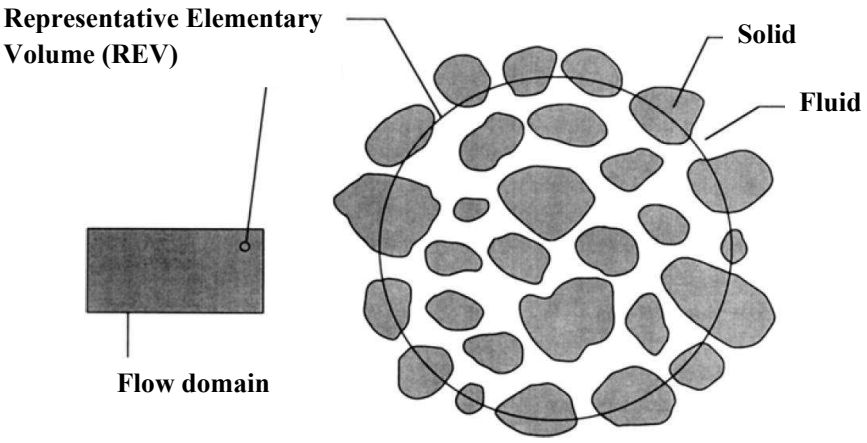

FIGURE 1.3: The averaging volume or the representative elementary volume REV: The figure is cited from Nield & Bejan (2006).

volume (REV) shown in figure 1.3. It can be seen that the length scale of the REV is much larger than the pore scale; however, it is noticeably smaller than the length scale of the macroscopic physical domain. Since there is an averaging volume associated with every point in space, i.e., in both the fluid and solid phases, a field of average values can be generated.

The literature often cites two approaches that are useful for averaging. The first approach which is referred to as the *(local volume average)* or the *(phase average)* is to average over the entire REV encompassing both phases. For example, in the fluid phase, this average is defined by:

$$\langle \Psi_f \rangle = \frac{1}{V} \int_{V_f} \Psi_f dV, \tag{1.5}$$

here Ψ refers to a general quantity, V_f represents the volume of the fluid phase contained within the averaging volume or the REV's volume V and the operator $< ... >$ denotes a local volume average of a quantity. In general, the *phase average* is not the average of choice in the analysis of multi-phase transport phenomena. Therefore, for the multi-phase transport it is usual to use another approach, *(intrinsic phase average)*, which requires a split averaging over each phase of the two phases, as follows:

$$\langle \Psi_f \rangle^f = \frac{1}{V_f} \int_{V_f} \Psi_f dV, \tag{1.6}$$

and the relationship between the two quantities is:

$$\langle \Psi_f \rangle = \varepsilon \langle \Psi_f \rangle^f. \tag{1.7}$$

1.3 Overview and aims of the study

For the investigations presented in this dissertation, a more reliable flow model that incorporates non-Darcian effects, combined with the *LTNE* assumption that includes the effect of thermal dispersion, is used to accurately predict time-dependent forced convective heat transfer around a horizontal circular cylinder or bank of cylinders embedded in a porous medium, i.e., a horizontal packed bed of spheres. This is done for steady or oscillatory hydro-dynamic inlet boundary conditions. The heat transfer augmentation produced by a porous medium is attributed to a combination of effects, including thinning of the hydrodynamic and thermal boundary layers around the cylinder, increased mixing, and direct conduction through the solid matrix. However, the efficiency of a porous medium in heat transfer enhancement depends on the porous medium structure, thermo-physical properties, and fluid flow conditions. Therefore, this study aims to develop a better understanding of the influence of the presence of porous packing material on the heat transfer enhancement, and on the fields of fluid flow, temperature, and pressure. Also, the effects of the pertinent parameters such as Reynolds number, solid-to-fluid thermal conductivity and diffusivity ratios, interfacial heat transfer coefficient, particle diameter and porosity on heat transfer from a single cylinder are considered. Another objective is to analyze the influence of flow interaction between four cylinders on the local and average heat transfer released from them to the surrounding porous medium. Both a staggered and in-line arrangement are investigated. In addition, the development in heat transfer when a harmonic term is superimposed on the steady state inlet velocity in both empty and porous channels is studied. The influence of frequency and amplitude of the inlet flow on heat transfer is thoroughly examined. An aim is to test the validity of the *LTE* assumption for the application of forced convective heat transfer from a circular cylinder under steady and pulsating inlet boundary conditions and find

the circumstances under which this assumption would be justifiable.

1.4 Structure of the thesis

The preface of the thesis, which comprises the preceding pages, includes a dedication, title page, statement of originality, abstract, acknowledgments, a list of the publications by the author pertaining to the thesis, nomenclature, the table of contents, and finally, this introduction.

The body of the thesis consists of a literature review in chapter 2, a numerical methods chapter (chapter 3), verification of the numerical code in chapter 4, results chapters (chapters 5−9), and conclusions (chapter 10).

Chapters 5−9 contain results from numerical investigations of: forced convection around a single cylinder embedded in a porous medium, i.e., the effect of thermal and structural properties of porous media (chapters 5 and 6). Chapter 7 presents the results obtained on the geometry investigated in chapters 5 and 6, but with a pulsatile inlet flow. Chapter 8 details an investigation of the validity of the *LTE* assumption for the application of forced convective steady and pulsatile flows over a cylinder embedded in a porous channel. A study of forced convection from a bundle of cylinders immersed in a porous medium is presented in chapter 9.

Chapter 2

A Review of the Literature

2.1 Introduction

In order to provide an understanding of and context for the research that was undertaken as part of this study, a review of the relevant literature was undertaken and is summarised in this chapter. There is a broad and considerable volume of published research in the field of convection heat transfer in porous media. Excellent review articles and monographs have been provided by, for example, Ingham & Pop (1998), Hadim & Vafai (2000), Vafai (2000), Vafai & Hadim (2000), Pop & Ingham (2001), Ingham & Pop (2002), Bejan & Kraus (2003), Ingham *et al.* (2004) and Nield & Bejan (2006). These indicate the current level of understanding of the transport mechanisms of momentum and thermal energy in porous media. However, much of the existing work on this topic has been focused on either convection near plane walls or channels filled with porous media. To date there has been relatively limited published work on convective heat transfer from heated bodies of *high* complexity, such as circular cylinders or arrays of cylinders, embedded in porous media. In addition, most of the published articles concerning these more complex cases has been devoted to either natural or mixed convection, whereas, forced convection, although encountered frequently in applications, appears less studied. Moreover, the majority of studies conducted in the forced convection regime have used the simple Darcy model and/or the idealised *LTE* energy model.

The analysis of heat transfer in porous media based on the *LTNE* energy model is more involved as detailed in chapter one. Therefore, many researchers

have utilised the *LTE* energy model for predicting flow and thermal fields in porous media without investigating the validity of the assumption of *LTE* which is very necessary. The previous published work in this regard indicates that the validity of the *LTE* assumption has been comprehensively assessed in the forced convection mode of heat transfer. However, this assessment has been only tested in porous channels or over flat plates where the flow fields are considerably simpler.

The topic of cross flow over a bank of circular cylinders or tubes continues to attract interest because of the importance of this flow configuration in the design of tubular heat exchangers. This kind of heat exchanger can be found in many energy conversion and chemical reaction systems ranging from nuclear reactors to refinery condensers. The literature reveals that convective flows around multiple cylinders without the presence of porous media have been elaborately studied to investigate the flow interaction between cylinders on heat transfer from them, and other different related issues. However, heat transfer enhancement from a bundle of cylinders using the idea of inserting a porous material between the cylinders has been rarely examined.

There has been a growing need in many modern technological thermal applications for using highly effective cooling techniques for achieving a satisfactory enhancement in heat transfer while minimising frictional losses. This includes a diversity of active and/or passive cooling techniques. One of the promising techniques is the use of porous media subjected to a pulsating flow. Porous media has appeared as a convincing passive cooling enhancer due to the large contact surface area and the strong mixing for the fluid flow. Also, the forced oscillation of the incoming fluid is considered as an active augmentation method for heat transfer. This is due to the hydrodynamic instability in the shear layer of the flowing fluid, which greatly increases the lateral flow mixing, and hence strengthens the convective thermal transport from the heat source. The research on oscillating flows through porous media aimed at modifying heat transfer and fluid flow characteristics appears relatively scarce and incomplete.

Over the sections to follow previous studies of natural, mixed, and forced con-

vection past a horizontal cylinder embedded in porous media are first reviewed. Next, works that investigate the effect of flow interaction between multi-cylinders on heat transfer with and without the presence of porous media are presented. Then, the research of pulsating convective flow in porous media is described. These two sections provide some clarity about the shortage of studies into oscillatory flows in porous media in general and over a single circular horizontal cylinder in particular, and moreover about convective flows over multiple cylinders surrounded by porous media. The final section deals with the validity of the *LTE* assumption.

2.2 Convection heat transfer from a horizontal cylinder immersed in a porous medium

As indicated, hear transfer by free, forced and mixed convection flow from cylinders and spheres immersed in fluid-saturated porous media is an important subject and has received attention because of its fundamental nature as well as many potential engineering applications. Cylindrical and spherical geometries arise in power plant stream lines, buried electrical cables and transformer coils, industrial and agricultural water distribution lines, oil and gas distribution lines, storage of nuclear waste, solar collectors, to name just a few. This section reviews work previously published on this subject.

2.2.1 Natural convection

Buoyancy-induced flow over horizontal heated cylinders in porous media is relevant to several of the engineering problems mentioned above especially those those involve thermal insulators. The thermal insulator typically includes a fibrous porous material, which is permeable to fluid motion. Consequently, natural convection may develop in the insulating material and contribute significantly to the heat transfer process, as has been demonstrated by many authors. Eckert & Drake (1972) and Thiyagarajan & Yovanovich (1974) represent early studies in this regard, but they have concentrated on the case of immersed cylinders assuming the surrounding porous medium to be solely conductive. However, for a

high-permeability porous medium, the assumption of pure conduction heat transfer from an immersed cylinder may not be valid. In fact, the medium which is permeable enough to fluid motion produces a temperature difference between the heated cylinder and the fluid penetrating within the medium giving rise to a natural convection flow. Therefore, the entire heat transfer from buried cylinders consists of both convection as well as conduction, and in the most cases the contribution of free convection is as large or larger than that of conduction.

The first similarity solutions for free convection adjacent to axisymmetric and two-dimensional bodies of arbitrary shaped cylinders and spheres, in a constant porosity medium of infinite extent were obtained by Merkin (1979) based on the Darcy's law in the boundary layer. Using the same approach, Cheng (1985) proposed a theoretical correlation for the average Nusselt number, Nusselt number, to the specific case of a horizontal circular cylinder heated at constant temperature. Fand *et al.* (1986) performed the first experimental investigation on free convection heat transfer from a cylinder buried in a randomly packed bed of glass spheres saturated by either water or silicone oil. They concluded that the whole range of Rayleigh number, Ra, can be divided into two low and high regions. In each region, the behaviour of Nusselt number is totally different. The results showed that the high-Ra region, which is usually located near the heated surface, corresponds to *Forchheimer* flow, whereas, the low-Ra region, somewhat further from the surface, corresponds to *Darcy* flow.

Ingham & Pop (1987) investigated numerically the problem under the assumption of the flow being governed by Darcy's law for the full range of Ra. They found it difficult to obtain accurate numerical solutions at small values of Ra, while the asymptotic solutions are only valid for $-log(Ra) \gg 1$. For $Ra \approx 1.0$, the numerical results were found to be in a reasonable agreement with the experimental findings of Fand *et al.* (1986). However, at larger Ra, there was a need for numerical solutions to the boundary-layer equations, but with an increasing difference between them and the experimental data as Ra increases. However, this difference should not be surprising because at large Ra the experimental results correspond to the Forchheimer model, thus the application of Darcy's law

loses validity.

Later, numerical and experimental investigations of free convection around a cylinder heated with constant heat flux were performed by Himasekhar & Bau (1988a). The results of the measured average Nusselt numbers were found to be higher than those obtained from the numerical solutions at large Ra. The numerical solutions were carried out using the Darcy's approximation with the assumption of negligible thermal dispersion. They attributed the difference between their theoretical and experimental results at high Ra to the flow transition from a steady two-dimensional flow to a transient three-dimensional one as observed in their experiments.

The problem of unsteady free convection about a cylinder embedded in an enclosed packed bed of spherical particles was studied numerically by Hsiao *et al.* (1992). Both uniform wall temperature and uniform heat flux thermal boundary conditions were considered at the cylinder surface. In addition, both non-Darcian effects and thermal dispersion effect were taken into account. The results illustrated that these effects have an appreciable influence on the heat transfer enhancement from the cylinder surface. Also, it was deduced that with these effects considered simultaneously, the predicted Nusselt number was in better agreement with the experimental results of Fand *et al.* (1986) and Himasekhar & Bau (1988a).

Oosthuizen & Naylor (1996) examined free convection heat transfer from a cylinder placed in a square enclosure partly filled with a layer of air-saturated porous medium and partly filled with a layer of only air, with a horizontal impermeable barrier between the two layers. The cylinder was assumed to be buried in the porous layer, and the barrier was assumed to offer a negligible resistance to heat transfer. The main objective of the study was to determine how the rates of heat transfer from the cylinder are influenced by the size of the air-gap at the top of the enclosure for different Ra, solid-to-fluid thermal conductivity ratio k_r, Darcy number Da and enclosure size. In all cases considered, a certain critical size of the fluid layer thickness was found to give a minimum Nusselt number.

The thermally non-equilibrium energy model with the Darcy's approxima-

tion were used by Saeid (2006) to numerically study natural convection in the boundary layer around an isothermal horizontal cylinder immersed in porous media. The effect of the interfacial heat transfer coefficient parameter H_v and the porosity-scaled thermal conductivity ratio parameter γ on the local and average Nusselt numbers were investigated. The results showed that an increase in any one of these two parameters results in an increase in the total average Nusselt number throughout the fluid and solid phases. However, it was found that the dependency of the total Nusselt number on the related parameters is different. This depended substantially on the conductivity ratio parameter and only slightly on the interfacial heat transfer parameter.

Saada *et al.* (2007) analysed the flow and heat transfer characteristics of natural convection about a cylinder coated by an air-saturated fibrous layer described in figure **??** by using a mathematical model incorporating non-Darcian effects. They did an optimisation study in order to find the better circumstances, coating layer thickness, effective/stagnant thermal conductivity ratio and Darcy number, that produce good thermal insulation or heat transfer augmentation. The results demonstrated that the efficient insulation, which corresponds to heat losses less than 10%, can be obtained for layer thicknesses higher than 0.8 cylinder diameters, for low $Da \leq 10^{-7}$ and conductivity ratio equal to 2, as shown in figure **??**. Whereas, for heat transfer enhancement purposes, the study found that a highly permeable and highly conducting porous layer is suitable.

Unsteady free convective flow over a cylinder buried in a semi-infinite porous medium bounded above by a liquid layer was studied by Kumari & Nath (2009). It was assumed that the flow is described by Darcy's law due to the small range of Rayleigh number $Ra < 200$ used. The unsteadiness condition in the problem arose from the cylinder which is suddenly isothermally heated or cooled and then maintained at that temperature. The average Nusselt number was shown to be significantly influenced by Ra and the ratio of burial depth to cylinder diameter. The Nusselt number increases as Ra increases at a constant value of burial depth ratio; however, it can be increased or decreased as the burial depth ratio increases depending on Ra.

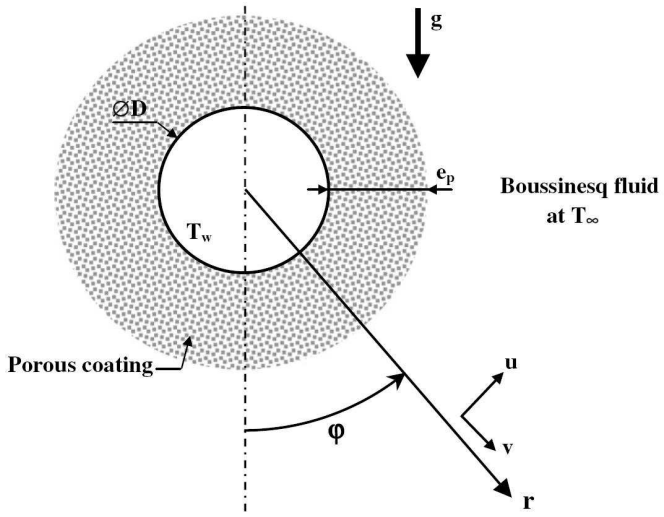

(a) The schematic diagram

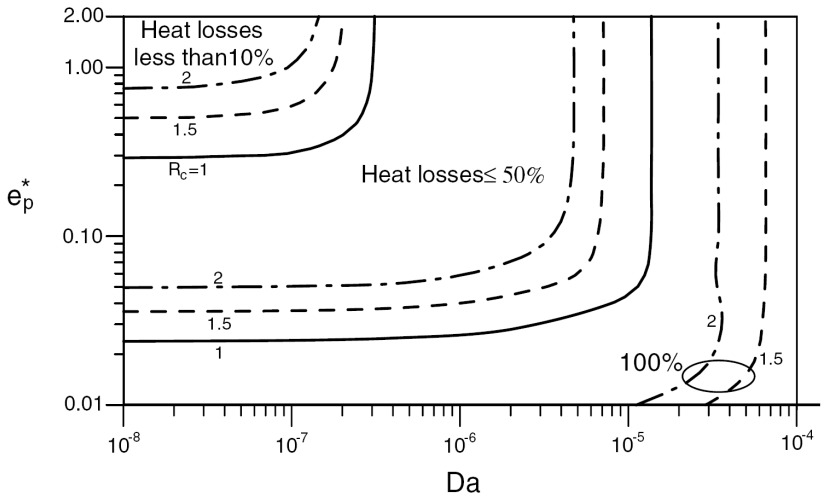

(b) Heat loss maps

FIGURE 2.1: Natural convection from a horizontal circular cylinder coated by a porous layer and heated at constant temperature. This problem was investigated by Saada *et al.* (2007) to find an optimal conditions for thermal insulation or heat transfer augmentation for different circumstances, i.e. porous layer thickness to cylinder diameter ratio e_p^* and Darcy number Da and at thermal conductivity ratio equals to 2.

Natural convection heat transfer for a cylinder of elliptic cross-section embedded in a porous medium has been examined by Pop *et al.* (1992), Facas (1995a), Cheng (2007a) and Cheng (2007b). Pop *et al.* presented numerical solutions to the governing boundary-layer equations for the steady state case. They obtained results for two cases; uniform temperature and uniform heat flux boundary conditions, with two body orientations; one where the major axis is considered to be the horizontal axis, i.e. called blunt orientation, and the other where it is regarded to be the vertical axis, i.e. called slender orientation. Based on their numerical results, the authors deduced that for the case of uniform surface temperature, higher rates of heat transfer can be generated using the former orientation; while, the opposite is true for the case of uniform surface heat flux.

Facas (1995a) subsequently obtained numerical solutions for free convective fluid flow and heat transfer for an elliptical heat source, but this time immersed beneath a semi-infinite, saturated porous medium with a top surface assumed to be permeable to the flowing fluid. Attention was focused on the effect of the ellipse aspect ratio, burial depth and body orientation on heat transfer rates. Also, both blunt and slender body orientations were taken into consideration. The numerical results disclosed that the boundary-layer approximations used by Pop *et al.* (1992) were not valid for low values of ellipse aspect ratio. In addition, the results indicated to that heat transfer from a hot source is independent on the burial depth, and the slender orientation is much better than the blunt one for yielding heat transfer, especially for low ellipse aspect ratio.

Cheng (2007a) and Cheng (2007b) used the $LTNE$ energy model to perform a non-similarity boundary-layer analysis for the same problem near an elliptical cylinder with constant wall temperature, for permeable and impermeable cylinder surfaces, respectively. These analytical works tended to extend the work of Saeid (2006) to incorporate eccentricity transpiration effects. Similar to Saeid, Cheng concluded that an increase in the porosity-scaled conductivity ratio γ or the interfacial heat transfer parameter H_v tends to increase the rates of heat transfer. He also found similar trends as for the results of Facas above with respect to the influence of the body orientation on heat transfer. In addition, the effect of

the transpiration parameter, examined by Cheng (2007a), was shown to have a tendency to decrease the thickness of the thermal boundary layer formed around the cylinder, and hence augments heat transfer between its heated wall and the porous medium used.

The problem of heat loss by natural convection from buried pipes or cables has also received attention by some researchers. This problem arises, for example, in connection with oil/gas lines in which the oil/gas is heated or chilled in order to reduce the pumping cost. Fernandez & Schrock (1982) carried out the first experimental investigation on natural convection heat transfer from a cylinder put horizontally beneath a liquid-saturated porous medium, and wrapped by an isothermal liquid layer. They also performed numerical simulations for the problem based on the Darcy-Brinkmann model in a constant porosity medium, and presented a correlation for the Nusselt number that fits the experimental data with a standard deviation of only 11.4%.

Later, Bau (1984a) performed an analytical study to calculate the flow and temperature fields associated with a pipe embedded in a semi-infinite porous medium with an inclined surface. Both cases of permeable and impermeable top surfaces were considered. A correlation for Nusselt number in the form of a power series in terms of Rayleigh number Ra was presented. However, it was revealed that this correlation is valid only for a very small range of Ra. Following this, the work of Bau (1984a) for the impermeable case was extended by Himasekhar & Bau (1987) to involve a convective boundary condition at the surface of the porous medium. They obtained analytical solutions for both hot and cold pipes by formulating a double perturbation expansion in terms of Ra and inverse Biot number Bi. They also presented a correlation for Nusselt number as a function of these two pertinent parameters, i.e. Ra and Bi, with burial depth. In the above two studies of Bau (1984b) and Himasekhar & Bau (1987), it was demonstrated that there exists an optimal burial depth for which the heat transport from the pipe is minimised to provide a good degree of thermal insulation.

Facas (1994) and Facas (1995b) considered the problem of a hot pipe with two baffles horizontally connected to the surface, and immersed beneath a semi-

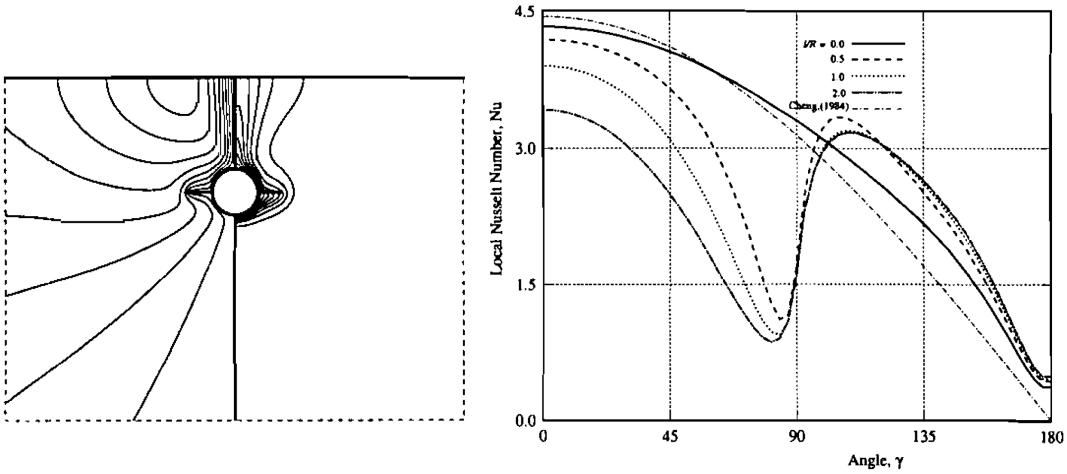

(a) Flow and thermal fields

(b) Local heat transfer

FIGURE 2.2: (a) Streamlines (Left) and isotherms (Right) for free convection from a pipe with external two baffles attached along its surface buried beneath a semi-infinite porous medium, at a baffle length/cylinder diameter ratio $l/D_{cy} = 1.0$, burial depth ratio $h/D_{cy} = 5.0$ and $Ra = 50$. (b) Local heat transfer distribution around the hot pipe for various baffle lengths $l/D_{cy} = 0.0, 0.5, 1.0$ and 2.0, also at $h/D_{cy} = 5.0$ and $Ra = 50$. These results are taken from Facas (1995b).

infinite porous medium as described in figure **??**. The surface of the medium was assumed to be impermeable to the fluid flow in the former study, whereas, it was assumed permeable in the later one. The results for both studies indicated to that the baffles provide a substantial energy saving as illustrated in figure **??**. Only a very weak dependence of heat transfer from the hot pipe on the burial depth was found.

Natural convection from a horizontal cylindrical annuli filled completely or partially with a porous medium has also been studied by number of investigators. The case of concentric cylinders has received the most attention in the literature. Burns & Tien (1979) reported the results of an analytical investigation of free convection in a porous medium bounded by two concentric spheres and horizontal cylinders using both a regular perturbation expansion and a finite-difference method. The effect of the modified Ra, the radius ratio and the external heat transfer coefficient on the overall heat transfer were quantitatively analysed. The

analysis pointed out that maximum values of Nusselt number are observed in both geometries depending solely on the radius ratio for each geometry. Moreover, Rao *et al.* (1988) examined the problem numerically in three dimensions using a Galerkin method. They obtained, in addition to the bi-cellular flow pattern, three-dimensional spiral flows for sufficiently strong initial perturbations. This was found to produce a higher maximum local heat transfer rate in the top region of the annulus, which consequently enhanced the overall heat transfer compared with that for two-dimensional unicellular flow.

The influence of the inclusion non-Darcian effects, i.e. inertia, boundary and velocity square terms, on heat transfer between two horizontal cylinders heated at constant temperature and filled by a saturated porous medium was reported numerically by Kaviany (1986). The results showed that all of these effects reduce the heat transfer rate, with the most significant influence produced from the boundary effect. He presented a diagram for the flow regime which illustrates the pseudo-conduction, Darcy and non-Darcy regimes, for radius ratios of 2 and 4. Following this, Charrier-Mojtabi *et al.* (1991) investigated numerically and experimentally free convective flows in a horizontal porous annulus. The characterisation of the multicellular two-dimensional $2D$ flows was estimated using both collocation-Chebyshev and full Fourier-Galerkin methods. Numerical results illustrated that the former method gives a better accuracy particularly for the description of the boundary layers developed near the inner and outer cylinders. The experimental study that was made using the Christiansen effect for the visualisation of the thermal isotherms allowed the authors to observe $2D$ bi-cellular flow patterns. It was also observed that the transition from unicellular to multicellular flow depends strongly on the initial experimental conditions.

Furthermore, the numerical work of Barbosa Mota & Saatdjian (1995) who studied the same problem of free convection in a saturated porous annulus, examined the effect of the annulus radius ratio on the heat transfer and the flow patterns generated inside the medium. The results displayed a closed hysteresis loop for the relationship between the Nusselt number and Rayleigh number Ra, when the radius ratio is above 1.7. This was assumed to be associated with

the transition from a two-cell to a four-cell flow regime. For small radius ratios less than 1.7, the steady-state flows comprising two, four, six and eight cells were progressively obtained in the porous layer as Ra increases, but no hysteretic behaviour was shown.

A conjugate formulation of the problem was investigated numerically by Kimura & Pop (1991) and Aldoss *et al.* (2004). Kimura and Pop described some features of the conjugate natural convection between two concentric cylinders entirely filled with a porous layer that were associated with inertia effects. They found that the rate of heat transfer, which is studied in terms of Ra, radius ratio, inertia parameter and the wall/medium thermal conductivity ratio, in the conjugate situation is lower than that in the non-conjugate case. From their results, there was a tendency for the inertia parameter to suppress commencement of convection; therefore, it was predicted that this parameter decreases the heat transfer rate whilst Ra increases it.

Whereas, Aldoss *et al.* (2004) considered a horizontal concentric annulus filled partially with porous media. The full DBF momentum model was used. The porous medium was introduced to simulate the insulation material. Therefore, the location, being adjacent to the inner cylinder or adjacent to the outer cylinder, with the main pertinent parameters such as Grashof Gr, Darcy Da numbers and the thickness of the porous layer, were considered. Comparisons with the reference cases, i.e. a completely filled annulus with porous media or no porous media, were made as well. An annulus completely filled with porous media was found to have the best insulation effectiveness, and was superior to partially filled annuli. The effect of Da on the effectiveness of the porous media used was found to be very significant.

Stability analysis for free convective flows between two concentric horizontal cylinders filled with porous media has been carried out by Caltagirone (1976) and Himasekhar & Bau (1988b). Caltagirone developed an experimental study by use the Christiansen effect for visualising the thermal fields in a porous medium bounded by two isothermal cylinders with radius ratio 2. He determined, by means of temperature measurements, the critical Ra for the transition between

the unicelluar two-dimensional convective flow and the three-dimensional fluctuating pattern. A three-dimensional numerical analysis using a finite-element method was also proposed, but no significant results were obtained to explain the experimentally observed flow structures. Himasekhar and Bau proposed a linear stability analysis of the multicellular $2D$ flows with $2D$ perturbations localised in the basic flow plane. It was stated that for a relatively large space parameter, i.e. radius ratio $> 2^{1/4}$, two solutions remain stable for some range of Ra above the transitional value until eventually they lose stability via Hopf bifurcations (i.e. a steady to unsteady transition). For relatively small radius ratio $< 2^{1/2}$, additional solutions appeared via a simple bifurcation process, i.e. one solution branch loses stability whereas another one gains it.

However, the study of the reduction of heat loss by the use of eccentric insulations, i.e. eccentric annuli filled by porous media, has been received less consideration. It was tested by, for example, Bau (1984a), Himasekhar & Bau (1986) and Barbosa Mota & Saatdjian (1997). Bau (1984a) reported analytical solutions for heat transfer by free convection in a saturated porous medium confined between two horizontal isothermal eccentric cylinders using a regular perturbation expansion in terms of Darcy and Rayleigh number. The results revealed that heat transfer from an insulated annulus can indeed be optimised by a proper choice of the eccentricity ϵ_c for a given radius ratio and Darcy-Rayleigh number. Himasekhar & Bau (1986) used a boundary-layer technique to present a correlation for the Nusselt number as a function of Ra, annulus radius ratio and ϵ_c. This correlation was found to be valid for a large range of Ra as long as the flow is $2D$, bi-cellular and steady. Barbosa Mota & Saatdjian (1997) used an accurate $2D$ finite-difference code to investigate numerically the conditions leading to a heat transfer reduction by the use of eccentric annuli at a radius ratio of 2. They found that for a moderate range of Ra, a transition from a $2D$ multicellular flow regime to a bi-cellular flow pattern, which results in an overall heat transfer reduction, can be induced by increasing ϵ_c, as illustrated in figure **??**. However, a minimum rate of heat transfer was shown to be located at a particular value of ϵ_c depending on Ra. For example, the results suggested that at $Ra = 110$, annuli

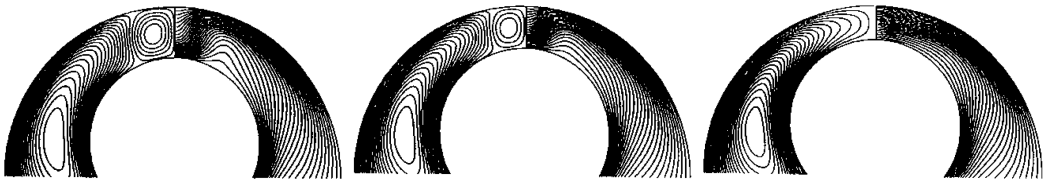

(a) $\epsilon_c = 0.4$ (b) $\epsilon_c = 0.5$ (c) $\epsilon_c = 0.6$

FIGURE 2.3: The results of streamlines (Left) and isotherms (Right) obtained by Barbosa Mota & Saatdjian (1997) for natural convection in the upper part of an annular filled with a porous medium, with radius ratio equal to 2.0 and Rayleigh number $Ra = 100$, for different eccentricity: (a) $\epsilon_c = 0.4$, (b) $\epsilon_c = 0.5$ and (c) $\epsilon_c = 0.6$.

with $\epsilon_c = 0.6$ can be a most efficient insulator with a heat reduction of 11.3% generated from the flow transition.

2.2.2 Mixed convection

Mixed convection is an interaction mechanism between the free and forced modes of convection. In contrast to forced convection flow where buoyancy effects are negligible, the mixed convection flow is influenced considerably by buoyancy effects, but they are not the only driving force of the flow. The theory of mixed convection shows that the ratio of the Grashof number to the square of Reynolds number (Gr/Re^2), which is known as the Richardson number Ri, has a great influence on the fluid flow and heat transfer mechanism. The forced convection dominates for small values of Ri while free convection takes over for large values of Ri, when the buoyancy forces become large. Initial research on mixed convection in porous media was motivated by Wooding (1960) and Wooding (1963) in an attempt to provide a basic understanding of the effect of through flow on the onset of instability in a semi-infinite porous medium. These works were perhaps motivated by flows associated with the geothermal region of Wairakei, New Zealand, where the subsurface groundwater is known to possess a general upward convective drift due to buoyancy induced by the high underground temperature.

Although substantial interest exists within the porous media community in the problem of mixed convection flow in porous media, the corresponding problem

of mixed convection flow over a horizontal cylinder immersed in porous media has received comparatively much less attention. By employing a generalised similarity transformation similar to that of Merkin (1979) for free convection problems, Cheng (1982) was able to obtain a similarity solution for the steady combined convection flow past a horizontal isothermal cylinder and a sphere. It was shown that using generalised similarity transformation reduces the resulting ordinary differential equations and boundary conditions for the isothermal cylinder to be similar to those of isothermal vertical plate in a porous medium (Cheng (1977)). Following this, using the same approach, but with a different transformation, Huang *et al.* (1986) obtained the solution for the constant heat flux case. Minkowycz *et al.* (1985) extended Cheng's analysis to consider adding mixed convection about a non- isothermal cylinder and a sphere. Based on a curvilinear orthogonal coordinate system, together with the boundary layer simplifications, approximate solutions were obtained by the local similarity and local non-similarity methods. Numerical simulations were also employed to the third level of truncation to disclose the effects of buoyancy and wall temperature variations on the thermal characteristics about the heated body.

Oosthuizen (1987) performed a numerical study on a mixed convective cross flow over a horizontal cylinder near an impermeable surface buried in a porous medium. The study aimed to investigate the effect of the presence of the surface on heat transfer from a cylinder. The results showed that the presence of the surface has a negligible influence on heat transfer when the buried depth of the cylinder is greater than three times its diameter. Also, it was shown that the presence of the surface tends to increase local heat transfer coefficients on the upper upstream quarter of the cylinder and decrease it on the upper downstream side of the cylinder. An experimental investigation of a combined convective cross flow past a non-isothermally heated horizontal cylinder was conducted by Fand & Phan (1987). The cylinder, $D_{cy} = 11.45\ mm$ diameter, was embedded in a porous medium composed of a randomly packed bed of glass spheres, with porosity $\varepsilon = 0.3606$ and diameter $d_p = 3\ mm$, saturated with water as a working fluid as described in figure **??**. A correlation hypothesis for convection heat transfer,

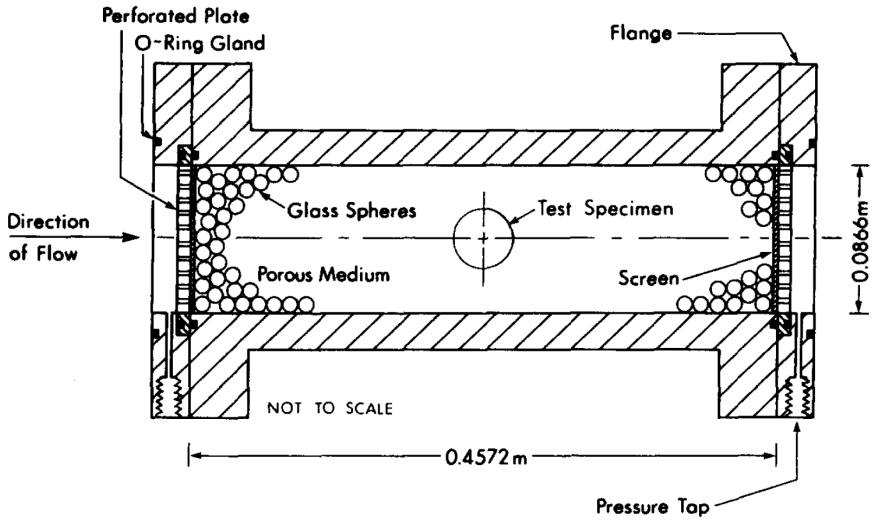

FIGURE 2.4: The geometry of a circular horizontal cylinder heated in a water-tunnel randomly packed with glass spheres. This apparatus was used in the experimental study of Fand & Phan (1987) to investigate mixed convection heat transfer from the cylinder.

which is based upon four plausible assumptions, primary among which is the assumption that a cross flow past a heated cylinder embedded in a porous medium can be decomposed conceptually into coarse and fine components, was determined. This hypothesis was shown to provide a basis for successfully correlating a set of experimental heat transfer data.

Badr & Pop (1988) examined combined convection for parallel and counter flows over a circular cross-sectional rod heated at constant temperature and placed in an air-saturated porous layer. The temperature of the rod surface was abruptly increased to and preserved at a constant value, which was assumed to be higher than the ambient air temperature. The flow patterns for the case of the counter-flow regime demonstrated an interesting observation, which was the occurrence of a peculiar behaviour owing to the presence of counter-rotating cells in each side of the symmetry line. These cells were found to shift toward the upper region of the hot rod as the Grashof number, Gr, increases, as displayed in figure **??**. Their predicted results for the local Nusselt number were compared with those obtained by Cheng (1982) and Minkowycz *et al.* (1985) based on boundary layer

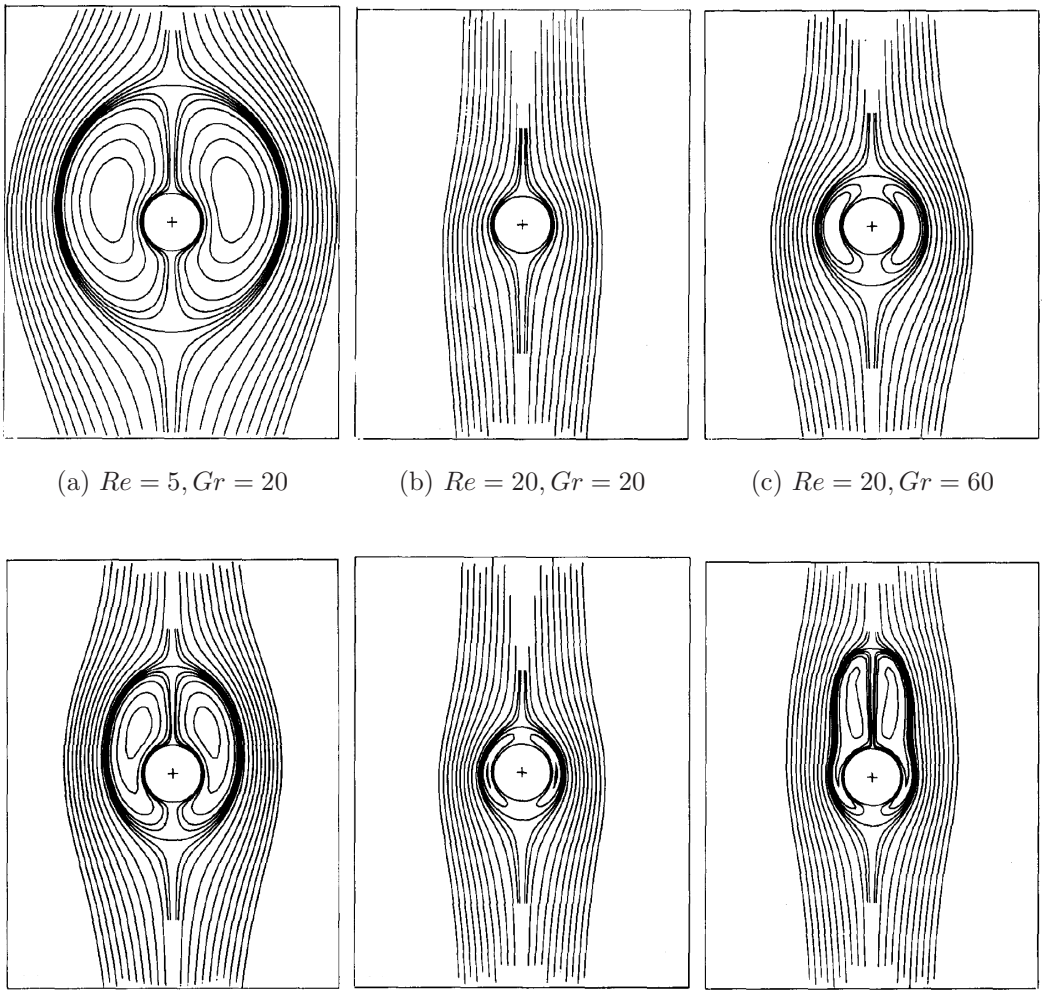

(a) $Re = 5, Gr = 20$ (b) $Re = 20, Gr = 20$ (c) $Re = 20, Gr = 60$

(d) $Re = 20, Gr = 80$ (e) $Re = 100, Gr = 300$ (f) $Re = 100, Gr = 400$

FIGURE 2.5: The streamline pattern of combined convective flows over a horizontal rod of circular cross-section embedded in a porous medium, for the case of counter flow studied by Badr & Pop (1988) at different values of Grashof Gr and Reynolds Re numbers.

theory. The comparison showed a good agreement over most of the rod surface, except for a small area in the vicinity of the upstream stagnation point, where this theory is not valid.

Zhou & Lai (2002) re-examined the problem of aiding and opposing mixed convection over a horizontal cylinder studied by Badr & Pop (1988) using a finite-difference method with body-fitted coordinates, to verify their solutions. The most important feature reported in their results was that for opposing flow,

oscillatory flows were found for several cases at $Re \geq 50$ and mixed convection parameter $Gr/Re \geq 4$. This oscillatory flow phenomenon was never exposed by Badr & Pop (1988), yet a steady solution was obtained for flow at $Re = 100$ and $Gr = 400$. However, similar behaviour was reported in the literature by Lai & Kulacki (1988) and Lai *et al.* (1990) for the case of combine convection in a horizontal porous layer partially heated from below by a long single heat source, and by multiple discrete heat sources done by Lai & Kulacki (1991). This flow instability was demonstrated by Zhou and Lai to be due to the interaction between the main flow that tends to push the secondary flow downstream of the cylinder and the thermal buoyancy forces that tend to lift it upstream, and by Lai and his co-workers to be due to the destruction and regeneration of the recirculating flows.

Investigation of heat transfer augmentation through the inclusion of a porous wrapper around a heated circular cylinder exposed to a mixed convective air flow was achieved by Bhattacharyya & Singh (2009). The porous layer used was of foam material with high porosity $\varepsilon = 0.9$. The results disclosed that a thin porous wrapper of high thermal conductivity can enhance the rate of heat transfer substantially even at low permeability. However, the porous wrapper was found to act as an insulator at low thermal conductivity even for high Reynolds number $Re = 200$ at Grashof number $Gr = 10^5$. A critical value of the porous layer thickness to provide optimal heat transfer from the cylinder was obtained. In addition, periodic vortex shedding behind the cylinder in the clear fluid was observed. The frequency of the periodicity was shown to be dampened due to the presence of the porous coating.

2.2.3 Forced convection

Although there have been numerous studies on forced convection heat transfer in porous media, a survey of the existing literature on this topic has revealed that relatively few investigations have been conducted to analyse fluid flow and heat transfer around bluff bodies, such as a horizontal circular cylinder, in the forced convection regime. The formulation of some of these investigations has

been based on the simple Darcy model to relate the flow velocity to the applied pressure gradient. Whereas, other studies have utilised modified or extended Darcy models. Therefore, in this section, the studies that have investigated forced convection from a horizontal circular cylinder in porous media are classified into two categories, namely Darcy and non-Darcy forced convection, according to the mathematical model used.

2.2.3.1 Darcy forced convection

Analytically, Sano (1980) and Pop & Yan (1998) used the Darcy model and presented analytical solutions of the energy equation in the boundary-layer region. In particular, Sano presented an asymptotic solution for the unsteady heat transfer from a circular cylinder immersed in a porous medium for large and small values of Péclet number Pe. The unsteadiness of the temperature field was produced by a step change in the cylinder wall temperature. It was suggested that these solutions are valid for $Pe \geq 200$ and $Pe \geq 0.1$, respectively. Pop & Yan (1998) obtained simple analytical expressions for the steady temperature field and local heat transfer rate for a cylinder and a sphere that are held at constant temperatures as a function of the angular coordinate for large Pe.

Kimura (1988) developed an integral solution to present an analytical expression for the average heat transfer for forced convection about an elliptic cylinder. This expression was found to be valid only for $Pe > 2.5$, and the critical Pe for the validity of the solution decreases with increasing the height/width ellipse ratio. Later, the same author Kimura (1989) analytically and numerically examined transient forced convection from a circular cylinder placed in a porous layer with cross flow. He presented the analytical solutions in terms of Nusselt number in the early stage of the transient process, as well as for the steady state. The numerical results showed the development of the thermal boundary layer with time, and it was found that the length of the transient period to reach the convective steady state was inversely proportional to Pe.

Only Layeghi & Nouri-Borujerdi (2006) used the Darcy model to analyze numerically the steady-state of the problem in the range of $Pe \leq 40$ with constant

Prandtl number $Pr = 1.0$ for gases, using a finite-volume approach based on staggered grids. Their analysis was conducted for different values of Reynolds number Re, porosity ε and permeability K on the distribution of the local Nusselt number and the velocity, temperature and pressure fields around the hot cylinder. They found that the Darcy model does not predict a (separated) wake behind the cylinder at this range of Pe. Also, it was concluded that the heat transfer rate increases with increasing Re or deceasing ε. The thermal field around the cylinder was shown to be strongly affected by ε of the porous medium and is not influenced by Kat all. However, the results showed that K has a positive impact on the pressure drop within the porous medium.

2.2.3.2 Non-Darcy forced convection

Other authors have used various types of extended Darcy models. Using the full DBF model, Murty *et al.* (1990) investigated the effects of Reynolds Re, Darcy Da and Forchheimer (Fs) numbers on forced convective heat released from a horizontal circular cylinder embedded in a porous medium. The authors reported that the effect of Re on the Nusselt number and the fields of temperature and velocity is more significant than other two parameters, i.e. Da and Fs. It was observed that at $Re < 10$, the main mode of heat transfer is conduction, while for higher values of Re, convection effects become important. In addition, the results demonstrated that a decrease in Da corresponds to an increase in the Nusselt number; however, beyond $Da = 10^{-4}$ this effect was found to be negligible. Also, the effect of inertial forces on the Nusselt number was shown to be dependent on the permeability of the porous medium used, for example, for high Da, the Nusselt number increases as Fs is increased, while for low Da, Fs has no effect on the Nusselt number.

Pop & Cheng (1992) reported an analytical study of the problem of a steady incompressible flow past a circular cylinder embedded in a constant porosity medium, i.e. spherical particles, based on the Brinkmann model. They obtained a closed form exact solution for the governing equations to formulate an expression for the separation parameter. They defined the separation parameter as the

vorticity on the wall near the rear stagnation point of the cylinder. Results in terms of streamlines and velocity profiles for the flow over the cylinder for different values of dimensionless particle diameter were presented, and it was found that separated flow does not occur at the rear stagnation flow region.

Thevenin & Sadaoui (1995) also used the Brinkmann model to investigate numerically steady forced convective flow over a cylinder immersed in a fibrous porous medium with high porosity $\varepsilon = 0.9$, by means of the finite-element method. The range of Re was chosen to be within $(1-100)$ to avoid the influence of thermal dispersion, at $Pr = 1.0$. Once again, as in the work of Layeghi & Nouri-Borujerdi (2006), the analysis revealed that the permeability of the porous medium does not have any effect on the temperature field; however, the velocity field was found to be strongly dependent on it. The same analysis done by Thevenin & Sadaoui (1995) was repeated by Thevenin (1995), but for transient forced convection around a suddenly heated isothermal cylinder, to investigate the effect of Péclet Pe and Darcy Da numbers on the mean Nusselt number. The respective successive conduction, transition and convection regimes were determined for a large range of dimensionless time. The duration required to reach steady-state convection heat transfer appeared to be a function of Pe and Da.

Fluid flow and heat transfer analysis for a single cylinder and an array of cylinders was performed by Layeghi & Nouri-Borujerdi (2004) by using the Darcy and the Darcy-Brinkmann models. The analysis was carried out with and without the presence of porous media at low $Pe \leq 40$ for the single cylinder, and at intermediate $Pe \leq 300$ for the arrays of cylinders, at $Pr = 1.0$. It was shown that the porous medium models predict different results at low $Da < 10^{-3}$. The results of the Darcy-Brinkmann model showed a decrease in the Nusselt number as the porosity ε decreases, whereas the Darcy model always predicts an increase in the Nusselt number when ε decreases. With regard to heat transfer augmentation, they found that more than 80% heat transfer enhancement can be obtained from the single cylinder by immersing it in a porous medium at high $Da > 10^{-3}$.

Furthermore, Younis (2010) also presented numerical results for forced convective cross-flow and heat transfer from a cylinder and a bundle of staggered

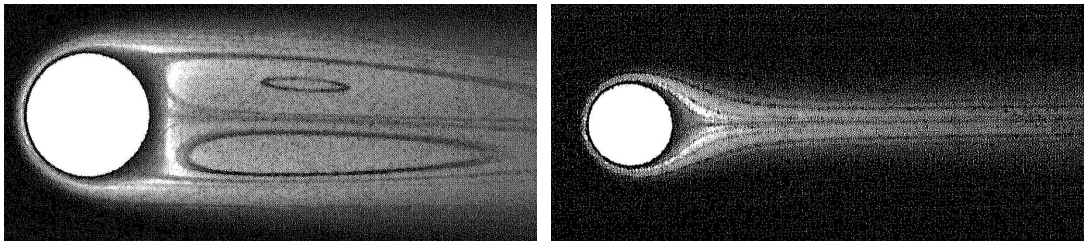

FIGURE 2.6: Streamlines (Upper portion) and isotherms (Lower portion) for forced convective flow over a bare single cylinder: (Left) placed in a clear fluid without the presence of porous media, and (Right) embedded in a porous medium at solid/fluid thermal conductivity ratio $k_r = 1.0$ and Darcy number $Da = 0.01$. This comparison was presented by Younis (2010) at $Re = 100$ and $Pr = 1.0$ for gases, to show the formation of vortex shedding in the downstream of the bare cylinder (without porous media) and its suppression with porous media.

cylinders, with and without a porous medium. The focus was on the effects of the permeability K and the thermal conductivity of the porous material on the fluid flow and the rate of heat transfer from a heated cylinder. The results for bare cylinders without porous media were compared with those for cylinders embedded in a porous medium. Part of this comparison for flow and thermal fields around a single cylinder, at $Re = 100$ are presented in figure **??**. It was found that it is possible to enhance the heat transfer rate from a cylinder placed in a cross-flow by several fold using a porous medium with high permeability and high thermal conductivity. Therefore, the author concluded that it is not beneficial to use a low-permeability medium for heat transfer enhancement because such a medium adds extra thermal resistance and may cause a decrease in heat transfer. Also, the results showed the formation of vortex shedding downstream of the bare cylinder at $Re = 100$, and its suppression in the presence of the porous medium.

In this section, all the previously mentioned investigations used the one-equation or *LTE* energy model to model the thermal response and calculate heat transfer. Thus, the porous medium was treated as a continuum by volume- averaging the properties of the fluid and solid phases. By reviewing the literature, it appears that the *LTNE* energy model which does not assume the idealised *LTE* assumption between the two phases has only been utilised by Rees *et al.*

(2003) and Wong *et al.* (2004) to study the problem of forced convection around a horizontal cylinder. They used this model to demonstrate how the thermal fields of the fluid and solid phases, and the rate of heat transfer around and from the cylinder, are affected by the absence of the *LTE* condition. The uniform temperature cylinder was assumed to be fixed perpendicular to an uniform fluid stream in a porous medium. Rees *et al.* examined the problem in the limit of high values of Pe. Their study was an analysis of forced convective heat transfer in the boundary layer regime by reducing the governing equations to a parabolic partial differential system. Whereas, Wong *et al.* investigated the same problem but at finite Pe by numerically solving the fully elliptic Darcy and two-equation energy models.

The authors, in both studies, reported that the surface heat transfer decreases with the distance from the leading stagnation point to the downstream stagnation point around the cylinder; however, the local rate of heat transfer for the fluid was found to be always higher than that of the solid matrix. It was pointed out that when the *LTNE* model applies the developing thermal fields in each phase is non-similar, for example, when the inter-phase heat transfer coefficient H_v is small, the solid thermal field occupies a region around the cylinder much greater that occupied by the fluid thermal field, as depicted in figure **??**. In addition, the results showed that the heat transfer in both phases increase by increasing the porosity-scaled thermal conductivity ratio γ for all values of the interfacial coefficient H_v tested. This occurred with no effect of this coefficient on the trend of convective heat transfer from the heated cylinder with γ. On the other hand, H_v was found to increase the rate of heat transfer in the solid phase and decreases it in the fluid phase. These investigations ignored non-Darcian effects and used the simple Darcy model, which is only valid for small Reynolds number (O(1) or less) based on the pore scale. Also, they omitted the effect of thermal dispersion, which has a significant influence on the process of heat transfer in porous systems as explained in the literature.

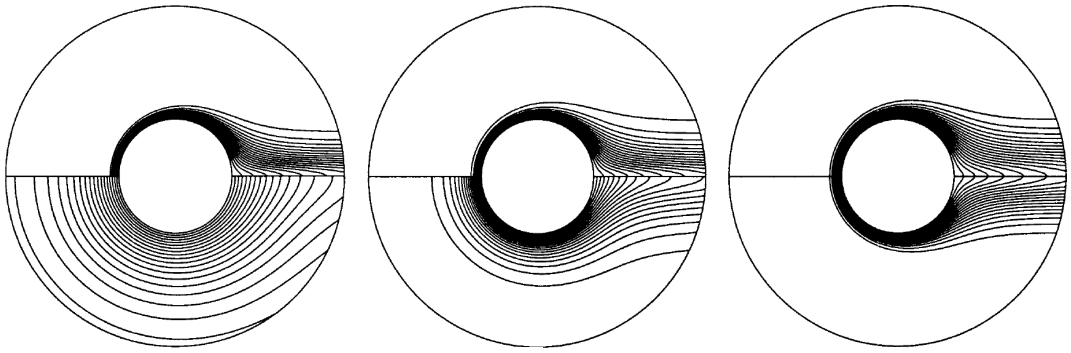

(a) $H_v = 0.01$ (b) $H_v = 0.1$ (c) $H_v = 100$

FIGURE 2.7: Effect of the dimensionless interfacial heat transfer coefficient H_v: (a) 0.01, (b) 0.1 and (c) 100, on the thermal fields of fluid (Upper) and solid (Lower) phases, in the problem of forced convection around a circular heated cylinder investigated by Wong *et al.* (2004) at Péclet number $Pe = 100$ and porosity-scaled thermal conductivity ratio $\gamma = 1.0$.

2.3 Convection over multiple cylinders in porous media

For industrial applications, depending on the application and design criteria, the arrangement of cylinders into arrays may have many possible variations. In-line and staggered arrangements of multiple cylinders are perhaps the most typical arrangements in the design of compact heat exchangers. Many related engineering applications of heat transfer and flow characteristics of multiple bare cylinders without porous media using these two arrangements have been presented. Most of the early works on this topic are experimental in nature. An extensive review of the experimental investigations up to 1970 is provided by Zhukauskas (1972). A considerable effort has been made in recent decades in the development of numerical models that predict hydrodynamic and thermal fields in cylinder bundles. This can be traced back to the pioneering work done by Thom & Apelt (1961), who employed a conformal mapping technique to transform the boundaries of the staggered tubes to coincide with equivalued surfaces of one of the independent variables. Amongst the vast number of studies in this regard, the most important

later works are listed in Wang *et al.* (2000) and Zhou & Yiu (2006).

It is important in cylinder bank flows to investigate the effect of flow interaction between multiple cylinders on the characteristics of heat transfer (Zdravkovic 1994). The literature discloses that the influence of the spacing parameter between cylinders on heat transfer has been discussed elaborately for the case of absence of porous media. For example, Aiba (1990) examined experimentally the effect of the longitudinal spacing parameter between four in-line circular cylinders above a plane wall and exposed to a cross-flow of air on the convective heat transfer characteristics from the third cylinder. It was noticed that although the spacing parameter does not play an important role in the behaviour of heat transfer as the gap between the cylinders and the plane wall, the average Nusselt number was found to be inversely proportional to this parameter. Jubran *et al.* (1993) reported also experimentally the effect of inter-fin spacing on convective heat transfer from cylindrical pin fins arranged in staggered and in-line arrays. They concluded that there is an optimal inter-fin spacing $2.5D_{cy}$ in both spanwise and streamwise directions, regardless of both type of array. Jue *et al.* (2001) tested numerically the influence of gap-to-diameter ratio of three cylinders arranged in an isosceles right-angle triangle between two parallel plates on the behaviour of the convective cross-flow and heat transfer. A maximum local and time-average Nusselt number were also obtained at a certain value of gap-to-diameter ratio 0.75. Also, Roychowdhury *et al.* (2002) observed numerically that the pitch ratio of a bank of staggered cylinders has a strong influence on the recirculatory vortex formation and growth, and consequently on heat transport properties, in the interior region between the cylinders.

Heat transfer enhancement from a bundle of cylinders using porous media between them with a fixed value of cylinder spacing has been studied only by Layeghi & Nouri-Borujerdi (2004), Layeghi (2008) and Younis (2010). They have made a numerical analysis for the problem of forced convection heat transfer from an array of staggered cylinders or tubes embedded in an air-saturated porous medium in an unconfined physical domain. Layeghi & Nouri-Borujerdi (2004) used the simple Darcy and Brinkmann-Darcy models to examine the effect of the

presence of a porous medium on the augmentation of heat transfer from two rows of cylinders at low and intermediate Péclet number $Pe \leq 300$ at $Pr = 1.0$. They concluded that the presence of the porous medium increases the heat transfer rate from the first and second rows in comparison with the no-porous case, with a very effective heat transfer augmentation for $100 \leq Pe \leq 300$. But, the increase in heat transfer from the first row was found to be more than that from the second one. However, they found that at $Pe \leq 20$, the use of the porous medium is not very effective for heat transfer augmentation from the first row, and it has a negative impact on the heat transfer from the second row.

Layeghi (2008) used the unsteady full *DBF* momentum model with the corresponding *LTE* energy model to analyze the effects of Reynolds number, i.e. $Re = 100$ and 300 at $Pr = 0.71$, for wooden porous materials with different thermal conductivities, i.e. wood/air thermal conductivity ratios $k_r = 2.5, 5.0$ and 7.5, on heat transfer enhancement from the first three rows of the staggered cylinder bundle. The results revealed that in some cases, more than 50% enhancement in heat transfer can be obtained from the bundle by using the wooden porous media. The highest conductivity ratio used $k_r = 7.5$ was shown to be the best choice for heat transfer enhancement for different Re, as displayed in figure **??**. However, it was noted that the total pressure drop also increases when the porous medium is inserted between the cylinders particularly at high Re. Therefore, the authors recommended that careful attention is needed for selecting porous materials with satisfactory heat transfer augmentation and acceptable pressure drop.

On the other hand, Younis (2010) pointed out that filling the gap between staggered cylinders with a porous medium may have an adverse effect on the overall rate of heat transfer. A comparison for the temperature field around multiple cylinders between the two cases with and without porous media was made, and it is presented here in figure **??**. It was reported that although increasing the effective thermal conductivity of the porous medium increases the rate of heat dissipation, the heat transfer rate from cylinders downstream of the first row decreases compared with that released from the first row. Therefore, for considering materials and operating costs, the author did not recommend to use porous media

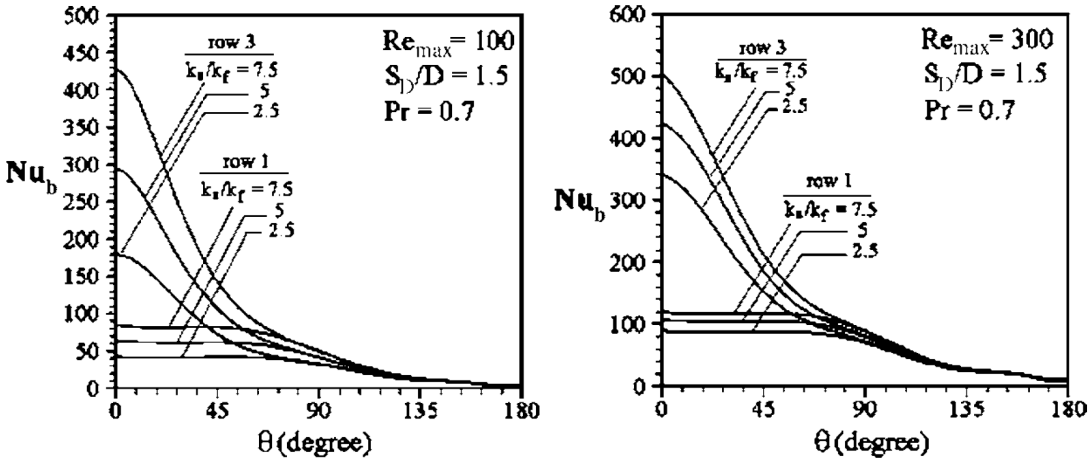

FIGURE 2.8: Effect of the solid/fluid thermal conductivity ratio $k_r = 2.5, 5$ and 7.5, on the local Nusselt number distribution on the first and third rows of a bundle of staggered cylinders embedded in an air-saturated porous medium with constant porosity $\varepsilon = 0.6$ and Darcy number $Da = 0.25$, at two values of Reynolds number (Left)100 and (Right)300. These results are taken from Layeghi (2008).

for heat transfer enhancement from multi-columns of heat exchangers.

2.4 Pulsating flow in porous media

The importance of unsteady internal flows has long been recognised. Of much practical interest are situations in which pulsations are superimposed on a mean flow inside a geometrically simple configuration, such as a pipe or a channel. In the absence of porous media, an early theoretical exposition was made by Uchida (1956) about an oscillating flow, but without consideration of heat transfer. The early numerical and experimental investigations on heat transfer in pulsating flow can be traced to Siegel & Perlmutter (1962) and Faghri *et al.* (1979) in a parallel channel and a pipe, respectively. The experimental data showed heat transfer enhancements, whereas the numerical analysis indicated to that for the case of constant wall temperatures, the presence of oscillations only slightly alters total heat transfer.

Following these studies, considerable research in this are has been undertaken. For example, Cho & Hyun (1990) performed comprehensive numerical simulations

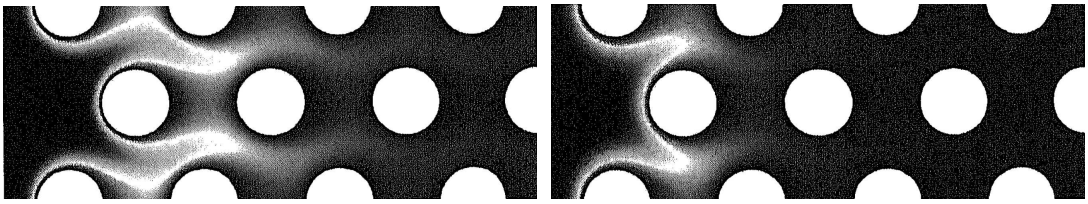

(a) With a porous medium

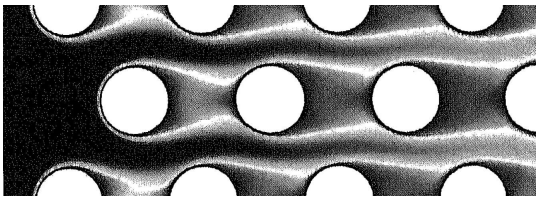

(b) Without a porous medium

FIGURE 2.9: Isotherms of a convective flow over staggered heated: (a) cylinders surrounding by a porous medium with solid/fluid thermal conductivity ratio; (Left) $k_r = 5.0$ and (Right) $k_r = 10$, at Darcy number $Da = 0.01$, and (b) bare cylinders without a porous medium. This comparison was made by Younis (2010) at Reynolds number $Re = 100$ and $Pr = 1.0$.

to delineate the flow and heat transfer characteristics for boundary-layer pulsating flow in a $2D$ cylindrical pipe. The attention was directed to relatively slow-moving pulsating flows with $Pr = 7.0$, such as those found in biofluid flows, to describe the subsequent unsteady motions of the fluid inside the pipe and to analyze the associated heat transfer characteristics. Kim *et al.* (1993) investigated the transient heat transfer characteristics of fully-developed pulsating flow but in the thermally developing region in a channel. This study was also made with a relatively slow throughflow at $Re = 50$ and $Pr = 0.7$. Experimental research to examine convective heat transfer from a heated floor of a rectangular duct subjected to a reciprocating airflow was conducted by Cooper *et al.* (1994). They obtained a non-dimensional correlation for the oscillatory-flow Nusselt number as a function of the pertinent parameters such as oscillatory Re, flow oscillation frequency f and duct height.

Zhao & Cheng (1995) presented a numerical solution for forced convection heat transfer of a periodically reversing flow in a pipe of finite length heated at constant temperature. A correlation formulation of the time-space average

Nusselt number for air in terms of kinetic Re, dimensionless pulsation amplitude A and length-to-diameter pipe ratio, was obtained. The same authors Zhao & Cheng (1996) extended their previous work to investigate experimentally and numerically forced convection in a long pipe heated by a constant heat flux and subjected to a hydrodynamically and thermally developing reciprocating flow of air. Once again, based on their experimental data, they formulated an empirical correlation for the cycle-space averaged Nusselt number in terms of the pertinent dimensionless parameters, for a laminar oscillatory flow of air in a long circular tube with constant heat flux.

Sert & Beskok (2003) studied numerically the same problem of reciprocating forced convection flows but in $2D$ channels subjected to periodic thermal boundary conditions. They compared their numerical results for the local time-average Nusselt number with the corresponding unidirectional flows. The possibility for determining a combination of the pertinent parameters such as the penetration length, Womersley Wo and Prandtl Pr numbers, to keep the maximum surface temperature below a desired value, which is important for cooling applications, was examined. Another numerical study for the enhancement of heat transfer from hot blocks mounted in a horizontal channel by pulsating flow was done by He *et al.* (2005). They performed comprehensive simulations to investigate the influence of several parameters, including Re based on the mean flow, Strouhal number St and pulsation amplitude A on the augmentation of heat dissipation from the hot blocks.

Only Iwai *et al.* (2004) and Ji *et al.* (2008) investigated fluid flow and heat transfer characteristics around immersed heated bodies, i.e. horizontal circular and square cylinders, respectively, placed inside an empty horizontal channel and exposed to an oscillating flow. Iwai *et al.* undertook experimental and numerical studies for a slowly oscillating flow with zero-mean velocity imposed, at different pulsation f and A. Figure **??** illustrates selected numerical results for the time variation of the thermal field around the circular cylinder for a half cycle of the flow oscillation. Whereas, Ji *et al.* performed experiments to investigate the convective heat transfer enhancement by using non-zero-mean pulsating flow, for

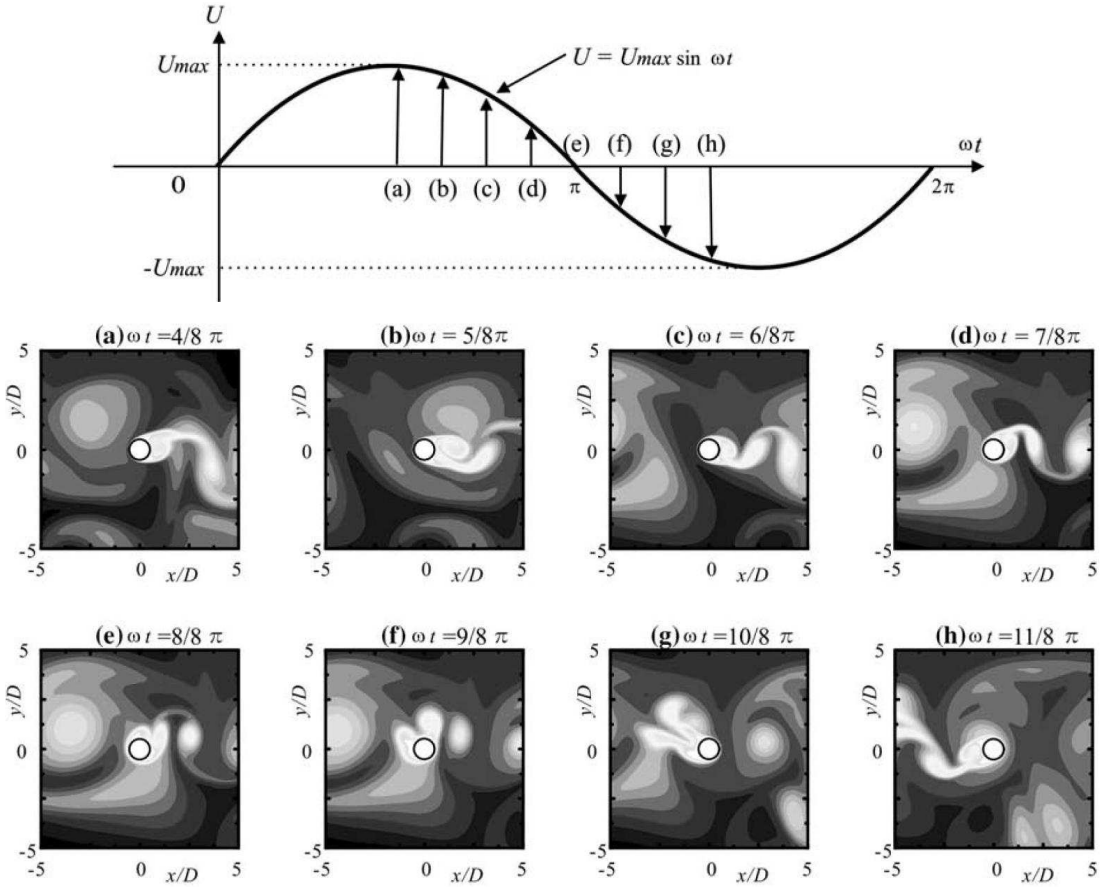

FIGURE 2.10: Time variation of temperature contours around a circular cylinder placed in an empty channel and exposed to a reciprocating flow. The results were presented by Iwai *et al.* (2004) for a half cycle of flow oscillation, at pulsating displacement amplitude $A/D_{cy} = 10$ and frequency $f = 1.0$.

different principal parameters, i.e. Reynolds number Re, pulsation f and the blockage ratio of the square cylinder, at low pulsation A.

In the presence of porous media, studies of the attendant heat transfer characteristics of a pulsating flow have been far less numerous. Efforts have been made to explore the utilisation of porous media as a heat sink in a confined channel subject to a pulsating flow. This has been motivated by the growing demand for achieving a higher rate of removal of heat from computing chips used in high-performance and high-power electronic devices. These studies are concerned with the aspect of forced-pulsating convective flows over full- or partial-porous systems. Paek *et al.* (1999) carried out an experimental study on the transient cool-down

of an insulated horizontal packed bed of spheres exposed to an pulsatile flow of air, wherein the pulsating component of the velocity is added to the inlet time-averaged flow. The results obtained at small $Da = 2.5 \times 10^{-5}$ indicated that the heat dissipation from the porous material is little affected by the introduction of flow pulsation if the pulsating amplitude $A < 1.0$ is small so that no reverse flows are induced. However, the heat transfer was shown to decrease when A becomes large enough to cause backward flows. Also, for a given A, the pulsating frequency represented by Womersly number Wo showed a positive effect on the rate of heat transfer between the packed bed and the flowing fluid; yet, these rates are still less than those for the case of steady flow.

Articles by Fu *et al.* (2001), Leong & Jin (2004), and Leong & Jin (2005) reported experimental results for heat transfer in porous channels subjected to steady and sinusoidal oscillatory air flows, with various porous materials, e.g. reticulated vitreous carbon (RVC) and metal foam, under constant heat flux thermal boundary conditions. All of these investigations have concluded that the oscillating flow is better than the steady flow for heat transfer purposes, where it was found that the averaged Nusselt number for the former flow is higher that for the later flow. They presented surface temperature distributions and local Nusselt number variations, and concluded that these distributions and variations for oscillating flow are more uniform than those for steady flow. Fu *et al.* pointed out that putting a channel filled with high conductivity porous media under a pulsatile flow represents a new effective technique for cooling electronic chips.

In the first study by Leong and Jin, the effects of thermal conductivity k and permeability K for different metal foam materials on heat transfer were analysed. It was shown that heat transfer from a porous channel subjected to an pulsating flow can be significantly enhanced by using materials of lower K and higher k. Their later study was an extension of that work to examine the effects of kinetic Re and dimensionless pulsation f and A. The results showed that the cycle-averaged Nusselt number increases with increasing A, and with increasing f, but for relatively low values. Also, the experimental data displayed a favourable range of Re, from 178 to 874, for augmenting heat transfer from a porous channel.

Khodadadi (1991) analysed using an analytical approach fully developed oscillatory flow within a horizontal porous channel bounded by two impermeable walls under the assumption of negligible inertia effects, showing that the velocity profiles exhibit maxima next to the solid walls. Therefore, it was suggested that for flow in porous media confined by two parallel walls with fast oscillation, a channeling phenomenon, similar to the one discussed by Vafai (1984) for variable porosity media, can be maintained. This study did not dealt with the issue of the associated effect on heat transport. However, it showed that the temporal average of the oscillatory frictional drag disappears over a period, suggesting that oscillations do not have a net influence on energy losses in the system, hence making it a good method for heat and mass transfer enhancement applications.

Kuznetsov & Nield (2006) also performed analytical work but for non-zero mean oscillatory flow in an iso-flux saturated porous channel and circular tube using a perturbation approach. In this work, analytical expressions for the velocity and temperature distributions, and for the transient Nusselt number, were presented for the problem of forced convection at constant small pulsation amplitude A and large Péclet number Pe. This study showed the effect of pulsation frequency f and modified Prandtl Pr and Darcy Da numbers on the transient Nusselt number. They found that the variation of the Nusselt number against f has a peak value. The magnitude of the peak was shown to decrease as the modified Pr increases, whereas, it first increases, reaches a maximum, and then decreases to zero as Da decreases.

Numerically, Sözen & Vafai (1991) simulated forced convective flow of a compressible ideal gas through an adiabatic packed bed. The effect of oscillating hydrodynamic and thermal inlet boundary conditions on the behaviour of the transport processes was investigated. Once again for insulated packed beds, the average energy storage characteristics were found to be very close, without major differences, for both cases of oscillating and constant inlet boundary conditions. It was observed that as A of the oscillations in the inlet pressure increases, the oscillations in the net energy stored become more pronounced. Larger f however, was shown to tend to smooth the variation in the net energy storage. Also,

the response of the field variables, temperature, pressure, density and velocity, was found to be more sensitive to an oscillating inlet pressure variation than an oscillating inlet temperature.

Numerical data of heat transport of forced pulsating convective flow in a porous channel with a uniform temperature walls was provided by Kim *et al.* (1994). Flow and thermal fields were examined over ranges of principal parameters, i.e. the flow pulsation amplitude A, the pulsation frequency parameter, the thermal conductivity, capacity ratios and Da. The comparison that was made with the case of non-pulsating flow showed that the existence of the oscillating flow in the porous medium brings almost forth a reduction in heat transfer in the entrance region of the channel, but an enhancement of heat transfer occurs at moderate downstream locations. The results illustrated that the influence of pulsation on heat transfer rates between the heated channel walls and the flowing fluid becomes stronger in the case of lower pulsation frequency and higher amplitude. However, this effect was found to be minor at extreme downstream locations. The peak value of heat transfer was found to be enhanced as Da decreases or the conductivity ratio increases, while, the effect of the capacity ratio appeared to be similar to that of frequency parameter.

Flow and thermal characteristics of forced pulsating convective flow in a parallel-plate channel with two discrete porous-block-mounted heat sources in tandem at the bottom wall was examined numerically by Huang & Yang (2008). They performed a detailed study of the effects of Darcy number Da, pulsation frequency represented by Strouhal number St, pulsation amplitude A and porous blockage ratio, on heat transfer. It was shown that both the presence of the porous blocks and the imposed inlet oscillating cause a periodic change in the the structure of recirculation flows, which are shown to have a significant influence on the flow and thermal behaviour near the heat sources. Some of the numerical results, reproduced in figure **??**, indicated that the effect of pulsation amplitude is considerably positive on the heat transfer enhancement factor for both heaters. A critical value of St to obtain a maximum heat transfer enhancement factor was obtained. Below and above this critical value, the enhancement factor was found

to decrease afterward. This occurred at low $A = 0.6$. Also, it is worth noting that their results showed that the values of the pulsating heat transfer enhancement factor are not always higher than those for the steady non-pulsating case, but depend on the values of A and St of the pulsating flow.

Steady and pulsatile forced convective flows in a horizontal channel partially filled with two porous layers adhering to the channel walls that are subjected to a uniform heat flux under $LTNE$ condition were investigated numerically by Forooghi *et al.* (2011). Effects of three determining parameters, namely Biot number Bi, solid-to-fluid thermal conductivity ratio k_r and the thickness of the porous layer, on the steady Nusselt number were considered. By comparing the results of the two convective flows, it was stated that the time-averaged Nusselt number for a pulsating flow is often higher than that of the steady flow. For pulsatile flow, though, the results revealed the same finding as for the above work of Huang & Yang (2008). That is, with respect to the pulsation A which has a positive influence on heat transfer, an entirely different trend of average Nusselt number against pulsating frequency, represented here by Womersley number Wo, was observed. The average Nusselt number that was obtained at different values of Bi and $k_r$was found to have a minimum value, instead of maximum, at a particular critical Wo, but surprisingly the maximum average Nusselt number occurred at the lowest Wo. This finding which is shown in figure **??** was predicted at high pulsation amplitude $A = 1.5$.

2.5 The validity of the LTE assumption

As mentioned in chapter one, it has been established that the LTE model for convection in porous media, which assumes thermal equilibrium between the solid and fluid phases, is not necessarily a good approximation depending on problem parameters. As such, more recently more attention has been paid to the $LTNE$ model to provide more physically realistic and accurate predictions of convection heat transfer processes in porous media. Representative works, for related problems of convection and for different applications include Carbonell & Whitaker (1984), Vafai & Sözen (1990a), Vafai & Sözen (1990b), Quintard & Whitaker

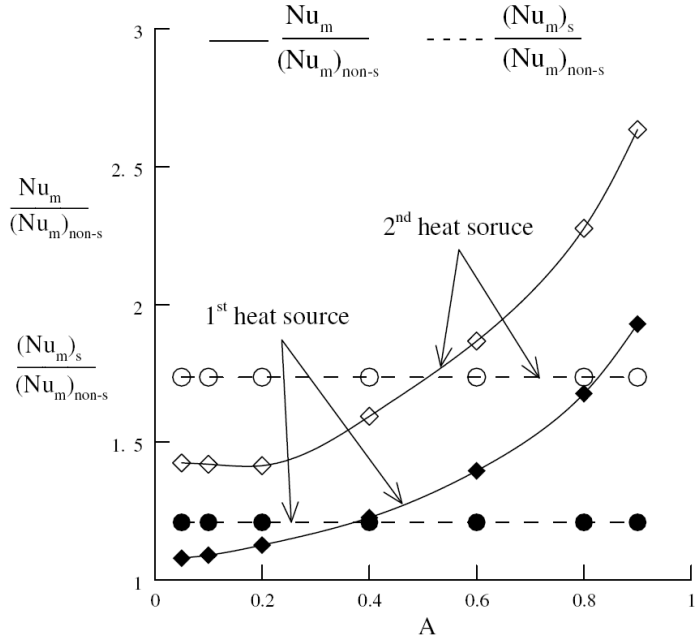

(a) Effect of pulsating amplitude

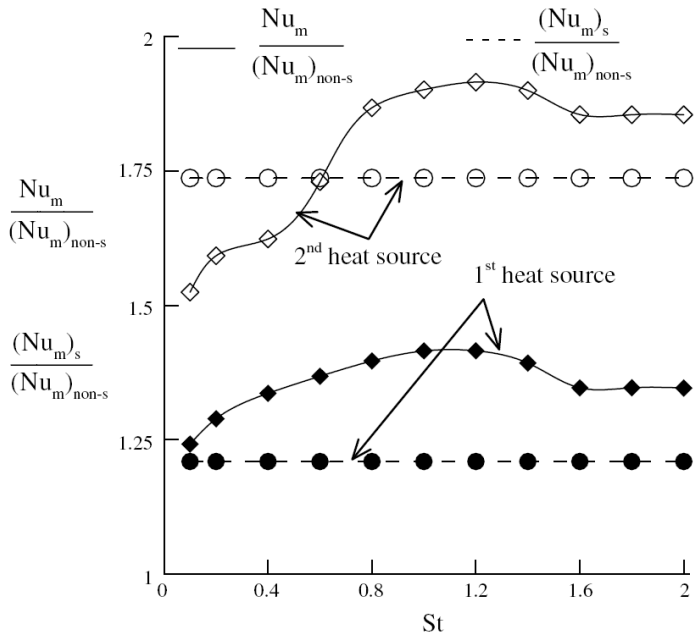

(b) Effect of pulsating frequency

FIGURE 2.11: Effects of: (a) pulsating amplitude at $St = 0.8$, and (b) Strouhal number at $A = 0.6$, of forced oscillating convective flow in a parallel-plate channel on the heat transfer from two discrete heat sources at the bottom wall with two porous-blocks mounted on them. The results were numerically obtained by Huang & Yang (2008) at Reynolds number $Re = 250$, Darcy number $Da = 3 \times 10^{-5}$ and effective thermal conductivity ratio equal to 1.0.

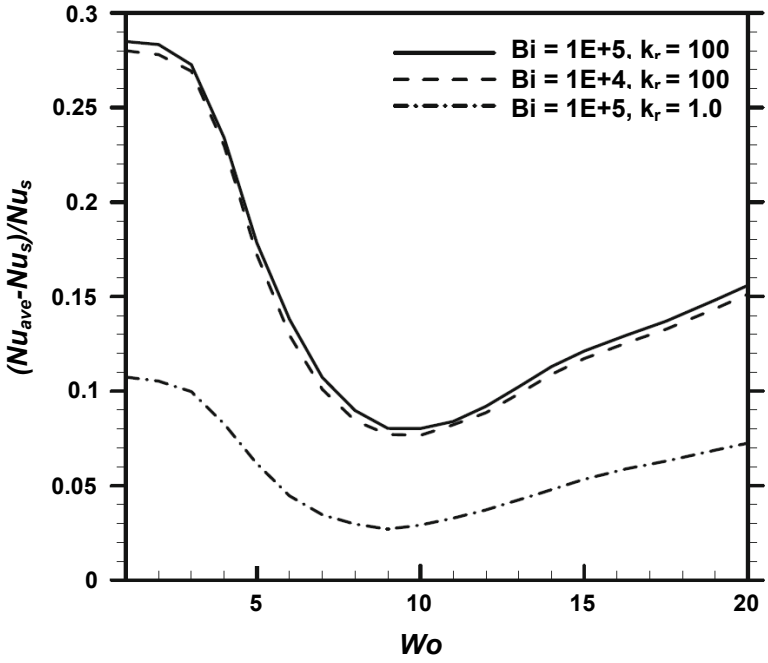

FIGURE 2.12: Variation of pulsation average Nusselt number against Womersley number at different values of Biot number and solid/fluid thermal conductivity ratio, of forced convective pulsatile flow in a channel partially filled with two porous layers with thickness $e/2H = 0.4$. The plots were obtained at $Re = 100$, $Pr = 1.5$, $\varepsilon = 0.5$ and $A = 1.5$, (reproduced from Forooghi *et al.* (2011)).

(1993), Amiri & Vafai (1994), Amiri *et al.* (1995), Jiang *et al.* (1996a), Jiang *et al.* (1996b), Kuznetsov (1997a), Kuznetsov (1997b), Quintard *et al.* (1997), Kuznetsov (1998), Amiri & Vafai (1998), Nield (1998), Minkowycz *et al.* (1999), Lee & Vafai (1999), Mohamad (2000), Rees & Pop (2000), Alazmi & Vafai (2000), Jiang & Ren (2001), Alazmi & Vafai (2002), Baytas & Pop (2002), Banu & Rees (2002), Baytas (2003), Jiang *et al.* (2004a), Saeid & Pop (2004), Wang & Wang (2006), Wong & Saeid (2009), etc.

Moreover, there have been considerable effort in assessing the validity of the LTE assumption. Some criteria have been suggested for this assumption in forced convection channel flow. Whitaker and his co-workers, Carbonell & Whitaker (1984), Whitaker (1991), Quintard & Whitaker (1995) and Quintard & Whitaker (2000), have performed pioneering work in this regard. Based on the order of magnitude analysis, they proposed a criterion in the case where the effect of

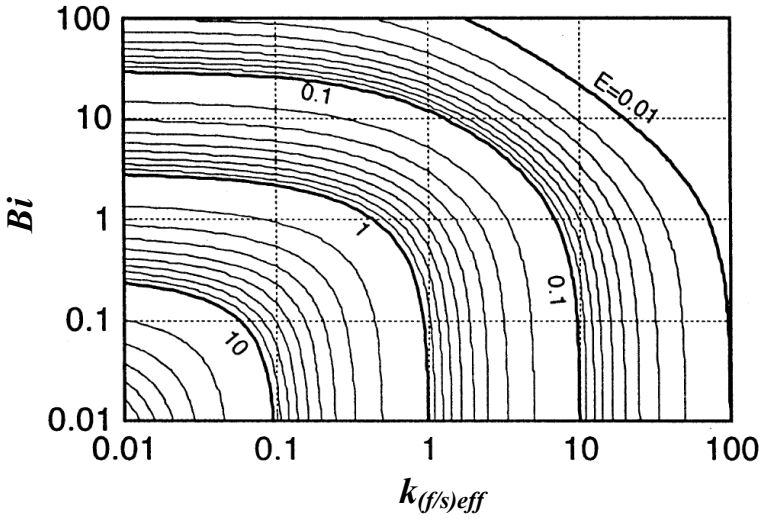

FIGURE 2.13: Contour error map plotted using the criterion proposed by Lee & Vafai (1999) for the validity of the *LTE* assumption. The criterion is a function of Biot number and effective thermal fluid/solid conductivity ratio.

conduction is dominant in the *REV* enclosing both the fluid and solid phases. Lee & Vafai (1999) presented a practical criterion for the case of forced convective Darcian flow in channels with different cross sections. This criterion, which is a function of Biot number Bi and effective thermal fluid-to-solid conductivity ratio, was utilised to present a qualitative error map given in figure **??**. It can be seen that the error in using the *LTE* model increases as both the conductivity ratio and Bi become smaller, hence causing that model to lose validity.

Later, Kim & Jang (2002) presented a general criterion for *LTE* expressed in terms of important engineering parameters, for instance Darcy Da, Prandtl Pr and Reynolds Re numbers. The criterion was checked when applied for conduction and/or convection heat transfer in porous media, which is more general than previous one suggested by Whitaker and his co-workers above. Also, it was confirmed to apply to various cases of convective heat transfer, such as micro-channel heat sinks and packed beds, and to well predict the validity of the *LTE* assumption in porous media. Following this, a new criterion was developed by Zhang & Liu (2008) for the case when convection heat transfer is dominant inside a channel filled with spherical particles under the condition of constant wall heat

flux. This criterion encompasses the influence of the effective solid/fluid thermal conductivity ratio in addition to the boundary heat flux, the area of cross section, characteristic length for pore size, porosity ε, fluid conductivity k_f, heat source of the solid phase and Nusselt number. The validity of the criterion was checked against numerical results obtained using the *DBF* model. The results showed that the effect of the *LTE* on porous media becomes larger with the increase of k_f, as well as with a decrease in boundary heat flux, characteristic length for pore size, heat source of the solid phase and the conductivity ratio.

In addition, other studies have attempted to determine the applicable region of the *LTE* assumption by calculating the temperature difference between both phases, i.e. fluid and solid, using the *LTNE* energy model. Analytically, Kuznetsov (1997c) obtained an analytical solution for the temperature difference between two phases in a channel with uniform wall heat flux utilising a perturbation technique. They concluded that this difference is proportional to the ratio of the flow velocity to the mean velocity. However, the analysis could not produce the velocity field, temperature field of any phase and nor lead to a Nusselt number, or even present an error map configuration.

Nield (1998) clarified the circumstances under which the *LTNE* condition may be important in a saturated porous channel using an analytical approach for the temperature fields and Nusselt number. They also suggested an important parameter ($N = k_s/H_{ch}^2 h_{sf}$), where parameters k_s and H_{ch} are the solid thermal conductivity and the channel height, respectively. The *LTNE* effect is negligible only when $N \ll 1.0$. It was found that the influence of *LTNE* was to reduce Nusselt number. Then, Nield & Kuznetsov (1999) extended the work of Nield (1998) by examining the effect of the conjugate situation involving the coupling of convection in the porous medium and conduction within a finite solid slabs on *LTNE*. They pointed out that the degree of *LTNE* is decreased due to the finite thermal resistance of the channel slabs.

The analytical work of Minkowycz *et al.* (1999) established a new area of failure for the *LTE* assumption corresponding to the presence of rapidly changing surface heat flux. They investigated the conditions when there is a relatively small

departure from the *LTE* condition due to a rapid transient heating for a saturated porous medium. It was concluded that the presence of the *LTE* state depends on the magnitude of the Sparrow number Sp which represents the thermo-physical properties of the porous medium used, and on the change to the rate in the heat input. A simple method of estimating Sp for the case of zero flow and forced flow was presented. For the case of no flow, a sufficiently large Sp was found to be indicative of the existence of the *LTE* condition. However, for the case with flow, the *LTE* condition appeared to be valid if Sp/Re is large.

The applicability of the *LTE* model for a micro-channel sink, which was modelled as a porous medium, was also analytically assessed by Kim *et al.* (2000) for the case where the bottom surface is uniformly heated by constant heat flux and the top surface is insulated. They obtained exact solutions for the temperature distributions by using both the 1− and the 2−equation energy models. A relative error map in terms of Da and the porosity-scaled fluid/solid thermal conductivity ratio γ to identify the applicable region of the *LTE* was presented. It was shown that the *LTE* assumption and the corresponding energy model can be valid as Da approaches zero or γ goes to infinity (see figure **??**).

Marafie & Vafai (2001) incorporated the effects of Da, Bi, inertial parameter Λ and the effective fluid/solid conductivity ratio in an analytical representation of the temperature field of both phases. They also presented error maps based on the Nusselt number to examine the validity of the *LTE* model for the above pertinent parameters. As in the work of Lee & Vafai (1999), smaller values of Bi and conductivity ratio were found to result in an increase in the error demonstrating a required use of the *LTNE* model instead of the *LTE* one. In addition, it was established that other two parameters, i.e. Da and Λ, have a smaller role in determining the validity of the *LTE* compared with Da and conductivity ratio.

The validation of the *LTE* assumption for transient forced convection channel flow was investigated analytically by Al-Nimr & Abu-Hijleh (2002). The porous channel was assumed to be bounded by two insulated parallel boundaries, and the cause of the transient behaviour was a sudden change in the inlet fluid temperature. Closed form expressions were presented for the solid and fluid temperature

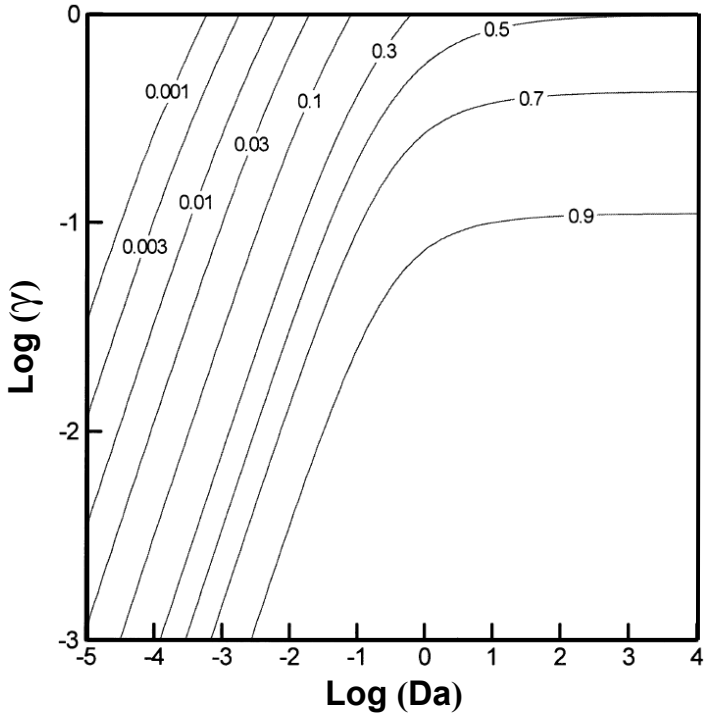

FIGURE 2.14: Contour error map in terms of Darcy number Da and the porosity-scaled fluid/solid thermal conductivity ratio γ. This map was presented from the analysis of Kim *et al.* (2000) for the validity of the *LTE* assumption in a micro-channel sink.

domains, and for a criterion which ensures the validity of this assumption. In order to investigate the conditions under which *LTE* is justified, they also considered a definition for the thermal relaxation time, which is the time required for both the solid and fluid to attain approximately the same temperature, and consequently *LTE* is ensured. It was found that four dimensionless parameters, namely: porosity ε, volumetric Biot number Bi, dimensionless channel length and solid/fluid thermal capacity ratio C_r, control the validity of the *LTE* condition in the channel. The results indicated to that the relaxation time is linearly proportional to the channel length and $1/Bi$, and to C_r but at small Bi and ε. The effect of ε was found to decrease the relaxation time at small Bi and large C_r, whereas, its effect is insignificant at large Bi and small C_r.

Celli & Rees (2010) analysed both analytically and numerically the effect of the *LTNE* condition on forced convective thermal boundary layer flow in a

saturated porous medium over a horizontal flat plate. The temperature fields of the medium phases were presented for different values of the conductivity ratio γ. The *LTNE* effects were found to be at their strongest close the leading edge where they were $O(x^{-1})$ in magnitude, but the maximum discrepancy between the temperature fields decreases with the distance from the leading edge, and the *LTE* condition is attained at large distance. This finding confirms the analytical work of Rees & Pop (2000) for a free convective boundary-layer flow close to a vertical plate, and the numerical results of Saito & Lemos (2009) for forced convection in a porous channel. In addition, the distance over which the *LTE* condition holds was shown to decrease in the neighbourhood of the leading edge for increasing γ due to the increase in heat transfer between the phases.

Yang *et al.* (2011) obtained exact solutions for the case of fully developed forced convective heat transfer in a two-dimensional tube filed with an air-saturated aluminium-foam under the *LTNE* assumption. The horizontal tube walls were assumed to be subjected to a constant wall heat flux. They presented profiles for the average temperature for both phases, i.e. air and aluminium. These profiles revealed that the aluminium temperature is always much higher than the air temperature. Therefore, it was concluded that the case of constant heat flux boundary conditions must be treated by using the *LTNE* energy model, since the two phases within the channel were found to be never at thermal equilibrium.

Numerically, Vafai & Sözen (1990a) analyzed transient forced convection of a gas flow through a packed bed of uniform spherical particles allowing for thermal non-equilibrium between the fluid and solid phases. They qualitatively assessed the validity of the *LTE* assumption by presenting an error contour maps based on qualitative ratings, shown in figure **??**, for three types of materials: lithium-nitrate-trihydrate, sandstone and steel. These maps were presented in terms of two pertinent parameters, Darcy Da and particle Reynolds numbers Re. The investigation allowed a simple characterisation scheme for understanding the applicability of the *LTE* hypothesis for different conditions of compressible flow and porous bed configurations. The results indicated to that the *LTE* condition is very sensitive to these parameters, but it was found to be valid as either Re or Da

approaches to zero. However, unexpectedly, the results showed that the validity of *LTE* is less affected by the thermo- physical properties.

Later, the same finding was reported by Amiri & Vafai (1994) who examined the validity of the *LTE* in a packed bed confined by walls at constant temperature, using the same qualitative error map variables used by Vafai & Sözen (1990a), that is, in terms of Re and Da at different values of solid/fluid thermal diffusivity ratio. Later the same authors (Amiri & Vafai 1998) examined the temporal *LTE* condition by computing the maximum temperature difference between the solid and fluid phases through the whole bed. They revealed that a larger discrepancy between the phases is encountered at early times as solid-to-fluid thermal conductivity ratio k_r approaches unity. However, this difference was shown to quickly vanish as the time progresses with the temperature difference smallest for k_r closest to unity. Once again, the *LTE* assumption appeared to become more justifiable for small values of Da. Also, it was noted that k_r is an essential parameter for examination the *LTE* assumption; however, it is not enough to use it solely to decide on the validity of *LTE*.

Khashan & Al-Nimr (2005) also numerically assessed the validity of the *LTE* assumption for the problem of non-Newtonian forced convective flow through channels filled with porous media. Quantitative *LTE* - *LTNE* region maps, reproduced in figure **??**, were presented for a broad ranges of representative dimensionless parameters such as Péclet number Pe, Biot number Bi, power-law index n, fluid/solid thermal conductivity ratio γ, and microscopic and macroscopic frictional flow resistance coefficients, to examine whether the *LTE* assumption can or cannot be used. The conditions of a higher Pe, a lower Bi, a lower γ a lower n and a lower frictional coefficient, were identified as unfavorable circumstances for this assumption to hold.

By utilising similar method used by Khashan & Al-Nimr (2005), Khashan *et al.* (2005) checked the validity of the *LTE* state for both hydro-dynamically and thermally developing forced convective flow in an isothermal porous tube. Their results also referred to the possibility of expanding the *LTE* validity over the *LTNE* region when Pe or the conductivity ratio γ decreases, or when Bi

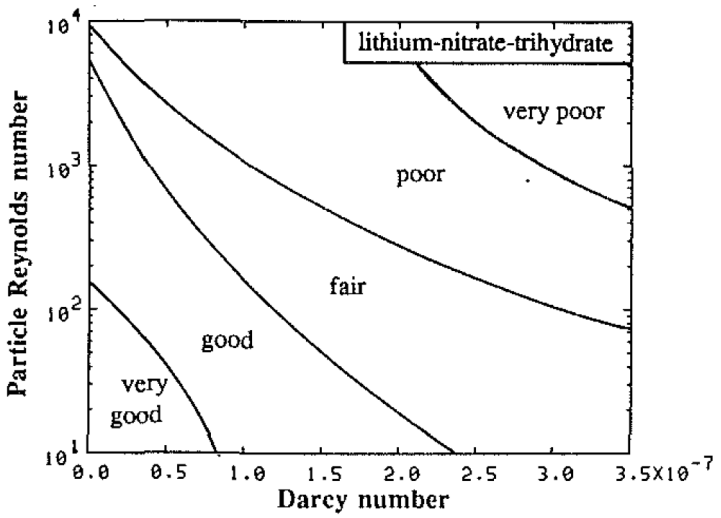

(a) For gas-saturated lithium-nitrate-trihydrate porous medium

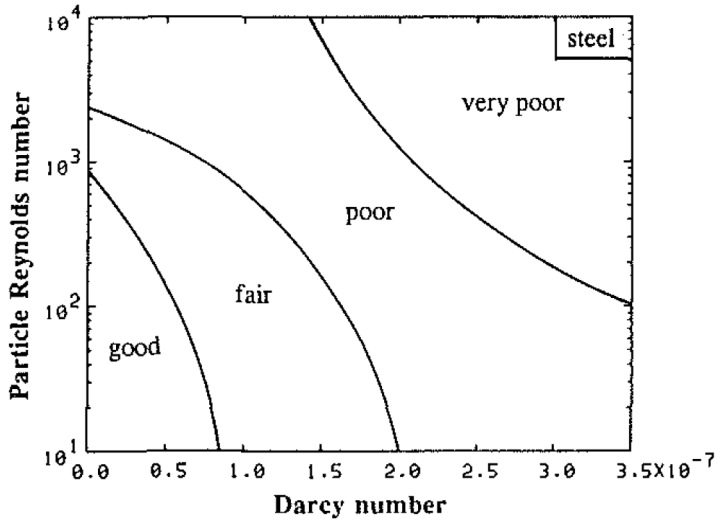

(b) For gas-saturated steel porous medium

FIGURE 2.15: Qualitative error maps for the *LTE* assumption for transient forced convective gas flow through a packed bed of two kinds of spherical materials: (a) lithium-nitrate-trihydrate, and (b) steel, in terms of Darcy and particle Reynolds numbers. The results are taken from Vafai & Sözen (1990a).

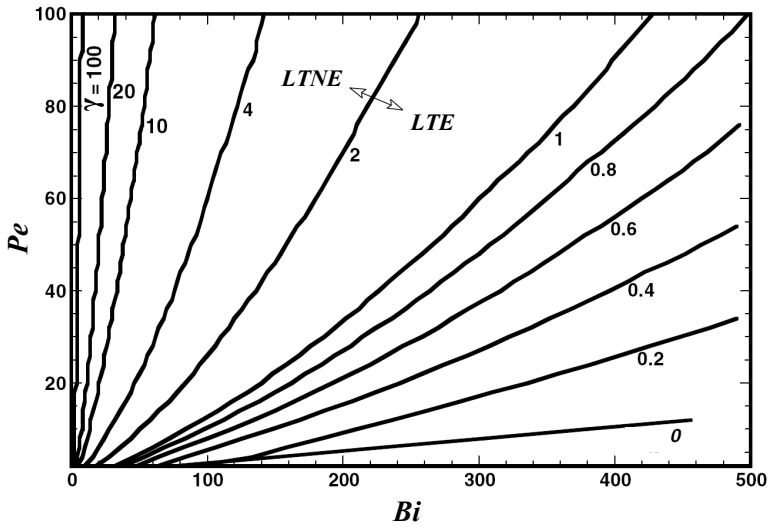

FIGURE 2.16: *LTE* - *LTNE* region map produced by Khashan & Al-Nimr (2005) for non-Newtonian forced convective flow through a channel filled with porous media, for a wide ranges of Biot number, Péclet number and fluid/solid thermal conductivity ratio.

increases. In addition, low Re, large dimensionless Forchheimer coefficient and low Da were all established to improve the validity of the *LTE* assumption, as low velocity flows allow sufficient thermal communication between the solid and fluid phases.

Saito & Lemos (2009) studied the effects of thermal and structural properties of a horizontal porous bed of spheres on forced convective heat transfer within from and around solid particles and the saturating fluid using the *LTNE* energy model, focusing on the effect of thermal dispersion. The bed was assumed to be bounded by two parallel plates at constant temperature. The results showed that high Re, low porosity ε, small particle diameter d_p and low solid-to-fluid thermal conductivity ratio k_r promote the thermal equilibrium between the fluid and solid phases in the bed leading to higher values of Nusselt number throughout both phases. The results also showed that the difference between the local solid and fluid Nusselt numbers with the longitudinal coordinate is large at the beginning of the bed, and it decreases with the distance downstream.

The validity of the equilibrium model has also been addressed for natural

convection, but with perhaps less attention, for various geometries and applications such as cavities, enclosures, horizontal cylinders, annuli and vertical and horizontal plates, against different parameters. Baytas & Pop (2002), Banu & Rees (2002), Baytas (2003), Saeid (2006), Badruddin *et al.* (2006) and Saeid (2007) all have found that when the interfacial heat transfer coefficient H_v and the porosity-scaled fluid-to-solid thermal conductivity ratio γ have large values then the thermal equilibrium state is approached in the two-phase porous system, i.e., both fluid and solid phases have the same thermal field and Nusselt number. In addition, the results of Mohamad (2000) indicated that the *LTE* model is difficult to justify for the non- Darcy regime, and when the thermal conductivity of the solid phase k_s is higher than that of the fluid phase k_f.

Rees & Pop (2000) who used an asymptotic analysis to investigate free convective boundary-layer flow close to a vertical plate emphasised on that the thermal equilibrium between the two phases is justified at increasing distances from the leading edge. Mohamad (2001) who used a different approach to examine numerically the same convective boundary-layer of Rees & Pop (2000) pointed out that the non-equilibrium parameter, fluid/solid conductivity ratio and the porosity ε of the porous medium used have a significant influence on the thermal equilibrium condition. It was revealed that this condition becomes unjustified if k_s is equal to or greater than k_f, the non-equilibrium parameter less than or equal to unity and ε is high.

Moreover, based on their numerical and experimental results, Phanikumar & Mahajan (2002) concluded that for the material of metal foams in general, the developed *LTNE* energy model must be employed instead of the traditional *LTE* model. They reported that the *LTNE* effects become significant at high Rayleigh *Ra* and Darcy *Da* numbers. Haddad *et al.* (2004) found that the *LTE* assumption is mainly controlled by four parameters which are *Bi*, *Ra*, *Da* and the ratio of effective to dynamic viscosity, in the problem of free convection over a vertical flat plate embedded in porous media. In their study, it was mentioned that this assumption is not valid for relatively low values of *Da*, *Bi* and viscosity ratio, and high values of *Ra*. Khashan *et al.* (2006) observed in a porous rectangular cavity

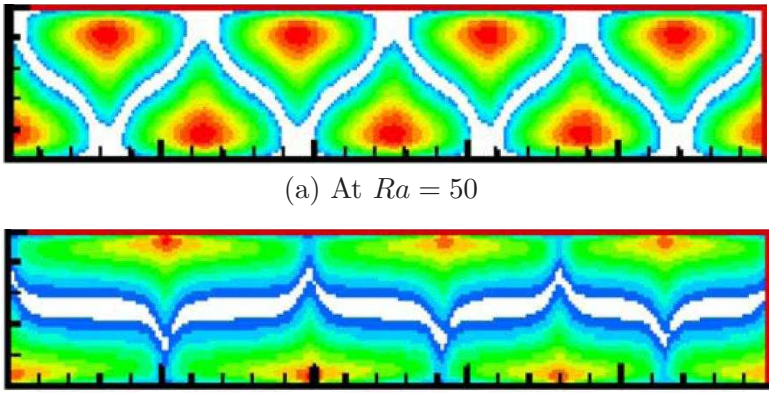

(a) At $Ra = 50$

(b) At $Ra = 400$

FIGURE 2.17: Contours of the local *LTNE* parameter, i.e. phase temperature difference, in a rectangular porous cavity heated from below. The contours were plotted for two values of Rayleigh number: (a) 50 and (b) 400, at Darcy number $Da = 10^{-3}$. The white regions represent the parameter values below 0.05, which was considered as an upper constraint for the *LTE* validity.

heated from below the effect of the *LTNE* depreciates as *Da* decreases, and as the effective fluid/solid conductivity ratio, *Ra* and *Bi* increase. They presented contours for the local *LTNE* parameter, which is the phase temperature difference, within the entire cavity, at various values of *Ra*, as illustrated in figure **??**.

In the mixed convection area, the validity of the *LTE* model has been assessed only by Wong & Saeid (2009) for vertical air jet impingement cooling of an isothermal heat source placed on the bottom wall of a horizontal channel filled with a high porosity metal foam under the condition of thermal non-equilibrium. Also, the authors emphasised in a part of their study, the effects of the interfacial coefficient H_v and the conductivity ratio γ on the equilibrium state. Once again, the results showed the same finding mentioned above related to these two parameters, which is that an increase in either renders the solid and fluid towards the thermal equilibrium condition.

2.6 Conclusion

Relevant background studies on thermal convection in channels containing porous media together with specific research which includes a heated body (generally a

circular cylinder) embedded within the porous medium provide the context for the current research. Concerning embedded cylinders, the literature reveals that considerable effort has been directed towards the natural convection case with fewer studies dealing with mixed and forced convection. Moreover, most of the existing studies include strong simplifying assumptions such as: adopting the *LTE* condition, neglecting the non-Darcian effects and/or omitting the thermal dispersion effect. Therefore, a theoretical study of forced convection over a circular cylinder within a porous medium, in which the effects of inertia, solid boundaries and thermal dispersion under the *LTNE* assumption is justified.

A natural and relevant extension is to consider the case of multiple embedded cylinders, given its obvious application to heat exchangers. The literature indicates that this subject has been elaborately investigated for the case without porous media, to examine the flow interaction between cylinders on heat transfer. However, using porous media to augment heat transfer from a bank of horizontal cylinders has been much less investigated. In those studies, the concentration has been only on testing heat transfer enhancement by inserting porous media amongst the cylinders with fixed values of cylinder spacing. The flow interaction between multiple cylinders and the convective effect on heat transfer has been not yet investigated throughly in the presence of porous media. This warrants further investigation to predict the enhancement effects of different porous media and cylinder bank arrangements on the local and average heat transfer from a cylinder bundle.

In this chapter the characteristics of heat transfer and fluid mechanics with and without porous media under pulsatile flow conditions also have been reviewed. This reveals that the majority of previous studies have focused on geometrically simple configurations, e.g. an *empty* pipe or channel. Thus the inclusion of a heated circular cylinder within a channel containing a porous medium subject to pulsating flow appears a relevant problem to address.

Finally, the literature indicates that the validity of the *LTE* energy model has been examined relative to the more accurate *LTNE* model for a restricted number of flow geometries, and conditions for the validity of the *LTE* model established

for ranges of governing parameters. However, the geometries tackled have not focused on the relevant case of bodies embedded within a porous medium such as a circular cylinder. Given this, one focus of the research is to fill this gap and provide parameter ranges for when the *LTE* model can produce acceptable predictions for the more complex geometry of a cylinder embedded in a porous medium.

Chapter 3

Methodology and validation

3.1 Introduction

This study aims for the accurate simulation of the complicated transport phenomena in packed beds. The analysis requires a general and rigorous model to describe the flow and heat transfer processes in porous media. In this chapter, the particular problem investigated in this thesis is described. Then, the coupled system of governing equations are introduced, which describe the complex physics involved, together with the specification of appropriate boundary conditions. Following this, the discussion continues on to discretising the governing equations, in this case, using the spectral-element method. Finally, numerical resolution studies are performed for the computational domain and grid.

3.2 Mathematical formulation

3.2.1 Statement of the problem

The problems considered in this thesis can be broadly categorised as predicting the flow and heat transfer from either a single or multiple circular cylinders embedded in a two-dimensional channel containing porous media. The upstream flow into the channel can be either steady or pulsatile. There are many physical parameters involved and an attempt is made to quantify the effect of varying these parameters on the flow and heat transfer. In addition, there are various approximations involved in translating the physics into mathematical models, both in terms of the hydrodynamics and the thermal modelling, and the effects of some of these

approximations are considered.

The schematic diagrams of the main cases considered are provided in figures 2.1 and 2.2. The cylinder(s) is/are assumed to be isothermally heated at a constant temperature T_h and cooled by the incoming external flow at T_o. The confining horizontal walls have the same temperature T_w as the flow at the inlet. The geometrical relationships are set such that:

- for the case of a single cylinder, shown in figure 2.1, the the blockage ratio of the bed is $D_{cy}/H = 0.25$, where D_{cy} is the cylinder diameter, which is considered to be the unit scale length in the present study, and H is the bed height.

- for the case of multi-cylinders, shown in figure 2.2, a larger blockage is incurred so a smaller diameter is used, $D_{cy}/H = 0.1666$, also to provide more flexibility to study the effect of changing the spacing between the cylinders. The longitudinal pitch p_l is taken as equal to that in the transverse direction p_t. Here, longitudinal pitch is the distance between the top and bottom cylinder centres, while transverse pitch is the distance between the front and back cylinder centres.

For both cases, the extent of the packed bed in the z-direction is assumed to be large enough so that the problem will essentially be two-dimensional.

3.2.2 Governing equations

Prior to analysing these problems, it is useful to state the assumptions on which the governing equations are based:

1. The fluid flow is laminar and incompressible.

2. Forced convection dominates the thermal field of the packed bed, i.e., natural convection effects can be ignored.

3. The fluid passing through the bed is Newtonian.

4. The porous medium is homogenous and isotropic.

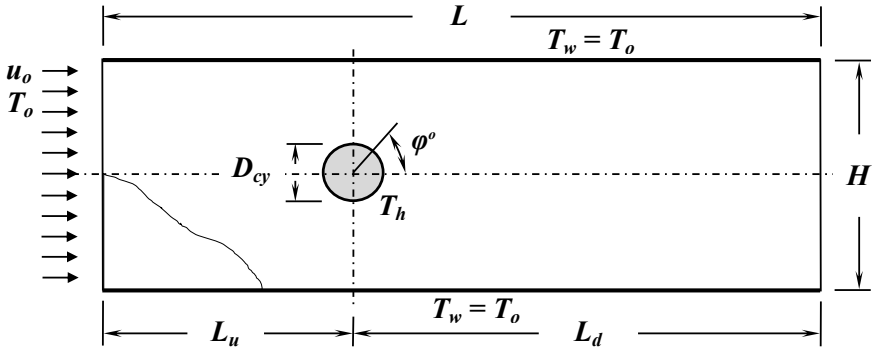

(a) Steady flow

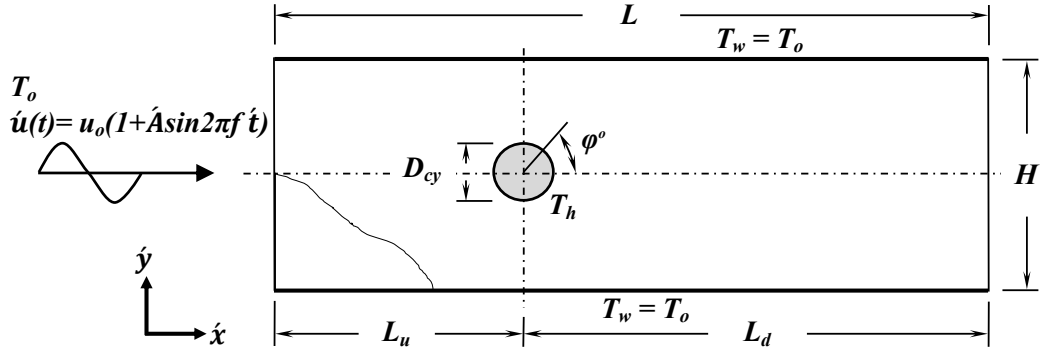

(b) Pulsatile flow

FIGURE 3.1: Schematic diagrams for forced convection for flow past a single cylinder with steady (top) and pulsatile (bottom) flows over a single heated circular cylinder embedded in a horizontal porous channel.

5. The variation of thermo-physical properties of the two phases with temperature can be neglected.

6. Inter-particle radiation heat transfer can be ignored.

7. No heat generation occurs inside the porous medium.

8. But, importantly, local thermal equilibrium between the two phases is not assumed.

Taking in account these assumptions, the system of the governing equations of the continuity, momentum and energy, can be presented in the following vectorial form as given in Vafai & Tien (1981), Kaviany (1995) and Nield & Bejan (2006),

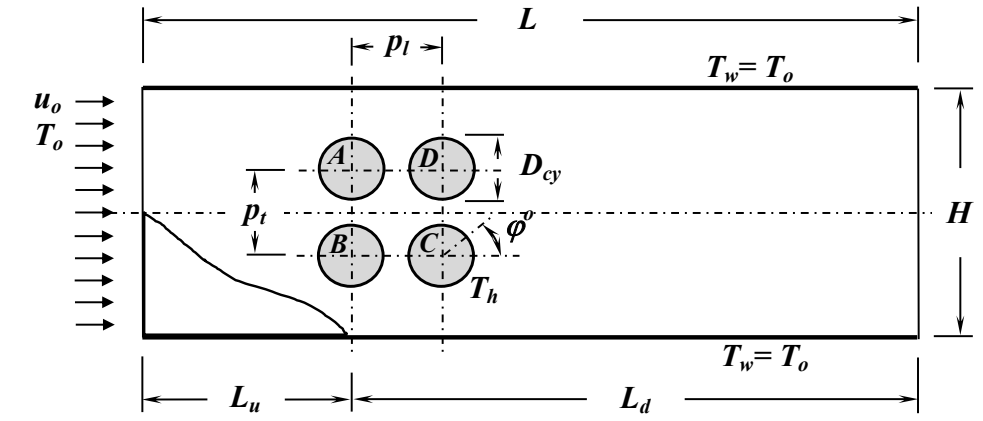

(a) Inline configuration

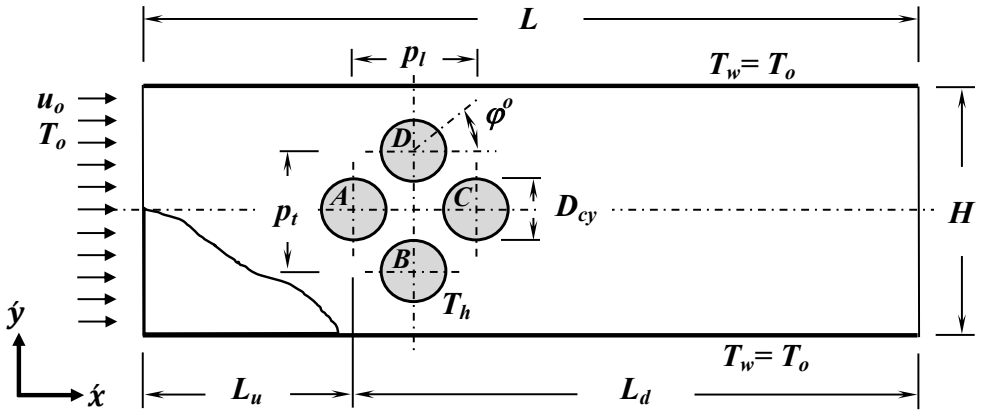

(b) Staggered configuration

FIGURE 3.2: Schematic diagram for steady forced convection flow over a bank of four heated circular cylinders: (a) in-line, and (b) staggered, configurations immersed in a horizontal porous channel.

based on the volume-average method:

a. Continuity equation:

$$\nabla \cdot \langle \acute{\mathbf{u}} \rangle = 0, \tag{3.1}$$

b. *DBF* momentum equation:

$$\frac{\rho_f}{\varepsilon}\left[\frac{\partial \langle \acute{\mathbf{u}} \rangle}{\partial \acute{t}} + \frac{1}{\varepsilon}\langle (\acute{\mathbf{u}} \cdot \nabla)\, \acute{\mathbf{u}} \rangle\right] = -\frac{\mu_f}{K}\langle \acute{\mathbf{u}} \rangle - \frac{\rho_f F \varepsilon}{\sqrt{K}} \left| \langle \acute{\mathbf{u}} \rangle \right| \langle \acute{\mathbf{u}} \rangle + \frac{\mu_f}{\varepsilon}\nabla^2 \langle \acute{\mathbf{u}} \rangle - \nabla \langle \acute{P}_f \rangle, \tag{3.2}$$

c. Two-phase energy equation:

- for fluid phase:

$$\varepsilon\left(\rho c_p\right)_f\left[\frac{\partial\langle\acute{T}_f\rangle}{\partial\acute{t}}+\langle\acute{\mathbf{u}}\rangle\cdot\nabla\langle\acute{T}_f\rangle\right]=\nabla\cdot\left[k_{f.\text{eff},(x,y)}\nabla\langle\acute{T}_f\rangle\right]+h_{sf}a_{sf}\left(\langle\acute{T}_s\rangle-\langle\acute{T}_f\rangle\right), \tag{3.3}$$

- for solid phase:

$$\left(1-\varepsilon\right)\left(\rho c_p\right)_s\frac{\partial\langle\acute{T}_s\rangle}{\partial\acute{t}}=\nabla\cdot\left[k_{s.\text{eff}}\nabla\langle\acute{T}_s\rangle\right]-h_{sf}a_{sf}\left(\langle\acute{T}_s\rangle-\langle\acute{T}_f\rangle\right), \tag{3.4}$$

d. One-phase energy equation:

The *LTE* model uses the same momentum equations but replaces the thermal equations with the following single energy equation:

$$\left(\rho c_p\right)_m\frac{\partial\langle\acute{T}\rangle}{\partial\acute{t}}+\varepsilon\left(\rho c_p\right)_f\left[\langle\acute{\mathbf{u}}\rangle\cdot\nabla\langle\acute{T}\rangle\right]=\nabla\cdot\left[k_{f.\text{eff},(x,y)}\nabla\langle\acute{T}\rangle\right], \tag{3.5}$$

where,

$$|\langle\acute{\mathbf{u}}\rangle|=\sqrt{\langle\acute{u^2}\rangle+\langle\acute{v^2}\rangle},\quad(\rho c_p)_m=\varepsilon(\rho c_p)_f+(1-\varepsilon)(\rho c_p)_s, \tag{3.6}$$

Here, $\acute{\mathbf{u}}$ is the velocity vector field, $\acute{t}$ is the time variable, $\acute{P}_f$ is the pressure field and $\acute{T}$ is the temperature field. Subscripts f and s denote the fluid and solid phases, respectively, and *eff* refers to an effective property. The following are other fluid and medium properties: K is the permeability, F the geometric function, μ_f the fluid dynamic viscosity, ρ the density, c_p the specific heat, ε the porosity, k the thermal conductivity, a_{sf} the specific surface area of the packed bed and h_{sf} the interfacial heat transfer coefficient. In addition, the primes refer to dimensional quantities and the operator $\langle ...\rangle$ denotes local volume average of a quantity.

In the momentum equation 2.2, the first term on the right-hand side represents the frictional resistance due to the presence of the micro-pore structure, while the square term, the second term on the right-hand side, is caused by the inertial effects from passing through the solid matrix. The third term on the right-hand side accounts for the effect of friction posed by an external boundary on the flow.

With regard to the energy equations, it can be seen that as the solid phase is stationary, the energy transport through the solid phase, i.e., equation 2.4, only needs to account for conduction. However, an additional mode of heat transfer emerges if there is a difference in the temperature distributions between the fluid and solid phases. This transfer mode can be conceived of as convective heat transfer that can be formulated via a fluid-to-solid heat transfer coefficient h_{sf}.

The equations $2.1-2.5$ can be transformed into a non-dimensional form $2.8-2.12$, respectively, by employing the following dimensionless variables:

$$x, y = \frac{\acute{x}, \acute{y}}{D_{cy}}, \quad \langle \mathbf{u} \rangle = \frac{\langle \acute{\mathbf{u}} \rangle}{u_o}, \quad t = \frac{\acute{t} u_o}{D_{cy}}, \quad \langle \theta \rangle = \frac{\langle \acute{T} \rangle - T_o}{(T_h - T_o)}, \quad \langle P_f \rangle = \frac{\langle \acute{P}_f \rangle}{\rho_f u_o^2}, \tag{3.7}$$

to give

$$\nabla \cdot \langle \mathbf{u} \rangle = 0, \tag{3.8}$$

$$\frac{1}{\varepsilon}\left[\frac{\partial \langle \mathbf{u} \rangle}{\partial t} + \frac{1}{\varepsilon}\langle (\mathbf{u} \cdot \nabla)\, \mathbf{u} \rangle\right] = -\frac{1}{Re_D Da}\langle \mathbf{u} \rangle - \frac{F\varepsilon}{\sqrt{Da}}\left|\langle \mathbf{u} \rangle\right| \langle \mathbf{u} \rangle + \frac{1}{\varepsilon Re_D}\nabla^2 \langle \mathbf{u} \rangle - \nabla \langle P_f \rangle, \tag{3.9}$$

$$\frac{\varepsilon}{k_r}\left[\frac{\partial \langle \theta_f \rangle}{\partial t} + \langle \mathbf{u} \rangle \cdot \nabla \langle \theta_f \rangle\right] = \frac{1}{Re_D Pr k_r}\nabla \cdot \left[\frac{k_{f.\text{eff},(x,y)}}{k_f}\nabla \langle \theta_f \rangle\right] + \frac{Bi}{Re_D Pr}\left(\langle \theta_s \rangle - \langle \theta_f \rangle\right), \tag{3.10}$$

$$\frac{(1-\varepsilon)}{\alpha_r}\frac{\partial \langle \theta_s \rangle}{\partial t} = \frac{1}{Re_D Pr}\nabla \cdot \left[\frac{k_{s.\text{eff}}}{k_s}\nabla \langle \theta_s \rangle\right] - \frac{Bi}{Re_D Pr}\left(\langle \theta_s \rangle - \langle \theta_f \rangle\right), \tag{3.11}$$

and the dimensionless form of the LTE energy model becomes

$$\frac{\partial \langle \theta \rangle}{\partial t} + \left(\frac{\varepsilon}{C}\right)\left[\langle \mathbf{u} \rangle \cdot \nabla \langle \theta \rangle\right] = \frac{1}{Re_D PrC}\nabla \cdot \left[\frac{k_{f.\text{eff},(x,y)}}{k_f}\nabla \langle \theta \rangle\right], \tag{3.12}$$

with

$$C = \left[\varepsilon + (1-\varepsilon)\left(\frac{k_r}{\alpha_r}\right)\right]. \tag{3.13}$$

Here, k_r and α_r are the solid-to-fluid thermal conductivity and diffusivity ratios, k_s/k_f and α_s/α_f, respectively. In addition, the key governing non-dimensional

groups: the Reynolds, Darcy, Prandtl, and Biot numbers are

$$Re_D = \frac{u_o D_{cy} \rho_f}{\mu_f}, \quad Da = \frac{K}{D_{cy}^2}, \quad Pr = \frac{\nu_f}{\alpha_f}, \quad Bi = \frac{D_{cy}^2 h_{sf} a_{sf}}{k_s}. \tag{3.14}$$

The empirical expression suggested by Dullien (1979) for the specific surface area of the packed bed a_{sf} is employed in the present investigation as follows:

$$a_{sf} = \frac{6(1-\varepsilon)}{d_p}, \tag{3.15}$$

where, d_p is the particle diameter. While, the formulation of the interfacial heat transfer coefficient h_{sf} is based on the empirical correlation proposed by Wakao *et al.* (1979) for packed beds and can be expressed as:

$$h_{sf} = \frac{k_f}{d_p}\left[2 + Pr^{1/3} Re_p^{0.6}\right], \tag{3.16}$$

where, Re_p is the *particle Reynolds number*

$$Re_p = \frac{\rho_f |\langle \mathbf{u} \rangle| d_p}{\mu_f}. \tag{3.17}$$

In turn, this allows the *Biot number* to be expressed as

$$Bi = 6(1-\varepsilon)\left(\frac{1}{k_r}\right)\left(\frac{D_{cy}}{d_p}\right)^2\left[2 + Pr^{1/3} Re_p^{0.6}\right], \tag{3.18}$$

which explicitly shows the strong effect of the interfacial heat transfer rate on the particle to cylinder diameter. The permeability of the porous medium K incorporated in the Darcy number and the geometric function F, in the momentum equation 2.9, are inherently tied to the structure of the porous medium. These are generally based on empirical fits from experimental findings, i.e., no universal representations exist. For a randomly packed bed of spheres such coefficients were reported by Ergun (1952), and were expressed in terms of porosity ε and particle diameter d_p as follows:

$$K = \frac{\varepsilon^3 d_p^2}{150\,(1-\varepsilon)^2}, \tag{3.19}$$

$$F = \frac{1.75}{\sqrt{150\varepsilon^3}}. \tag{3.20}$$

The effective thermal conductivity of the fluid phase $k_{f.eff}$ is composed of a sum of the stagnant k_{st} and dispersion k_d conductivities:

$$k_{f.\text{eff},(x,y)} = k_{st} + k_{d(x,y)}. \tag{3.21}$$

Typically, the stagnant conductivity is the product of the phase fractions and the individual thermal conductivities of the fluid and the solid phases. In the ongoing investigation, the semi-theoretical model of Zehner & Schluender (1970) for calculating the stagnant conductivity is used:

$$\frac{k_{st}}{k_f} = (1-\sqrt{1-\varepsilon}) + \frac{2\sqrt{1-\varepsilon}}{1-\lambda B} \times \left[\frac{(1-\lambda)B}{(1-\lambda B)^2} \ln(\lambda B) - \frac{B+1}{2} - \frac{B-1}{1-\lambda B} \right], \quad (3.22)$$

where $\lambda = 1/k_r$, and $B = 1.25\left[(1-\varepsilon)/\varepsilon\right]^{\frac{10}{9}}$. Whereas, the dispersion conductivity that incorporates the additional thermal transport due to the fluid's tortuous path around the solid particles is determined in both longitudinal and lateral directions based on the experimental correlation reported by Wakao & Kaguei (1982), and is given by:

$$\frac{k_{dx}}{k_f} = 0.5 PrRe_p, \quad (3.23)$$

$$\frac{k_{dy}}{k_f} = 0.1 PrRe_p. \quad (3.24)$$

While, the effective thermal conductivity for the solid phase consists merely of the phase fraction component which is the stagnant component since the solid phase is stationary:

$$k_{s.eff} = (1-\varepsilon)k_s. \quad (3.25)$$

Heat transfer characteristics are evaluated based on the time-mean local and average Nusselt numbers along the heated surface of the cylinder. The Nusselt number is defined for the fluid and solid phases separately and is expressed as:

Fluid phase local and average Nusselt numbers:

$$Nu_{f\varphi} = \frac{h_{cy}D_{cy}}{k_f} = \frac{-k_{f.eff}[\partial\langle \acute{T}_f\rangle/\partial\hat{n}]D_{cy}}{k_f(T_h - T_o)}, \quad Nu_f = \frac{1}{S}\int_0^S Nu_{f\varphi} ds. \quad (3.26)$$

Solid phase local and average Nusselt numbers:

$$Nu_{s\varphi} = \frac{h_{cy}D_{cy}}{k_s} = \frac{-k_{s.eff}[\partial\langle \acute{T}_s\rangle/\partial\hat{n}]D_{cy}}{k_s(T_h - T_o)}, \quad Nu_s = \frac{1}{S}\int_0^S Nu_{s\varphi} ds, \quad (3.27)$$

where $\hat{n}$ and s denote to the normal and tangential directions at the cylinder surface, respectively, and S is the circumference of the cylinder. Consequently,

the time-mean average total Nusselt number Nu_t is defined as the summation of Nu_f and Nu_s:

$$Nu_t = Nu_f + Nu_s. \tag{3.28}$$

The dimensionless DBF momentum equation 2.9 allows for a smooth transition between fluid flow through porous media and the Navier-Stokes equations in a space without porous media by taking $\varepsilon = 1$ and $K \to \infty$. Also, the one-equation energy model 2.12 can be transformed to the standard fluid energy equation by taking the constants $C = 1$ and $k_{f.eff} = k_f$ to predict the thermal fields in the absence of porous media.

3.2.3 Boundary conditions

The problem is not completely specified without the provision of proper boundary conditions. In the problems under investigation Dirichlet boundary conditions, for the pertinent hydrodynamic and thermal variables, i.e., the velocity and temperature fields, are imposed at the inlet and solid boundaries. For example, the cylinder surface and the channel walls are maintained at constant temperatures, and a no-slip boundary condition is imposed at the cylinder surface and the confining walls. In addition, both fluid and solid phases are at the same temperature at the inlet of the packed bed. At the exit, Neumann boundary conditions are imposed on the normal velocity and the solid and fluid temperatures. In addition, the pressure is set to zero at the outlet boundary. At other boundaries the pressure satisfies a Neumann condition obtained by taking the dot-product of the Navier-Stokes equations with the surface normal vector. This higher-order boundary condition also ensures mass conservation at solid boundaries (**?**).

Thus, the dimensional initial and boundary conditions can be mathematically expressed as:

$$
\begin{aligned}
&\text{at } \acute{t}=0: \ \langle \acute{u}\rangle = \langle \acute{v}\rangle = \langle \acute{T_f}\rangle = \langle \acute{T_s}\rangle = 0 \\
&\text{at } \acute{t}>0: \ \textbf{at inlet} \qquad\qquad (\acute{x}=0,\ 0<\acute{y}<H) \\
&\qquad \langle \acute{u}\rangle = u_o \quad \text{(for steady flow)} \\
&\qquad \langle \acute{u}(\acute{t})\rangle = u_o(1+\acute{A}sin(2\pi f \acute{t})) \qquad \text{(for pulsatile flow)} \\
&\qquad \langle \acute{v}\rangle = 0,\ \langle \acute{T_f}\rangle = \langle \acute{T_s}\rangle = T_o \\
&\qquad \textbf{at outlet} \qquad\qquad (\acute{x}=L,\ 0<\acute{y}<H) \\
&\qquad \frac{\partial\langle \acute{u}\rangle}{\partial \acute{x}} = \frac{\partial\langle \acute{T_f}\rangle}{\partial \acute{x}} = \frac{\partial\langle \acute{T_s}\rangle}{\partial \acute{x}} = \langle \acute{v}\rangle = 0 \\
&\qquad \textbf{at the walls} \qquad (0<\acute{x}<L,\ \acute{y}=0 \text{ and } H) \\
&\qquad \langle \acute{u}\rangle = \langle \acute{v}\rangle = 0,\ \langle \acute{T_f}\rangle = \langle \acute{T_s}\rangle = T_w \\
&\qquad \textbf{at the cylinder boundary} \qquad (0<\varphi^o<360) \\
&\qquad \langle \acute{u}\rangle = \langle \acute{v}\rangle = 0,\ \langle \acute{T_f}\rangle = \langle \acute{T_s}\rangle = T_h. \qquad\qquad (3.29)
\end{aligned}
$$

By using the dimensionless variables in equation 2.7, the dimensionless initial and boundary conditions become as follows:

$$
\begin{aligned}
&\text{at } t=0: \ \langle u\rangle = \langle v\rangle = \langle \theta_f\rangle = \langle \theta_s\rangle = 0 \\
&\text{at } t>0: \ \textbf{at inlet} \qquad\qquad (x=0,\ 0<y<H/D_{cy}) \\
&\qquad \langle u\rangle = 1 \quad \text{(for steady flow)} \\
&\qquad \langle u(t)\rangle = 1 + Asin(2\pi St\ t) \qquad \text{(for pulsatile flow)} \\
&\qquad \langle v\rangle = \langle \theta_f\rangle = \langle \theta_s\rangle = 0 \\
&\qquad \textbf{at outlet} \qquad\qquad (x=L/D_{cy},\ 0<y<H/D_{cy}) \\
&\qquad \frac{\partial\langle u\rangle}{\partial x} = \frac{\partial\langle \theta_f\rangle}{\partial x} = \frac{\partial\langle \theta_s\rangle}{\partial x} = \langle v\rangle = 0 \\
&\qquad \textbf{at the walls} \qquad (0<x<L/D_{cy},\ y=0 \text{ and } H/D_{cy}) \\
&\qquad \langle u\rangle = \langle v\rangle = \langle \theta_f\rangle = \langle \theta_s\rangle = 0 \\
&\qquad \textbf{at the cylinder boundary} \qquad (0<\varphi^o<360) \\
&\qquad \langle u\rangle = \langle v\rangle = 0,\ \langle \theta_f\rangle = \langle \theta_s\rangle = 1. \qquad\qquad (3.30)
\end{aligned}
$$

For these boundary conditions, the thermal equilibrium assumption is imposed

at heated boundaries, e.g., the fluid and solid phases have the same temperature as that of the isothermal cylinder's surface, see Alazmi & Vafai (2002) and Wong & Saeid (2009).

3.3 Numerical method of solution

The above equations $2.8 - 2.12$ form the mathematical model for analysing the transient momentum and energy transport in unsteady forced convective flow in a porous media. This is a system of highly coupled equations describing the evolution of the four pertinent fields, i.e. velocity $\langle \mathbf{u} \rangle$, fluid temperature $\langle \theta_f \rangle$, solid temperature $\langle \theta_s \rangle$ and pressure $\langle P_f \rangle$. To numerically solve this system of equations, it is necessary to discretise the problem in both time and space.

3.3.1 Temporal discretisation

The temporal discretisation method used for this study is a two- and three-step time-splitting scheme for the energy and momentum equations, respectively. The name of time-splitting for this method is because the right-hand side of the equations is divided into two or three groups, and integrated separately, which results in the overall integration over one time-step being split into two or three sub-steps. The method is thoroughly described in Chorin (1968), Karniadakis *et al.* (1991) and Thompson *et al.* (2006).

For brevity, the discretisation for the Darcy-Brinkmann-Forchheimer *DBF* momentum equation 2.9 is described in this section. This equation is rearranged as follows:

$$\frac{\partial \langle \mathbf{u} \rangle}{\partial t} = \left(-\frac{1}{\varepsilon} \langle (\mathbf{u} \cdot \nabla) \mathbf{u} \rangle - \frac{F\varepsilon^2}{\sqrt{Da}} |\langle \mathbf{u} \rangle| \langle \mathbf{u} \rangle - \frac{\varepsilon}{Re_D Da} \langle \mathbf{u} \rangle \right) + \frac{1}{Re_D} \nabla^2 \langle \mathbf{u} \rangle - \varepsilon \nabla \langle P_f \rangle. \tag{3.31}$$

For use of this method with the Navier-Stokes equations as in the aforementioned references, the three sub-steps of the time-splitting process treat the advection, mass conservation/pressure, and diffusion terms. Therefore, for the above momentum equation 2.31, the non-linear terms accounting for convection and Forchheimer inertial effect, with the linear Darcy term accounting for fractional

resistance, are first integrated over the entire time-step, providing a primary intermediate velocity field $\langle \mathbf{u}^* \rangle$. Then, the primary velocity field is employed as an initial condition for the integration of the pressure step, which produces a secondary intermediate velocity field $\langle \mathbf{u}^{**} \rangle$. Last, this secondary intermediate velocity field is utilised as the starting condition for the integration of the diffusion term, for obtaining the final velocity field $\langle \mathbf{u}^{(n+1)} \rangle$ at the end of the time-step. Consequently, the following three discretised sub-step equations are obtained:

$$\langle \mathbf{u}^* \rangle - \langle \mathbf{u}^{(n)} \rangle = -\frac{1}{\varepsilon} \int_t^{t+\Delta t} \langle (\mathbf{u}.\nabla)\mathbf{u} \rangle dt - \frac{F\varepsilon^2}{\sqrt{Da}} \int_t^{t+\Delta t} |\langle \mathbf{u} \rangle| \langle \mathbf{u} \rangle dt - \frac{\varepsilon}{Re_D Da} \int_t^{t+\Delta t} \langle \mathbf{u} \rangle dt \tag{3.32}$$

$$\langle \mathbf{u}^{**} \rangle - \langle \mathbf{u}^* \rangle = -\varepsilon \int_t^{t+\Delta t} \nabla \langle P_f \rangle dt \tag{3.33}$$

$$\langle \mathbf{u}^{(n+1)} \rangle - \langle \mathbf{u}^{**} \rangle = \frac{1}{Re_D} \int_t^{t+\Delta t} \nabla^2 \langle \mathbf{u} \rangle dt, \tag{3.34}$$

where $\langle \mathbf{u}^* \rangle$ and $\langle \mathbf{u}^{**} \rangle$ are the primary and secondary intermediate velocity fields at the end of the first and second sub-steps, respectively, and n is the current time-step. The righthand side of the first sub-step equation 2.32 is treated using a second-order Adams-Bashforth approximation as follows:

$$\langle \mathbf{u}^* \rangle - \langle \mathbf{u}^{(n)} \rangle = -N_{adv} - N_{Forch} - L_{Darcy} \tag{3.35}$$

and,

$$\begin{aligned} N_{adv} &= \frac{\Delta t}{\varepsilon} \left(\frac{3}{2} \left(\langle (\mathbf{u}.\nabla)\mathbf{u} \rangle \right)^{(n)} - \frac{1}{2} \left(\langle (\mathbf{u}.\nabla)\mathbf{u} \rangle \right)^{(n-1)} \right) \\ N_{Forch} &= \frac{\Delta t F \varepsilon^2}{\sqrt{Da}} \left(\frac{3}{2} \left(|\langle \mathbf{u} \rangle| \langle \mathbf{u} \rangle \right)^{(n)} - \frac{1}{2} \left(|\langle \mathbf{u} \rangle| \langle \mathbf{u} \rangle \right)^{(n-1)} \right) \\ L_{Darcy} &= \frac{\Delta t \varepsilon}{Re_D Da} \left(\frac{3}{2} \left(\langle \mathbf{u} \rangle \right)^{(n)} - \frac{1}{2} \left(\langle \mathbf{u} \rangle \right)^{(n-1)} \right), \end{aligned} \tag{3.36}$$

where N_{adv} and N_{Forch} represent the non-linear advection and Forchheimer terms, respectively, while L_{Darcy} represents the linear Darcy term, and n is the time-step. The pressure sub-step equation 2.33 is treated in two parts as both the two unknown velocity and pressure fields in the equation must be integrated forward

in time. A second-order Adams-Moulton method is first used to formulate the integration of the pressure sub-step, giving

$$\langle \mathbf{u}^{**} \rangle - \langle \mathbf{u}^{*} \rangle = -\frac{\Delta t \varepsilon}{2} \left(\nabla \langle P_f^{(n+1)} \rangle + \nabla \langle P_f^{(n)} \rangle \right). \tag{3.37}$$

Further simplifying for this equation can be obtained by considering the pressure field at the middle of the time-step,

$$\langle \mathbf{u}^{**} \rangle - \langle \mathbf{u}^{*} \rangle = -\Delta t \varepsilon \left(\nabla \langle P_f^{(n+\frac{1}{2})} \rangle \right). \tag{3.38}$$

In the second part, taking the divergence of equation 2.38, and enforcing the continuity for the velocity field at the end of the sub-step (using equation 2.8), leads to a Poisson equation for the pressure,

$$\nabla^2 \langle P_f^{(n+\frac{1}{2})} \rangle = \frac{1}{\Delta t \varepsilon} \nabla . \langle \mathbf{u} \rangle^{*}, \tag{3.39}$$

from which the velocity field at the end of the sub-step, $\langle \mathbf{u}^{**} \rangle$ in equation 2.38, can be solved. In the third sub-step, the final velocity field $\langle \mathbf{u}^{(n+1)} \rangle$ is computed by approximating the diffusion sub-step equation 2.34 employing an implicit second-order Adams-Moulton method, rendering it to the following form,

$$\langle \mathbf{u}^{(n+1)} \rangle - \langle \mathbf{u}^{**} \rangle = \frac{\Delta t}{2 Re_D} \left(\nabla^2 \langle \mathbf{u} \rangle^{(n+1)} + \nabla^2 \langle \mathbf{u} \rangle^{(n)} \right) \tag{3.40}$$

The integration over the time-step is now completed by solving the above equation for $\langle \mathbf{u}^{(n+1)} \rangle$. The implicit Crank-Nicholson technique retains second-order accuracy in space and time, see Canuto (1988). In general, the splitting method attains a second-order accuracy in time for the velocity field when first-order pressure boundary conditions are imposed, as explained by Karniadakis *et al.* (1991).

For the energy equations, 2.10, 2.11 and 2.12, this method results in separate equations being formed for merely the nonlinear advection term and the linear diffusion term. Also, similar to the momentum equations, the nonlinear advection equation is solved using an explicit second-order Adams-Bashforth method, and the linear diffusion equation is solved using an implicit second-order Crank-Nicholson method. Because of the non-linear coupling between the equations, it

is necessary to iterate over each time-step. Iteration is required until convergence is achieved. In the present study, it is assumed that this occurs when $\langle \mathbf{u} \rangle$ velocity components and the time-mean average fluid and solid Nusselt numbers, Nu_f and Nu_s, respectively, in two consecutive iterations differ by less than the convergence criterion of 10^{-10}.

3.3.2 Spatial discretisation

The nodal-based spectral-element method, which is a high-order Galerkin finite-element approach, is implemented to discretise the governing equations in space. In this method, the computational domain is usually subdivided coarsely into a series of discrete macro-elements. Refinement can be made to the generated macro-mesh in regions of the domain that experience high gradients ($h-$refinement). The spatial discretisation employed here is based on quadrilateral elements, although these elements are free to have curved sides. The treatment of spatial discretisation using the Galerkin method is well-documented by, for example, Fletcher (1984), Fletcher (1991) and Karniadakis & Sherwin (2005).

The following is a brief description for the solution procedure of the Galerkin method used in the present algorithm. This process can be applied on each of the temporally integrated sub-step equations defined in equations 2.35-2.40. For brevity, only the spatial discretisation for the first sub-step equation 2.35 is described here. The first step starts with calculating the residual $\mathbf{R}$. The residual is formed by moving all terms to the right hand side, and substituting a trial solution for the variables. This results in the expression

$$\begin{aligned}\left(\mathbf{u}^{*}_{\text{trial}} - \mathbf{u}^{(\text{n})}_{\text{trial}}\right) + \frac{\Delta t}{\varepsilon}\left(\frac{3}{2}\left((\mathbf{u}_{\text{trial}}.\nabla)\mathbf{u}_{\text{trial}}\right)\right)^{(n)} - \frac{1}{2}\left((\mathbf{u}_{\text{trial}}.\nabla)\mathbf{u}_{\text{trial}}\right)\right)^{(n-1)}\Bigg) + \\ \frac{\Delta t F \varepsilon^2}{\sqrt{Da}}\left(\frac{3}{2}\left(|\mathbf{u}_{\text{trial}}|\,\mathbf{u}_{\text{trial}}\right)^{(n)} - \frac{1}{2}\left(|\mathbf{u}_{\text{trial}}|\,\mathbf{u}_{\text{trial}}\right)^{(n-1)}\right) + \\ \frac{\Delta t \varepsilon}{Re_D Da}\left(\frac{3}{2}\left(\mathbf{u}_{\text{trial}}\right)^{(n)} - \frac{1}{2}\left(\mathbf{u}_{\text{trial}}\right)^{(n-1)}\right) = \mathbf{R},\end{aligned} \tag{3.41}$$

where $\mathbf{u}_{\text{trial}}$ is the trial solution for the velocity field, and the operator $\langle ... \rangle$ is eliminated for simplicity. It is shown in equation 2.41 that the residual is an error term introduced through the use of the trial function. Where if the residual $\mathbf{R} = 0$,

the trial solutions is the exact solution, otherwise the trial solution represents the approximate solution for the velocity field.

Next, the method of weighted residuals (MWR) is employed to weight the residual. This is accomplished by taking the inner product of the residual with respect to the weighting function over the computational domain Ω and set the weighted residual to zero as follows:

$$\int\int_{\Omega}\left[\left(\mathbf{u}^{*}_{\text{trial}}-\mathbf{u}^{(\text{n})}_{\text{trial}}\right)+\frac{\Delta t}{\varepsilon}\left(\frac{3}{2}\left((\mathbf{u}_{\text{trial}}.\nabla)\mathbf{u}_{\text{trial}}\right)\right)^{(n)}-\frac{1}{2}\left((\mathbf{u}_{\text{trial}}.\nabla)\mathbf{u}_{\text{trial}}\right)\right)^{(n-1)}\Bigg)+ \frac{\Delta t F\varepsilon^{2}}{\sqrt{Da}}\left(\frac{3}{2}\left(|\mathbf{u}_{\text{trial}}|\,\mathbf{u}_{\text{trial}}\right)^{(n)}-\frac{1}{2}\left(|\mathbf{u}_{\text{trial}}|\,\mathbf{u}_{\text{trial}}\right)^{(n-1)}\right)+ \frac{\Delta t\varepsilon}{Re_{D}Da}\left(\frac{3}{2}\left(\mathbf{u}_{\text{trial}}\right)^{(n)}-\frac{1}{2}\left(\mathbf{u}_{\text{trial}}\right)^{(n-1)}\right)\Bigg].N_{i,j}(\xi,\eta)dxdy=0, \tag{3.42}$$

where $N_{i,j}(\xi,\eta)$ is referred to as the weight function or test function in two dimensions and (ξ,η) are the orthogonal element coordinates. Here, the weight functions are derived from the product of the quadratic Lagrangian interpolation functions within each element. Therefore, the weight functions can be written as a tensor-product Lagrange polynomials in two dimensions,

$$N_{i,j}(\xi,\eta)=\prod_{\substack{q=1\\ s=1\\ q\neq i\\ s\neq j}}^{p+1}\frac{(\xi-\xi_{q})}{(\xi_{i}-\xi_{q})}\frac{(\eta-\eta_{s})}{(\eta_{j}-\eta_{s})} \tag{3.43}$$

where i,j,q and s are the indices of the internal node points within each element, p is the order of the Lagrange polynomials, and $p+1$ represents the total number of points N of the element. Therefore, for increasing the number of points for further improving the grid resolution, the order of these polynomials p can be increased from 2 to 14. This kind of refinement is known as p-refinement, which leads, together with the h-refinement mentioned above, to so-called h-p method. In fact, this is the main advantage of the h-p discretisation method. Where the computational domain can be discretised once merely with an approximately optimal macro-element grid, and then an accurate converged solution can be achieved by only increasing p at run-time until convergence is obtained.

The integral of the equation 2.42 can be achieved separately for each compo-

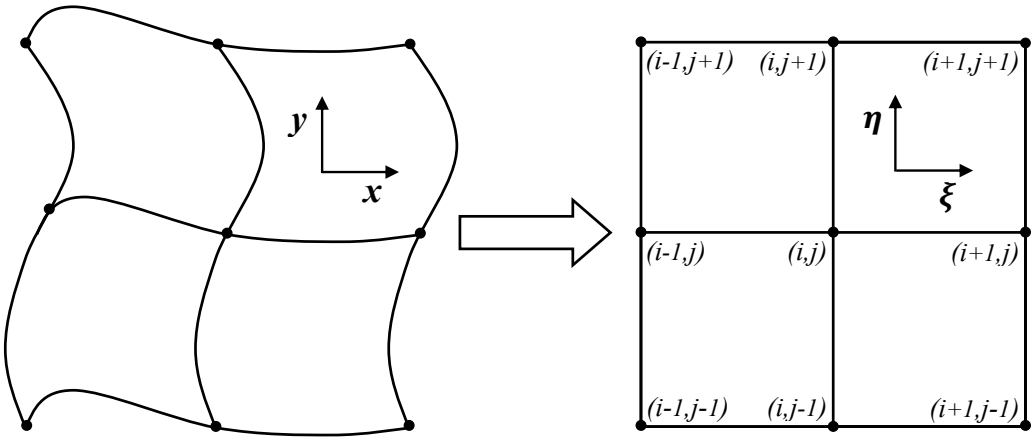

FIGURE 3.3: A general four curved quadratic macro-elements transformed into a linear square elements with new elemental coordinates ξ and η.

nent existing in the equation. Therefore, the first term which is defied as:

$$\int \int_{\Omega} \mathbf{u}^*_{\text{trial}}.N_{i,j}(\xi,\eta)dxdy, \tag{3.44}$$

is used to demonstrate the solution procedure of the Galerkin method. The integration of the equation 2.44 has to be done first over each macro-element separately, and then the contributions of the total elements are summed together to be evaluated over the whole domain. To simplify the approximation of this integral, the Jacobian is employed for transforming the curved quadratic macro-element into a square element defined over the range of -1,1 in both ξ and η directions as shown in figure 2.3. Thus, the integral over each element is expressed as

$$\int \int_{El} \mathbf{u}^*_{\text{trial}}.N_{i,j}(\xi,\eta)J(\xi,\eta)d\xi d\eta, \tag{3.45}$$

where El represents the element domain, and $J(\xi,\eta)$ is the Jacobian. Finally, by using Gauss-Lobatto-Legendre quadrature, the integral of the equation 2.46 can be approximated as:

$$\sum_{a,b} W_{a,b}(\xi,\eta) \sum_{i,j} \widehat{\mathbf{u}^*_{\text{i,j}}}.N_{i,j}(\xi,\eta)J(\xi,\eta), \tag{3.46}$$

where $\widehat{\mathbf{u}^*}$ represents the velocity field at the nodal points, $W_{a,b}(\xi,\eta)$ is the weighting coefficients of the Gauss-Lobatto-Legendre quadrature at these points, and a

and b are the points' locations in two directions ξ and η, respectively. Similar process is repeated for other components in equation 2.42, and the elemental results are then assembled to construct the global mass matrix system that may be solved with an appropriate boundary conditions for new field of the primary intermediate velocity. The same procedure is also repeated for the rest of the substep equations to complete the spatial discretisation for the momentum equation and obtain the final unknown field of velocity.

3.4 Resolution studies

Tests are conducted to ensure that the numerical results obtained are independent of the domain size and the spatial grid resolution. Domain size and grid resolution studies are undertaken for the two configurations described in figures 2.1 and 2.2 for a single circular cylinder and bundle of staggered and inline four cylinders, respectively, mounted in a horizontal channel. Nu_f and Nu_s are monitored in these studies as an indicator of convergence.

3.4.1 Domain size study

The study of domain size is first performed for steady flow in the first geometrical configuration shown in figure 2.1(a). Four physical domains, i.e. $M1$, $M2$, $M3$, and $M4$, according to their upstream L_u and downstream L_d lengths from the centre of the cylinder as explained in table 2.1, are chosen. The four domains are examined with and without the presence of porous media at two values of Reynolds number $Re_D = 10$ and 250, with polynomial order $p = 6$. To sufficiently resolve the higher temperature gradients near the heated cylinder the macro-element distribution is concentrated around its surface. The macro-mesh resolution is decreased in both the upstream and downstream directions to the inlet and outlet boundaries where gradients are smaller. To capture the boundary layers in the y-direction a finer mesh is employed near the walls with coarsening towards the core of the channel. The results of the study presented in table 2.2, show that the $M2$ and $M3$ domains are appropriate choices for the porous and empty channels, respectively, with numerical errors less than 0.1% as mea-

Domain	L_u	L_d	macro-elements	macro-nodes
$M1$	$3D_{cy}$	$10D_{cy}$	670	615
$M2$	$5D_{cy}$	$12D_{cy}$	742	683
$M3$	$8D_{cy}$	$15D_{cy}$	850	785
$M4$	$8D_{cy}$	$20D_{cy}$	940	870

TABLE 3.1: Four physical domains chosen, with their upstream and downstream lengths, and the total number of macro-elements and nodes.

	(a) Empty channel		(b) Porous channel			
	$Re_D = 10$	$Re_D = 250$	$Re_D = 10$		$Re_D = 250$	
Domain	Nu_f	Nu_f	Nu_f	Nu_s	Nu_f	Nu_s
$M1$	5.057827	19.441979	7.984645	0.129630	69.705124	0.130727
$M2$	5.122665	19.539155	7.968639	0.128593	69.699884	0.129716
$M3$	5.153913	19.660151	7.965108	0.128553	69.698501	0.129681
$M4$	5.153913	19.660764	7.965108	0.128553	69.698501	0.129681

TABLE 3.2: Domain size study for a steady forced convective flow in two; (a) empty, and (b) porous, channels for two values of $Re_D = 10$ and 250, with order of polynomial $p = 6$.

sured by fluid and solid Nusselt number convergence. The distribution of the computational macro-meshes for the $M2$ and $M3$ domains are described in figure 2.4.

The same domain lengths of $M2$ and $M3$ shown in table 2.1 are used for the problem of steady flow over multi-cylinders, but with different numbers of macro-elements and nodes due to the number of cylinders, for the cases with and without the presence of porous media. Figures 2.5 and 2.6 show the computational macro-element meshes for the configurations of staggered and inline multi-cylinders, respectively, for $M2$ and $M3$ channels. The mesh of the staggered arrangement is plotted at spacing parameter $SP = 2.75$, while the mesh of the inline arrangement is plotted at $SP = 0.75$. Once again, it is seen from the distribution of the computational meshes in figures 2.5 and 2.6 that the resolution of the macro-mesh is concentrated around the heated cylinders, and this resolution decreases in both the upstream and downstream directions to the inlet and outlet boundaries. Also, a finer mesh is employed close the walls and coarser mesh close the core of the

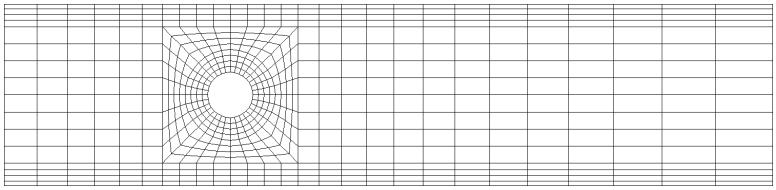

(a) $M2$ domain

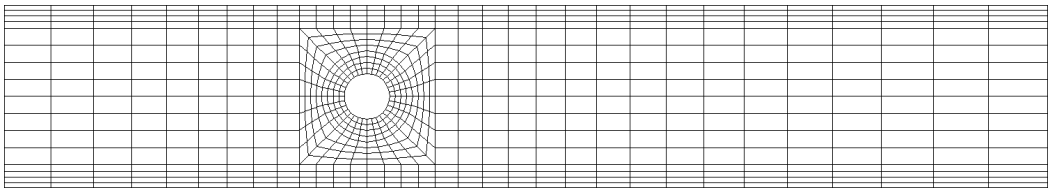

(b) $M3$ domain

FIGURE 3.4: Typical computational macro-meshes for the; (a) $M2$ physical domain used for steady flow in a porous channel, and (b) $M3$ physical domain used for steady flow in an empty channel.

	Staggered arrangement		Inline arrangement	
Domain	elements	nodes	elements	nodes
$M2$	1836	1713	2328	2182
$M3$	2156	2023	2600	2449

TABLE 3.3: The total number of macro-elements and nodes used in the computational meshes of the staggered and inline multi-cylinders' arrangements, described in figures 2.5 and 2.6, for the cases of with $M2$ and without $M3$ of porous media.

channel. The total number of the macro-elements and nodes used in the meshes of the staggered and inline arrangements are given in table 2.3, for $M2$ and $M3$ channels.

To use the $M2$ and $M3$ physical domains for the problem of pulsatile flow over a single cylinder inside porous and empty channels, and to ensure that they are relevant for this application, the effect of the their upstream length L_u on heat transfer from the cylinder Nu_f and Nu_s, is investigated. This investigation is done by changing the upstream length within the range of $5D \leq L_u \leq 10D$ for the $M2$ domain, and within $8D \leq L_u \leq 12D$ for the $M3$ domain. This is

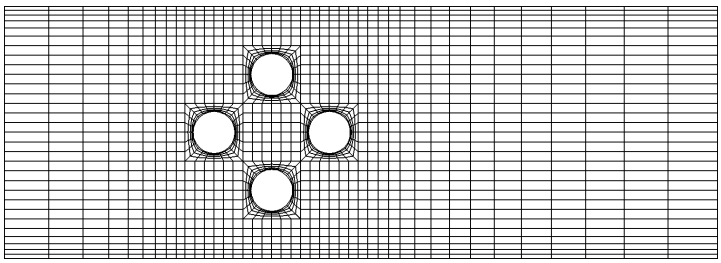

(a) $M2$ domain

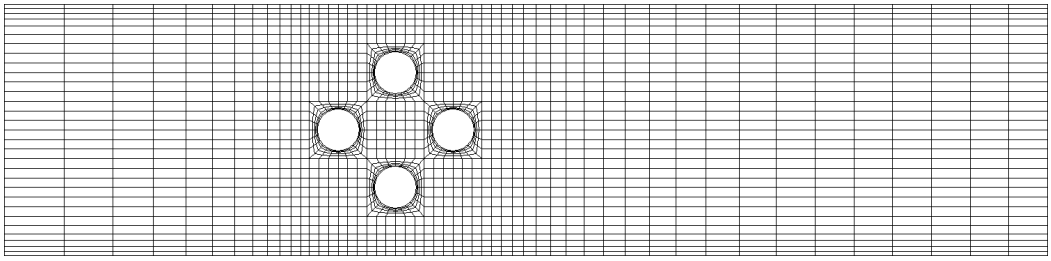

(b) $M3$ domain

FIGURE 3.5: Typical computational macro-mesh for banks of four staggered cylinders with spacing parameter $SP = 2.75$, for; (a) the $M2$ domain used for the porous case, and (b) the $M3$ domain used for the case of without porous media.

achieved at the highest pulsation amplitude examined, i.e. $A = 3.0$ in the porous channel, and $A = 0.7$ in the empty channel, for the lowest and highest limits of pulsation frequency $St = 0.1$ and 2.0, and for $Re_D = 1.0$ and 250. The results of the investigation are presented in tables 2.4 and 2.5, for both channels. It is found that the $M2$ domain with $L_u = 6D_{cy}$, and the $M3$ domain with the same original upstream length $L_u = 8D_{cy}$, are appropriate for oscillatory flows in these channels with numerical errors less than 0.1%. Figure 2.7 depicts the influence of L_u on the transient variation of N_f over one period of a pulsating flow in the porous channel, at $A = 3.0$ and $St = 0.1$, and for $Re_D = 1.0$ and 250.

3.4.2 Grid resolution study

In order to ascertain at what spectral resolution the solution becomes grid independent and subsequently which resolution provides a satisfactory compromise between accuracy and computational expense, a grid resolution study (GRS) for

	(a) $Re_D = 1.0$			
	$St = 0.1$		$St = 2.0$	
Lu	Nu_f	Nu_s	Nu_f	Nu_s
$5D$	2.791911	0.191021	2.477719	0.187402
$6D$	2.759714	0.189347	2.477754	0.187405
$7D$	2.742694	0.188456	2.477729	0.187403
$8D$	2.737184	0.188149	2.477730	0.187403
$9D$	2.734957	0.188044	2.477730	0.187403
$10D$	2.734706	0.188030	2.477730	0.187403

	(b) $Re_D = 250$			
	$St = 0.1$		$St = 2.0$	
Lu	Nu_f	Nu_s	Nu_f	Nu_s
$5D$	72.006157	0.290494	68.311690	0.301378
$6D$	71.038944	0.289071	68.311707	0.301378
$7D$	71.023951	0.288897	68.311714	0.301378
$8D$	71.023224	0.288896	68.311721	0.301378
$9D$	71.022825	0.288895	68.311722	0.301378
$10D$	71.022387	0.288893	68.311722	0.301378

TABLE 3.4: The effect of upstream length of the $M2$ domain allocated for the porous channel, subjected to a non-zero pulsate flow at its highest amplitude $A = 3.0$, on Nu_f and Nu_s at (a) $Re_D = 1.0$ and (b) 250, and for two minimum and maximum frequency limitations $st = 0.1$ and 2.0.

	$Re_D = 1.0$		$Re_D = 250$	
	$St = 0.1$	$St = 2.0$	$St = 0.1$	$St = 2.0$
Lu	Nu_f	Nu_f	Nu_f	Nu_f
$8D$	2.328386	2.381161	24.002609	24.374326
$9D$	2.328386	2.381161	24.002609	24.374326
$10D$	2.328386	2.381161	24.002609	24.374326
$11D$	2.328386	2.381161	24.002609	24.374326
$12D$	2.328386	2.381161	24.002609	24.374326

TABLE 3.5: The effect of upstream length of the $M3$ domain allocated for the empty channel, subjected to a non-zero pulsate flow at its highest amplitude $A = 0.7$, on Nu_f at $Re_D = 1.0$ and 250, and for two minimum and maximum frequency limitations $st = 0.1$ and 2.0.

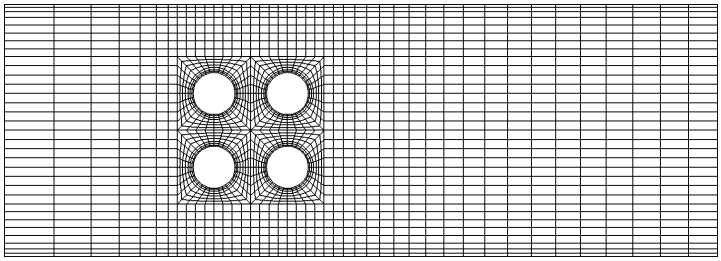

(a) $M2$ domain

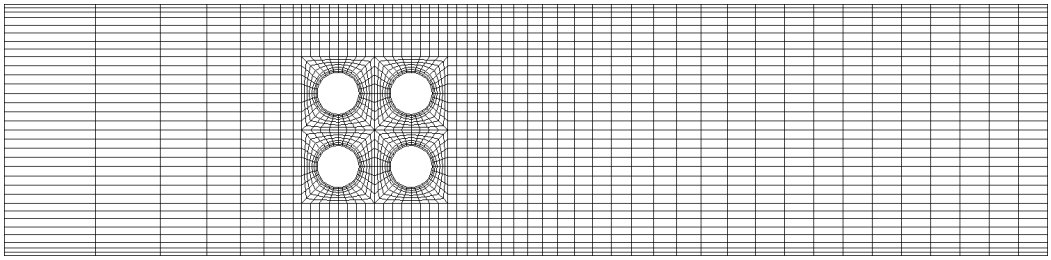

(b) $M3$ domain

FIGURE 3.6: Typical computational macro-mesh for banks of four inline cylinders with spacing parameter $SP = 0.75$, for; (a) the $M2$ domain used for the porous case, and (b) the $M3$ domain used for the case of without porous media.

the aforementioned meshes is undertaken. As described earlier, interpolants of order $p = N - 1$ are employed to represent the solution variables throughout the spatial discretisation. This leads to a set of $N \times N$ internal node points during each macro-element of the mesh, while keeping the macro-element layout the same. Therefore, in the present study the mesh resolution is varied by changing the order of these interpolants from 2 to 8.

The GRS is carried out for the macro-element meshes of the $M2$ and $M3$ domains shown in figure 2.4 assigned for the case of a single cylinder placed in a horizontal channel, and for the macro-element meshes of the $M2$ and $M3$ domains shown in figures 2.5 and 2.6 assigned for the case of staggered and inline multi-cylinders mounted in a horizontal channel. For the case of single cylinder, the GRS is first achieved for the porous channel, i.e., $M2$, at two lowest and highest values of Reynolds number $Re_D = 1$ and 250, and at two minimum and maximum values of each of the following parameters: solid-to-fluid thermal conductivity

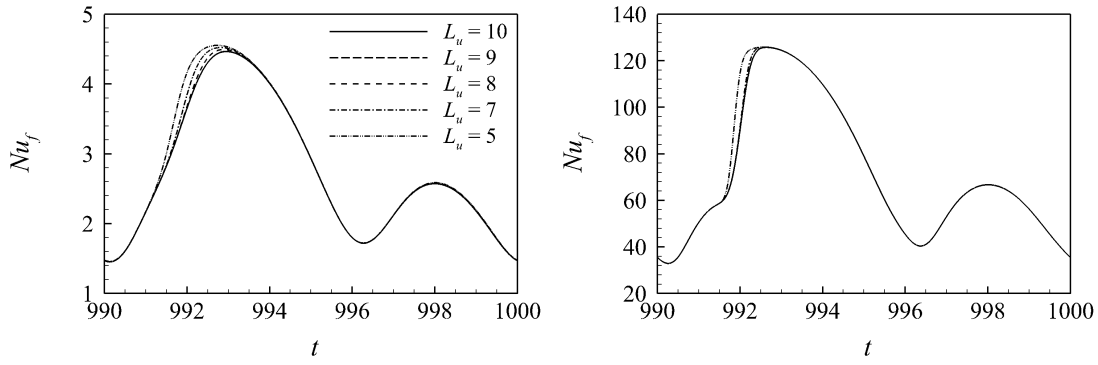

(a) Fluid Nusselt number

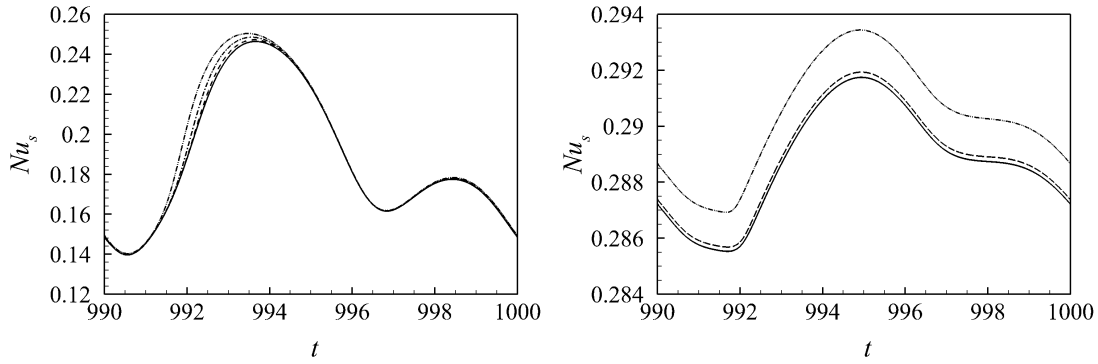

(b) Solid Nusselt number

FIGURE 3.7: The effect of upstream length of the $M2$ domain for the porous channel under a non-zero pulsate flow with amplitude $A = 3.0$ and frequency $St = 0.1$, on the transient variation of; (a) Nu_f, and (b) Nu_s for a one period, at (Left) $Re_D = 1.0$ and (Right) $Re_D = 250$.

ratio $k_r = 0.01$ and 1000; Biot number $Bi = 0.01$ and 100; and cylinder-to-particle diameter ratio $d_p = 10$ and 100, which govern the porous system. Then, the GRS study is done for the empty channel, i.e., $M3$, at only $Re_D = 1$ and 250. Again, Nu_f and Nu_s are monitored as an indication of accuracy. The results of this case are presented in tables 2.6, 2.7, 2.8 and 2.9. Here the selection of an appropriate p value relied rather on the range of p for which the solution does not diverge. These results show that Nu_f and Nu_s are converged by $p = 6$ for the porous channel, and Nu_f is converged by $p = 7$ for the empty channel, with a relative error of less than 0.5%.

For the case of multi-cylinders, the GRS is implemented for both inline and staggered arrangements, and for the empty and porous channels as well, at only

$Re_D = 1.0$				
	$k_r = 0.01$		$k_r = 1000$	
p	Nu_f	Nu_s	Nu_f	Nu_s
2	2.093937	0.208724	1.945964	0.124746
3	2.084829	0.208389	1.940192	0.124378
4	2.082658	0.208095	1.935207	0.124058
5	2.081221	0.207893	1.931993	0.123852
6	2.080121	0.207749	1.929790	0.123711
7	2.079330	0.207646	1.928184	0.123608
8	2.078717	0.207566	1.926967	0.123529

$Re_D = 250$				
	$k_r = 0.01$		$k_r = 1000$	
p	Nu_f	Nu_s	Nu_f	Nu_s
2	66.31117	0.303586	54.95857	0.260723
3	65.98328	0.302715	54.71937	0.259967
4	65.99555	0.302373	54.74098	0.259612
5	65.99180	0.302171	54.74359	0.259411
6	65.97858	0.302032	54.73227	0.259271
7	65.96869	0.301929	54.72206	0.259169
8	65.96135	0.301852	54.71413	0.259092

TABLE 3.6: Grid resolution study of the computational domain $M2$ for a single cylinder embedded in a horizontal porous channel, at two minimum and maximum values of solid-to-fluid thermal conductivity ratio $k_r = 0.01$ and 1000, and at two lowest and highest values of Reynolds number $Re_D = 1.0$ and 250. This is done by varying the interpolation polynomial order p within the range $2 - 8$, while keeping the macro-element layout the same.

the smallest and largest values of the spacing parameter $SP = 1.5$ and 3 between the cylinders. This case is a little more difficult than the previous case since the numerical accuracy has to be satisfied for Nu_f and Nu_s of all the four cylinders. This is accomplished also at $Re_D = 1$ and 250, and the results of this case indicate that the values of Nu_f and Nu_s for the four cylinders are well within again 0.5% with $p = 6$ for the porous channel, and with $p = 7$ for the empty channel. Here, for brevity, only the results of the front cylinder A in each arrangement are presented in tables 2.10, 2.11, 2.12 and 2.13.

The numerical simulations for the domain and mesh resolution studies have been performed at a time-step $\Delta t = 0.001$ (determined by a Courant time-step restriction), on the Monash (University) Sun Grid (MSG) and National Compu-

$Re_D = 1.0$				
	$Bi = 0.01$		$Bi = 100$	
p	Nu_f	Nu_s	Nu_f	Nu_s
2	2.544630	0.126913	2.453301	0.235783
3	2.535916	0.126555	2.445354	0.235100
4	2.533012	0.126237	2.442494	0.234799
5	2.531002	0.126031	2.440490	0.234597
6	2.529496	0.125890	2.438990	0.234452
7	2.528403	0.125787	2.437900	0.234346
8	2.527562	0.125709	2.437062	0.234266

$Re_D = 250$				
	$Bi = 0.01$		$Bi = 100$	
p	Nu_f	Nu_s	Nu_f	Nu_s
2	67.99546	0.130639	67.89319	0.655912
3	67.64925	0.130263	67.54869	0.650291
4	67.66128	0.129938	67.56126	0.649493
5	67.65795	0.129724	67.55809	0.649283
6	67.64456	0.129577	67.54474	0.649137
7	67.63441	0.129473	67.53458	0.649034
8	67.62685	0.129395	67.52701	0.648956

TABLE 3.7: Grid resolution study of the computational domain $M2$ for a single cylinder embedded in a horizontal porous channel, at two minimum and maximum values of Biot number $Bi = 0.01$ and 100, and at two lowest and highest values of Reynolds number $Re_D = 1.0$ and 250. This is done by varying the interpolation polynomial order p within the range $2 - 8$, while keeping the macro-element layout the same.

tational Infrastructure (NCI) high-performance computers.

3.5 Chapter summary

In this chapter, a description for the physical problem under consideration in this thesis is first stated. Next, the mathematical model, i.e. the Darcy-Brinkmann-Forchheimer DBF momentum and the one- and two-equation energy models, that describes the flow and heat phenomenon in porous media is presented with an appropriate assumptions. Then, a normalisation process using a proper dimensionless variables to formulate a general non-dimensional form for the macroscopic mathematical model used, is performed. Following this, relevant Dirichlet and Neumann boundary conditions are specified that are employed in the current in-

$Re_D = 1.0$				
	$D_{cy}/d_p = 10$		$D_{cy}/d_p = 100$	
p	Nu_f	Nu_s	Nu_f	Nu_s
2	2.409024	0.185074	2.596653	0.193798
3	2.404260	0.184718	2.583461	0.193727
4	2.400991	0.184395	2.578620	0.193615
5	2.398749	0.184185	2.575193	0.193461
6	2.397186	0.184042	2.573881	0.193360
7	2.396063	0.183938	2.573185	0.193281
8	2.395210	0.183859	2.572616	0.193215

$Re_D = 250$				
	$D_{cy}/d_p = 10$		$D_{cy}/d_p = 100$	
p	Nu_f	Nu_s	Nu_f	Nu_s
2	91.56000	0.273684	40.92436	0.349061
3	91.37153	0.273048	40.55497	0.347402
4	91.35897	0.272731	40.61156	0.347006
5	91.31966	0.272529	40.76205	0.346781
6	91.29128	0.272388	40.80610	0.346625
7	91.27201	0.272286	40.81810	0.346518
8	91.25765	0.272209	40.82188	0.346440

TABLE 3.8: Grid resolution study of the computational domain $M2$ for a single cylinder embedded in a horizontal porous channel, at two minimum and maximum values of cylinder-to-particle diameter ratio $D_{cy}/d_p = 10$ and 100, and at two lowest and highest values of Reynolds number $Re_D = 1.0$ and 250. This is done by varying the interpolation polynomial order p within the range $2 - 8$, while keeping the macro-element layout the same.

	$Re_D = 1.0$	$Re_D = 250$
p	Nu_f	Nu_f
2	2.086845	22.453573
3	2.084753	19.399868
4	2.082221	18.992643
5	2.080529	19.377584
6	2.079362	19.465532
7	2.078513	19.435192
8	2.077858	19.425336

TABLE 3.9: Grid resolution study of the computational domain $M3$ for a single cylinder placed in a horizontal empty channel, at two lowest and highest values of Reynolds number $Re_D = 1.0$ and 250. This is done by varying the interpolation polynomial order p within the range $2 - 8$, while keeping the macro-element layout the same.

	$Re_D = 1.0$			
	$SP = 1.5$		$SP = 3.0$	
p	Nu_f	Nu_s	Nu_f	Nu_s
2	1.465940	0.105811	2.485226	0.180932
3	1.459136	0.105163	2.477214	0.180329
4	1.455365	0.104777	2.473191	0.179935
5	1.452807	0.104525	2.470577	0.179681
6	1.450975	0.104348	2.468757	0.179505
7	1.449566	0.104212	2.467463	0.179380
8	1.448953	0.104153	2.466449	0.179282

	$Re_D = 250$			
	$SP = 1.5$		$SP = 3.0$	
p	Nu_f	Nu_s	Nu_f	Nu_s
2	48.89282	0.169444	69.00218	0.301128
3	48.73988	0.168676	68.73723	0.300299
4	48.70266	0.168271	68.72283	0.299898
5	48.72026	0.168015	68.70536	0.299644
6	48.73662	0.167985	68.68897	0.299468
7	48.74995	0.167882	68.67657	0.299341
8	48.75491	0.167861	68.66711	0.299244

TABLE 3.10: Grid resolution study of the computational domain $M2$ for four staggered cylinders embedded in a horizontal porous channel. This table shows the results of only the front cylinder A at two minimum and maximum values of spacing parameter $SP = 1.5$ and 3.0, and at two values of Reynolds number $Re_D = 1.0$ and 250.

	$Re_D = 1.0$		$Re_D = 250$	
	$SP = 1.5$	$SP = 3.0$	$SP = 1.5$	$SP = 3.0$
p	Nu_f	Nu_f	Nu_f	Nu_f
2	1.066199	2.038929	15.25015	19.43185
3	1.059792	2.033090	13.65182	18.27510
4	1.055753	2.029119	13.59634	18.32084
5	1.053185	2.026571	13.65323	18.41300
6	1.051421	2.024817	13.66191	18.40881
7	1.050147	2.023539	13.65659	18.40993
8	1.049140	2.022570	13.65459	18.40991

TABLE 3.11: Grid resolution study of the computational domain $M3$ for four staggered cylinders placed in a horizontal empty channel. This table shows the results of only the front cylinder A, for $SP = 1.5$ and 3.0, and at $Re_D = 1.0$ and 250.

	$Re_D = 1.0$			
	$SP = 1.5$		$SP = 3.0$	
p	Nu_f	Nu_s	Nu_f	Nu_s
2	2.133478	0.136744	2.545001	0.191963
3	2.116174	0.135757	2.526682	0.191016
4	2.112479	0.135371	2.522761	0.190630
5	2.109931	0.135119	2.520189	0.190377
6	2.108127	0.134944	2.518384	0.190202
7	2.106812	0.134817	2.517058	0.190075
8	2.105780	0.134717	2.516046	0.189977

	$Re_D = 250$			
	$SP = 1.5$		$SP = 3.0$	
p	Nu_f	Nu_s	Nu_f	Nu_s
2	68.29207	0.254285	69.61140	0.304836
3	68.06833	0.253375	69.34052	0.303930
4	68.05973	0.252970	69.32607	0.303520
5	68.03801	0.252716	69.30967	0.303266
6	68.02065	0.252541	69.29255	0.303091
7	68.00807	0.252413	69.28008	0.302964
8	67.99868	0.252316	69.27054	0.302866

TABLE 3.12: Grid resolution study of the computational domain $M2$ for four inline cylinders embedded in a horizontal porous channel. This table shows the results of only the front cylinder A at two minimum and maximum values of spacing parameter $SP = 1.5$ and 3.0, and at two values of Reynolds number $Re_D = 1.0$ and 250.

	$Re_D = 1.0$		$Re_D = 250$	
	$SP = 1.5$	$SP = 3.0$	$SP = 1.5$	$SP = 3.0$
p	Nu_f	Nu_f	Nu_f	Nu_f
2	1.255058	2.010588	19.949738	18.473362
3	1.249006	2.005596	18.341549	16.647298
4	1.245032	2.001674	18.480191	16.636018
5	1.242487	1.999131	18.567784	16.822433
6	1.240740	1.997380	18.580809	16.818516
7	1.239449	1.996097	18.584627	16.815137
8	1.238494	1.995110	18.584108	16.814505

TABLE 3.13: Grid resolution study of the computational domain $M3$ for four inline cylinders placed in a horizontal empty channel. This table shows the results of only the front cylinder A, at $SP = 1.5$ and 3.0, and at $Re_D = 1.0$

vestigation to describe the pertinent hydrodynamic and thermal variables, i.e. the velocity and temperature, on the inlet, outlet and solid boundaries. The numerical technique, e.g. the spectral-element method, is also introduced, for which the discretisation of the system of highly-coupled governing equations in both time and space is shown in some detail. In the last section, the computational meshes for the physical domains are developed, and a detailed domain- and grid-resolution studies are presented.

Chapter 4

Validation of the numerical code

4.1 Introduction

In order to validate the implementation, results from the present code have been compared with previously published numerical and experimental results. A number of test problems have been used to provide benchmarks. Initially, the numerical results of the code have been compared with numerical and experimental results for mixed and forced convective flows inside a channel and over a single cylinder. Following this, it is validated for thermal predictions for multiple heat sources, e.g. multiple cylinders, in both the presence and absence of porous media against related numerical studies.

4.2 Mixed convection of a jet impingement

As described in the literature review, to date there has been no complete analysis of unsteady non-equilibrium forced convective flow past a cylinder embedded in porous media. Therefore, the numerical algorithm used in the existing code is first verified against a closely related mathematical problem reported by Wong & Saeid (2009). They analysed the problem of steady mixed convection arising from an air cooling jet impinging on an isothermal heated surface contained within a channel containing porous media under the *LTNE* condition. They used a finite-volume numerical approach with a lower-order power-law scheme for the convection-diffusion formulation to discretise the generalised *DBF* momentum model and other governing equations. Their problem is modeled using our

approach.

The channel is filled by highly porous metal foam at constant porosity $\varepsilon = 0.87$. Non-Darcian effects are taken into consideration, where the coefficient of friction is fixed at $C_F = 0.1$, during this study. The fluid-to-solid thermal conductivity ratio is modeled as a porosity-scaled thermal conductivity ratio parameter $\gamma = \varepsilon k_f/(1-\varepsilon)k_s$, and the interfacial convective heat transfer coefficient is normalized with respect to fluid thermal conductivity to obtain the volumetric convective heat transfer parameter $H_v = (h_{sf} a_{sf} H^2)/k_f$. The schematic diagram of the physical system with the macro computational mesh used here are provided in figure 3.1. The heat transfer and fluid flow characteristics are considered to be symmetrical about the y-axis, hence only one half of the physical model is considered for the computational domain. The upper wall of the channel is assumed to be cold with a temperature θ_c, while the bottom wall contains a hot surface at temperature θ_h in the middle section and adiabatic surfaces covering the rest of the wall. The aspect ratio of the channel is (length/height)$= (2S + 2L)/L = 10$ and the jet opening width is taken as one tenth of the heat source length $(2d/2L = 0.1)$. The heat source length is set to double the channel height.

The boundary conditions used are as follows:

$$
\begin{aligned}
&\text{at } x = 0 \quad \textbf{(Symmetry axis)} : \\
&\quad \frac{\partial \theta_s}{\partial x} = \frac{\partial \theta_f}{\partial x} = \frac{\partial v}{\partial x} = u = 0 \qquad \text{for} \quad (0 < y < L) \\
&\text{at } x = L + S \quad \textbf{(Flow exit)} : \\
&\quad \frac{\partial \theta_s}{\partial x} = \frac{\partial \theta_f}{\partial x} = \frac{\partial u}{\partial x} = \frac{\partial v}{\partial x} = 0 \quad \text{for} \quad (0 < y < L) \\
&\text{at } y = 0 \quad \textbf{(Bottom surface)} : \\
&\quad u = v = 0 \\
&\quad \theta_s = \theta_f = 1 \quad \text{for} \quad (0 < x < L), \quad \text{otherwise} \quad \frac{\partial \theta_s}{\partial y} = \frac{\partial \theta_f}{\partial y} = 0 \\
&\text{at } y = L \quad \textbf{(Top surface)} : \\
&\quad \theta_s = \theta_f = u = 0 \\
&\quad v = -1 \quad \text{for} \quad (0 < x < d), \quad \text{otherwise} \quad v = 0
\end{aligned}
\tag{4.1}
$$

The size of the macro-grid used in this work is (49×18) elements, with high

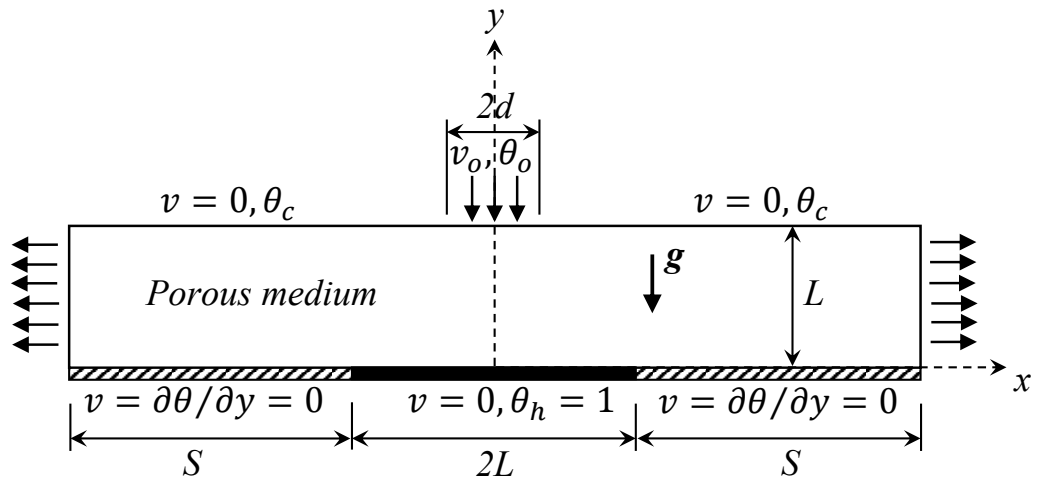

(a) Physical domain with the coordinate system

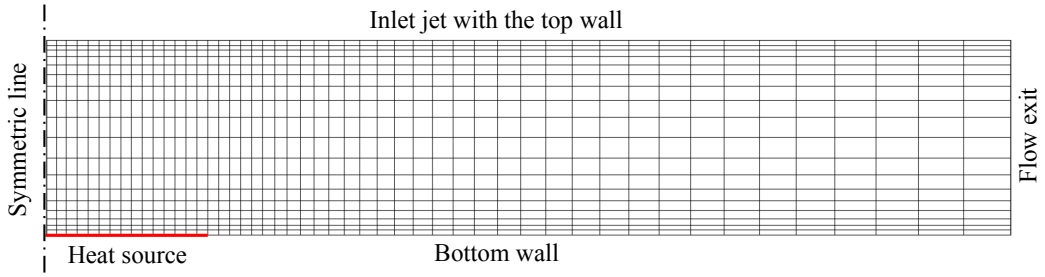

(b) Computational macro-mesh

FIGURE 4.1: (a) Schematic diagram of the full physical system for the problem of jet impingment cooling an isothermal heated surface immersed in a horizontal porous channel together with the coordinate system, studied by Wong & Saeid (2009), and (b) the computational macro-mesh used in the present study.

order of polynomial basis function $p = 7$. The computational grid is compressed in the x-direction towards the heat source, where steep variations in thermal and velocity fields are expected, while in the y-direction a finer mesh is employed in the vicinity of the solid boundaries and a coarser mesh near the core of the channel. The present code is tested for different values of Péclet number, Pe, and H_v, and at a constant values of Rayleigh number $Ra = 100$, Darcy number $Da = 10^{-3}$ and $\gamma = 1.0$.

Figures 3.2 and 3.3 show a comparison between the results reported by Wong & Saeid (2009) and those predicted by the code for streamlines and isotherms for the fluid and solid phases, for $Pe = 10, 40$, and 100, and at $H_v = 1.0$. In

figure 3.2, the streamlines of the fluid flow at low $Pe = 10$ refer to the dominance of free convection in the channel close to the heat source. Hence, the jet flow enters the channel vertically downwards through the porous medium and hits the heated segment making a turn, then passes through the middle of the two secondary generated vortices towards the exit. It can be seen that the strength of these two vortices decreases and they shift towards the upstream direction as Pe increases to 40, and then they disappear at $Pe = 100$, which means that forced convection becomes now dominant. The isotherms in figure 3.3 indicate that a thermal plume forms in the region between the two vortices. It is clear that as the flow becomes stronger the plume pushes towards the upstream direction. The comparisons of both streamlines and thermal fields are favourable, although the predictions from the current code are not identical to the published results. It is difficult to ascertain the cause of the differences, but it is worth noting that they are small.

Figure 3.4 illustrates the comparison between the two numerical models for the variation of fluid and solid average Nusselt numbers Nu_f and Nu_s respectively, versus Pe over the range $1 - 1000$, for two values of $H_v = 1.0$ and 1000. In figure 3.4(a), Nu_f is quite different from Nu_s which is relatively insensitive to Pe. However, in figure 3.4(b), it can be noticed that the difference between Nu_f and Nu_s is small and their values are almost identical which indicates thermal equilibrium. This is caused by increasing the heat transfer coefficient parameter H_v which represents the thermal contribution between the fluid and solid phases. As shown in these figures, there are small differences in the results between the two numerical models – typically about 10%. The differences may be a result of the lower-order numerical model used by Wong and Saeid. However, they did not state their values of the thermal diffusivity and heat capacity of the alloy of metal foam used as their porous medium. These values had to be estimated from data for the original alloy components $[Fe(73\%)Cr(20\%)Al(5\%)Y(2\%)]$ based on their percentages. However, again, the figures show very similar trends, which helps provide confidence in the implementation of the current code.

Another comparison for the velocity distribution close to the wall impinged

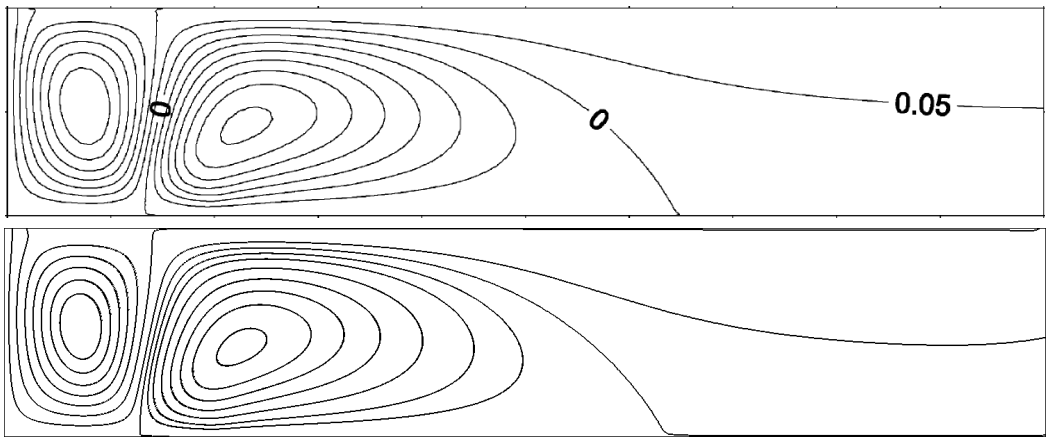

(a) $Pe = 10$

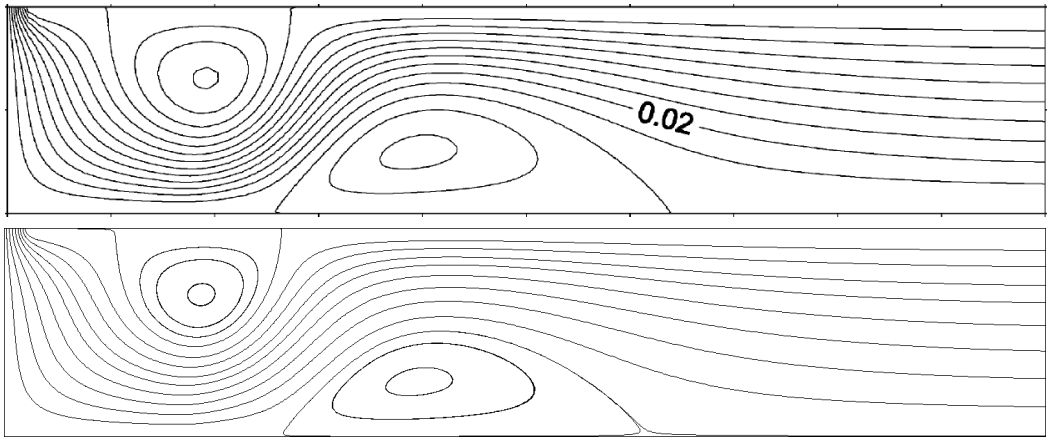

(b) $Pe = 40$

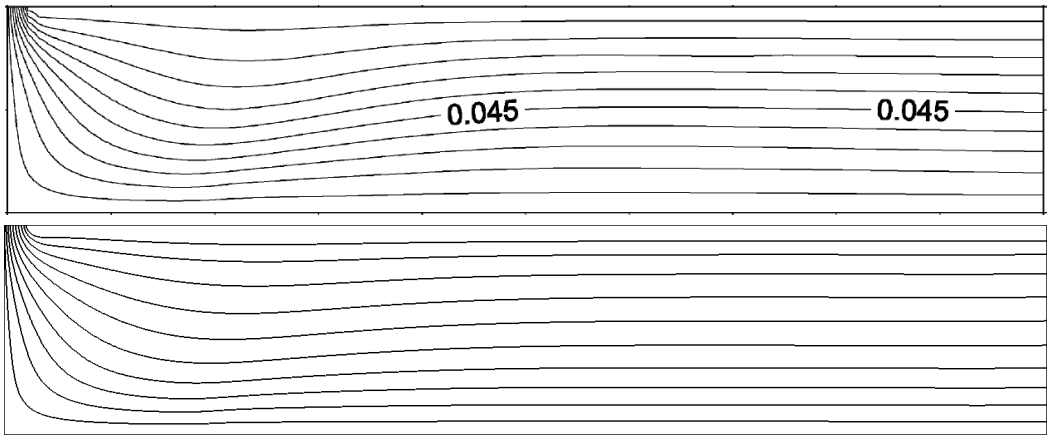

(c) $Pe = 100$

FIGURE 4.2: Comparison between the results of Wong & Saeid (2009) (Top) and those predicted by the present code (Bottom), for streamlines of air jet impingement cooling of a heat source immersed in a porous channel, at three values of Péclet number; (a) $Pe = 10$, (b) 40 and (c) 100.

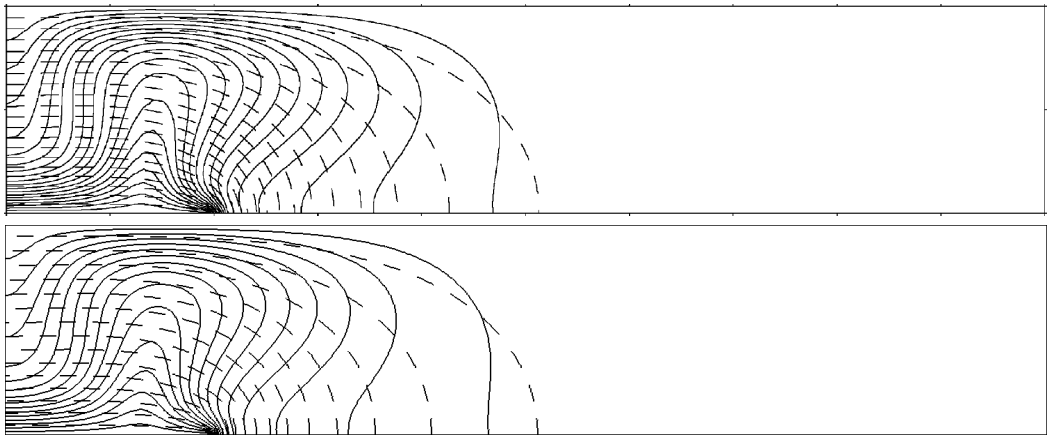

(a) $Pe = 10$

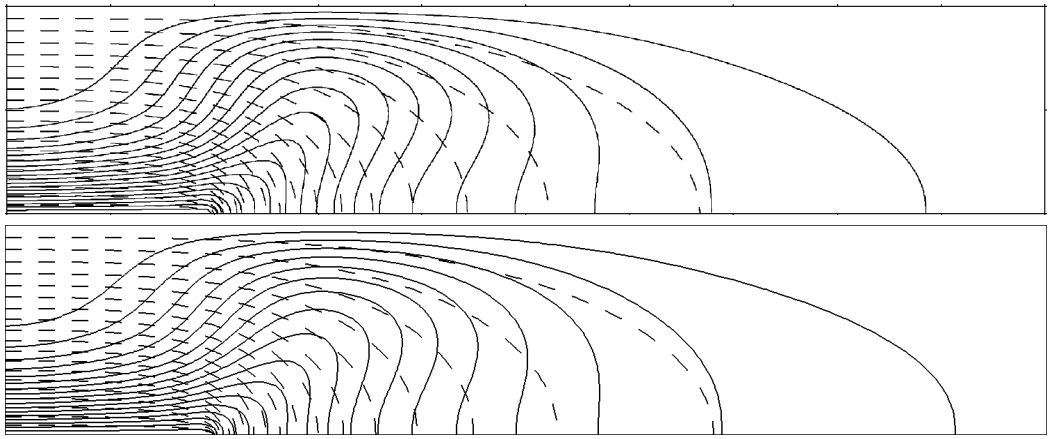

(b) $Pe = 40$

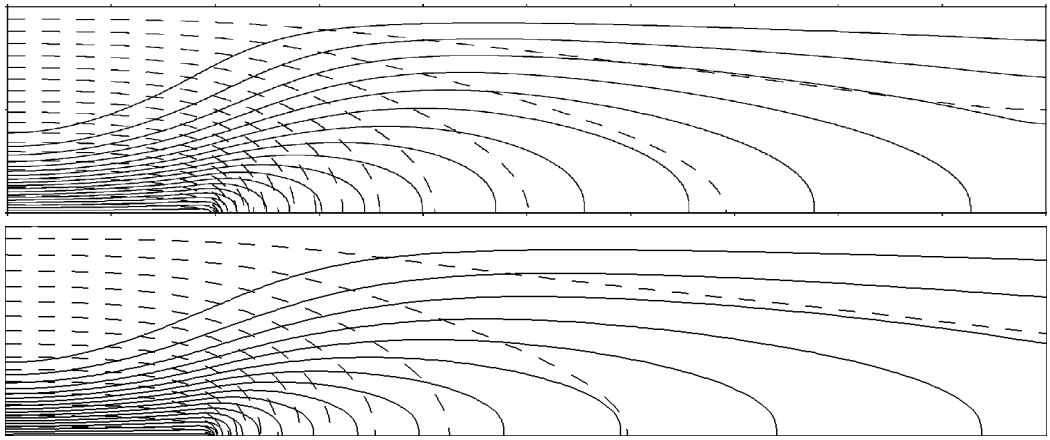

(c) $Pe = 100$

FIGURE 4.3: Comparison between the results of Wong & Saeid (2009) (Top) and those predicted by the present code (Bottom), for isotherms of the fluid phase (solid lines), and the solid phase (dash lines), for an air jet impingement cooling of a heat source immersed in a porous channel, at Péclet number (a) $Pe = 10$, (b) 40 and (c) 100.

upon by the jet, at $y = 0.002$ above the heated segment, for $Pe = 10$ and 20, at $H_v = 1.0$, and for the variation of the $LTNE$ parameter against H_v, at $Pe = 100$, are presented in figure 3.5. Here, the $LTNE$ parameter is defined as:

$$LTNE = \frac{\Sigma_N |\theta_s - \theta_f|}{N}, \tag{4.2}$$

where N is the total number of nodes in the domain. This is a simple measure of the mean difference between the fluid and solid over the domain. Even through this parameter is a weak function of the grid point distribution, which is different in each case, excellent agreement between the two numerical results can be seen in this figure.

4.3 Forced convection over a single cylinder

It is essential that the numerical results be verified against reliable experimental work to investigate the degree of accuracy of the current numerical findings. Therefore, in this section, the numerical results are benchmarked against experimental results obtained by Nasr *et al.* (1994) for air forced convection heat transfer from an unbounded circular cylinder surrounded by spherical particles, as shown in figure 3.6(a). In their experimental set up, the cylinder is embedded in a large vertical bed to avoid the effects of the solid boundaries. It is heated at a constant temperature T_w and cooled by the external flow T_o coming from the top of the bed. The comparison is made for three kinds of particle materials, nylon, glass and aluminum as the solid phase, with solid/fluid thermal conductivity ratios $k_r = 8.7, 38$ and 7605, and with different sizes, $d_p = 6.35, 2.85$ and 12.23 mm, respectively. Constant values of porosity $\varepsilon = 0.37$ and cylinder diameter $D = 12.7$ mm are used. In their work, they reduced the experimental data to dimensionless parameters such as Nusselt number and Péclet number. According to their recommendation, the model of Zehner & Schluender (1970) is used to calculate the effective stagnant thermal conductivity in the energy equation while the dispersion-enhanced conductivity is neglected. Thus, the porous medium is treated as a continuum by volume-averaging the thermal diffusivity of the solid and fluid phases. Therefore, the present code was adjusted to fit this particular

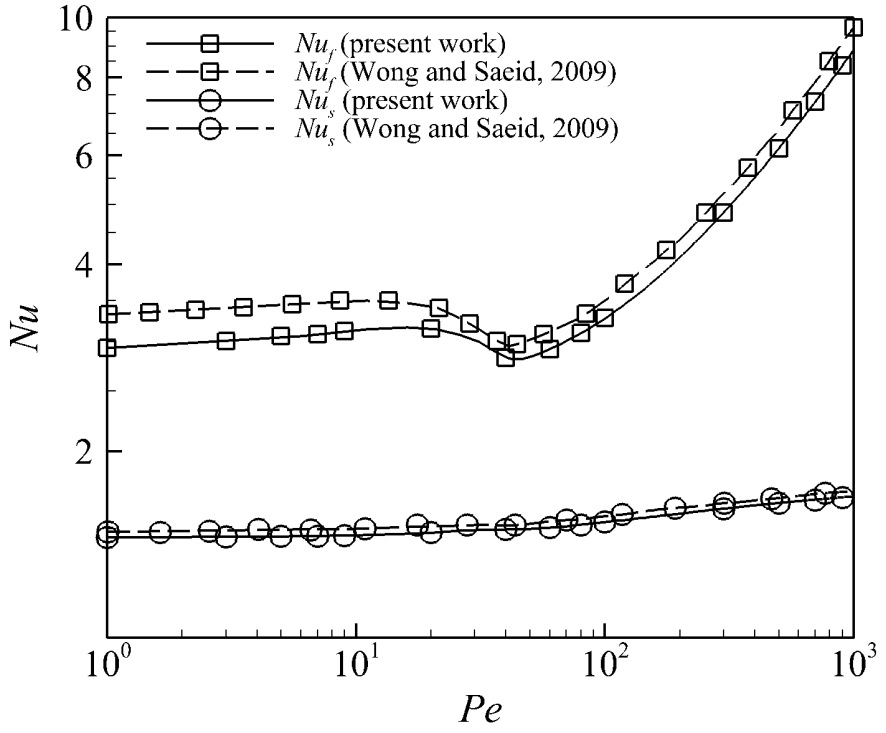

(a) At $H_v = 1.0$

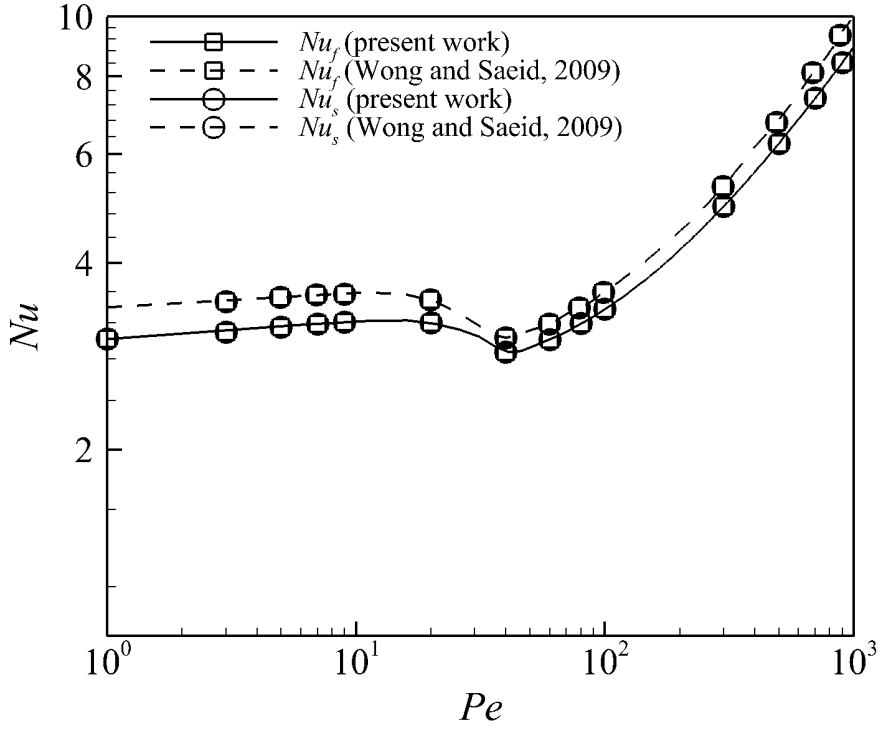

(b) At $H_v = 1000$

FIGURE 4.4: Comparison between the results of Wong & Saeid (2009) and those reproduced by the present code for the variation of average Nusselt number for the fluid and solid phase against Péclet number at: (a) $H_v = 1.0$, and (b) $H_v = 1000$.

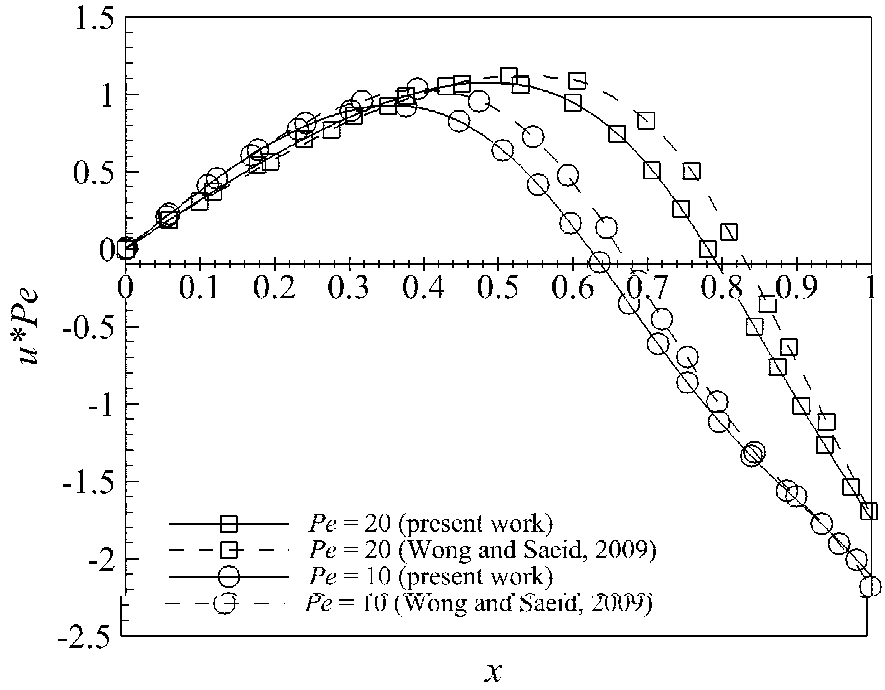

(a) The local velocity variation

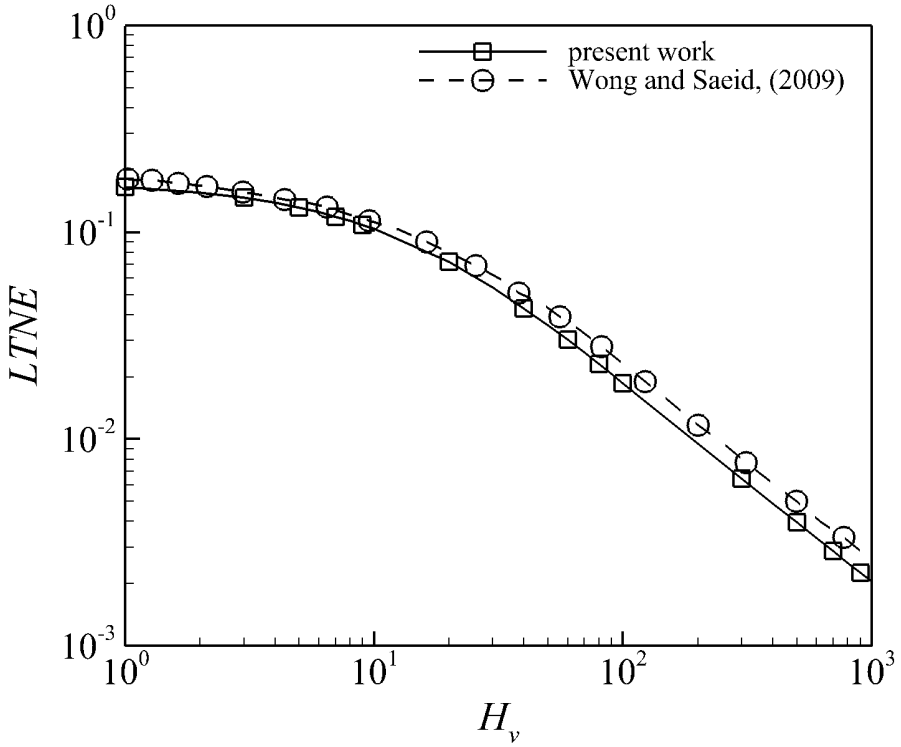

(b) The $LTNE$ variation

FIGURE 4.5: Comparison between the two numerical models: the present model and the model used by Wong & Saeid (2009), (a) for the variation of (u-velocity $\times Pe$) at $y = 0.002$ along the heat source, for two values of $Pe = 10$ and 20, with $H_v = 1.0$, and (b) for the variation of the $LTNE$ parameter against H_v at $Pe = 100$.

case, and reproduce the experimental results. The computational macro-mesh used in the numerical work is shown in figure 3.6(b). The large dimensions of the computational domain were chosen to limit boundary effects. The height of the computational domain is selected to be $H = 12D_{cy}$, while the total width is $L = 10D_{cy}$. The boundary conditions employed here are as follows:

$$
\begin{aligned}
&\text{at } y = +H/2 \ \textbf{(Flow inlet)} : \\
&\quad v_0 = -1, u = \theta = 0 \quad \text{for} \quad (-L/2 < x < +L/2) \\
&\text{at } y = -H/2 \ \textbf{(Flow exit)} : \\
&\quad \frac{\partial \theta}{\partial y} = \frac{\partial u}{\partial y} = \frac{\partial v}{\partial y} = 0 \quad \text{for} \quad (-L/2 < x < +L/2) \\
&\text{at } x = \mp L \ \textbf{(Free flow)} : \\
&\quad \frac{\partial v}{\partial x} = \frac{\partial \theta}{\partial x} = u = 0 \quad \text{for} \quad (-H/2 < y < +H/2) \\
&\text{at} \quad \textbf{(Cylinder surface)} : \\
&\quad \theta = 1, u = v = 0
\end{aligned}
\tag{4.3}
$$

Figures 3.7 and 3.8 show the results of the comparison for the variation of Nusselt number with Péclet number, Pe_D based on the cylinder diameter, for the three particle materials mentioned above. There is clearly good agreement between the numerical predictions, the experimental results and, as a further comparison, with the analytical solutions made by Cheng (1982) for mixed convection about a horizontal cylinder embedded in a fluid-saturated porous medium. Cheng obtained similarity solutions using the Darcy model in the boundary-layer region.

4.4 Forced convection over a bundle of cylinders

The validity of the present numerical scheme for its ability to predict thermal results in the case of heated multiple cylinders is verified in this section. Validation is achieved in two steps; with and without the presence of porous media.

4.4.1 With porous media

First, the case of multi-cylinders embedded in a porous medium was examined and comparison made with the numerical predictions of Layeghi (2008). They

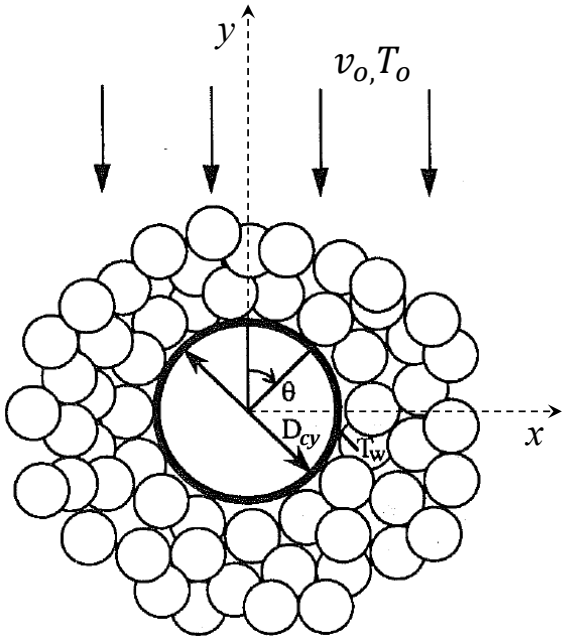

(a) The physical domain and coordinate system

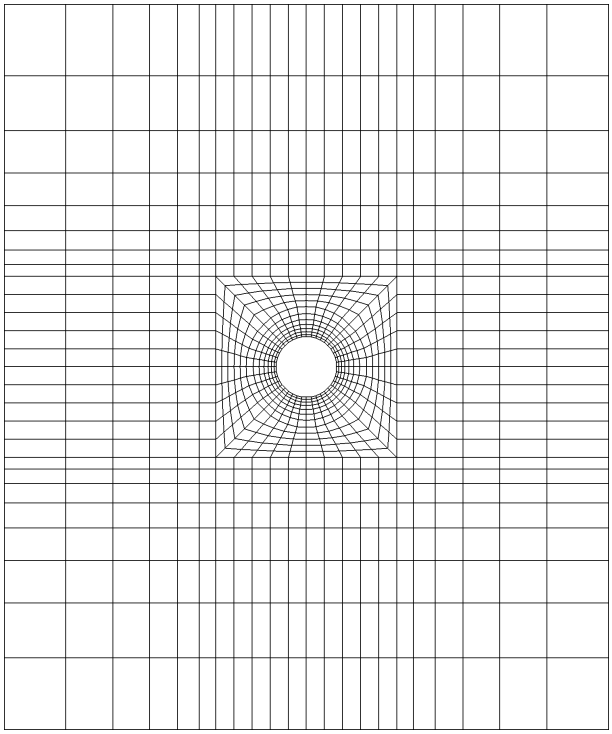

(b) Computational macro-mesh

FIGURE 4.6: (a) Schematic diagram of the problem of forced convection from an unbounded circular cylinder surrounded by spherical particles, investigated experimentally by Nasr *et al.* (1994), and (b) the computational macro-mesh used here to reproduce their results.

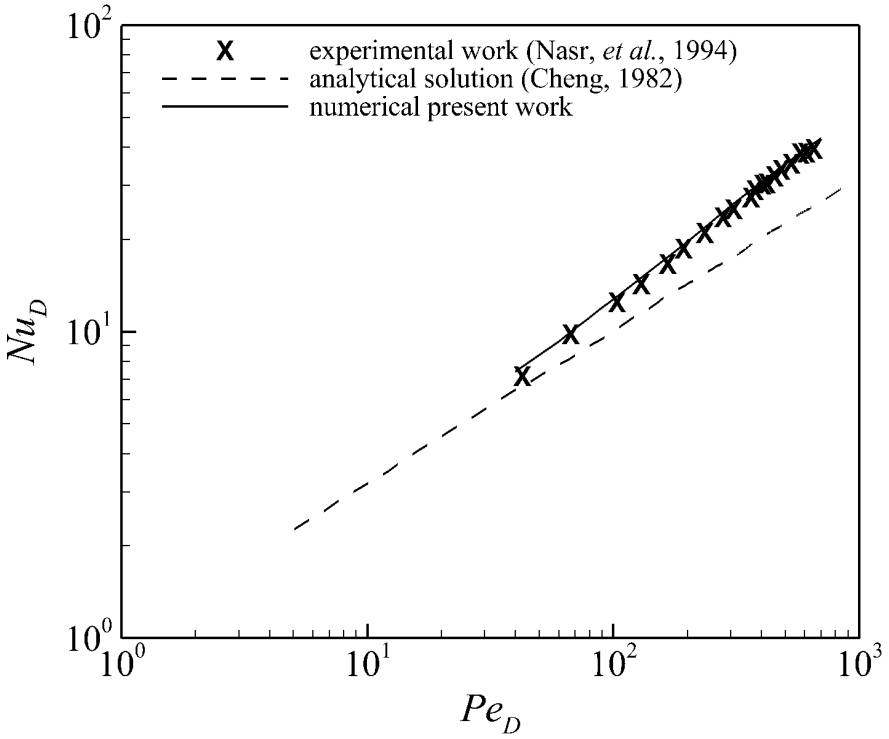

(a) For packed bed of nylon spheres

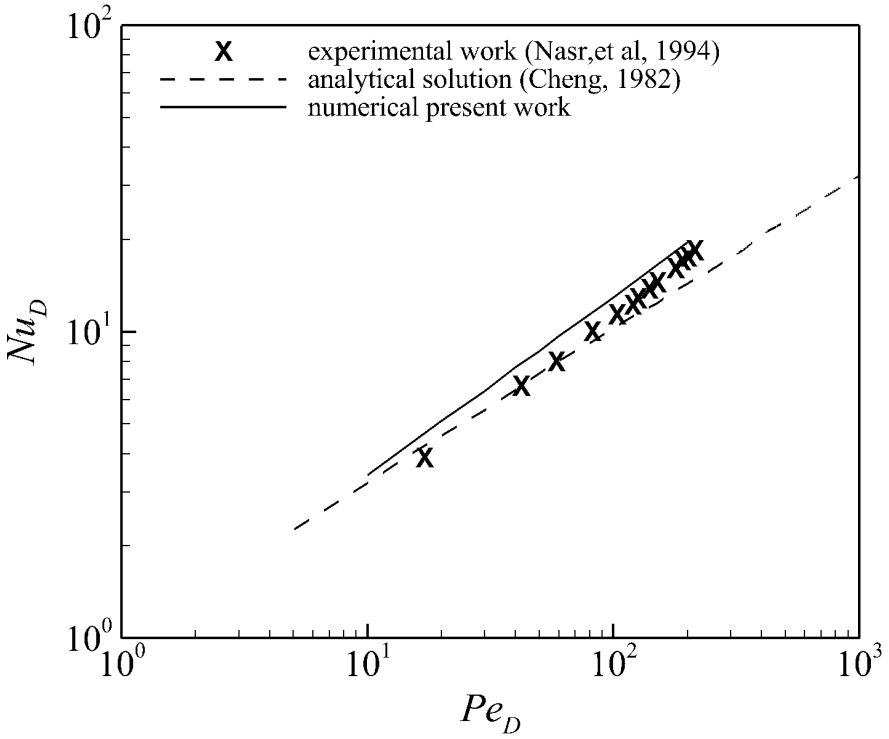

(b) For packed bed of glass spheres

FIGURE 4.7: Comparison between the present algorithm with the experimental data obtained by Nasr *et al.* (1994) for air forced convection heat transfer from a circular cylinder, $D = 12.7\ mm$, embedded in a packed bed of: (a) nylon spheres with $d_p = 6.35\ mm$, and (b) glass spheres with $d_p = 2.85\ mm$.

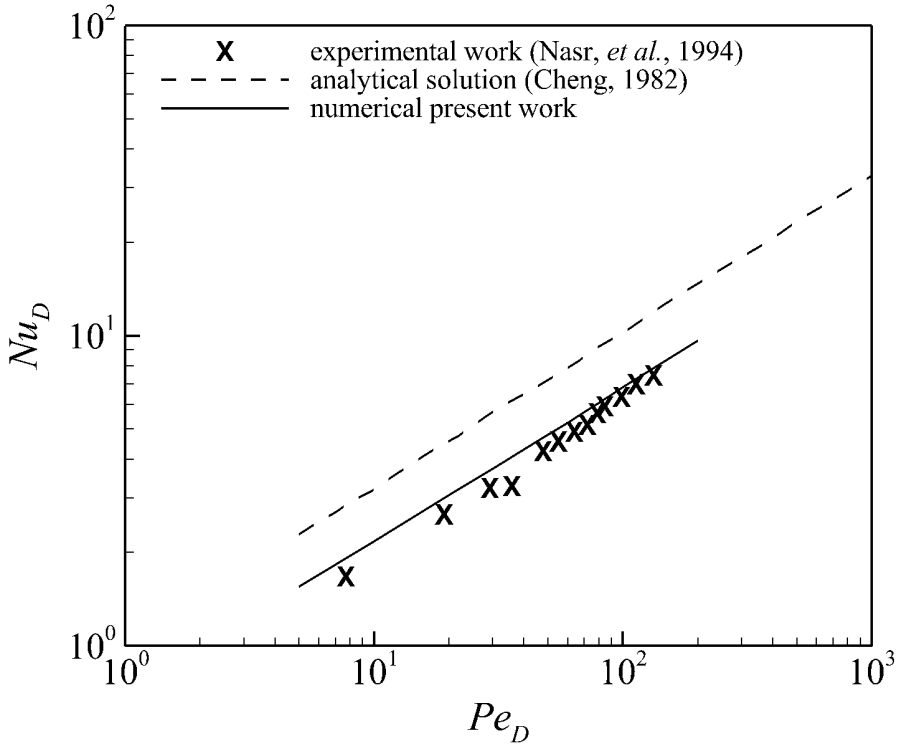

FIGURE 4.8: Comparison between the present algorithm with the experimental data obtained by Nasr *et al.* (1994) for air forced convection heat transfer from a circular cylinder, $D = 12.7\ mm$, embedded in a packed bed of aluminum spheres with $d_p = 12.23\ mm$.

analyzed forced convective heat transfer from the first three rows of staggered heated tube bundles immersed in a low thermal conductivity wooden porous medium using a finite-volume approach. The *DBF* momentum model, and the simple one-equation energy model, were used in their study to estimate the flow and thermal fields, respectively. The continuum assumption was employed to calculate the thermal properties of the porous medium, and the dispersion effect was incorporated into their model. The current model has been run for the same parameters. Four tubes from the bundle have been selected in the present study to test the heat transfer from the first three rows. The schematic diagram for this case and a typical computational mesh used for the computations, are shown in figure 3.9. The staggered tubes are arranged in an equilateral triangle form with longitudinal pitch $p_l = 1.3$, and transverse pitch $p_t = 0.75$. The relevant

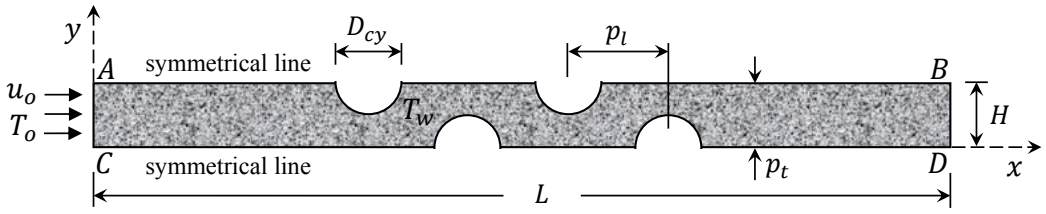

(a) Schematic diagram with the coordinate system

(b) Computational mesh used

FIGURE 4.9: (a) Physical domain for the problem of forced convective heat transfer from a staggered tube bundle embedded in a porous medium examined by Layeghi (2008), and (b) computational mesh used in the present study.

boundary conditions for the solution domain are as follows:

at $x = 0$ **(Flow inlet)** :

$$u_0 = 1, v = \theta = 0 \qquad \text{for} \quad (0 < y < H)$$

at $x = L$ **(Flow exit)** :

$$\frac{\partial u}{\partial x} = \frac{\partial v}{\partial x} = \frac{\partial \theta}{\partial x} = 0 \quad \text{for} \quad (0 < x < H)$$

at $y = 0$ and H **(Symmetrical lines AB and CD except tubes)** :

$$\frac{\partial u}{\partial y} = \frac{\partial \theta}{\partial y} = v = 0 \qquad \text{for} \quad (0 < x < L)$$

at **(Tubes' surfaces)** :

$$\theta = 1, u = v = 0 \tag{4.4}$$

The numerical simulations have been performed at Prandtl number $Pr = 0.7$ for air with a solid-to-fluid thermal conductivity ratio $k_s/k_f = 2.5$, Darcy number $Da = 0.25$ and porosity $\varepsilon = 0.6$, for two values of Reynolds number $Re_{max} = 100$ and 300. Where Re_{max} is based on the maximum velocity u_{max} which is the average velocity at the minimum cross-sectional area, and calculated by the following expression:

$$\frac{u_{max}}{u_o} = max \left\{ \frac{p_t/D_{cy}}{p_t/D_{cy} - 1}, \frac{0.5p_t/D_{cy}}{[(0.5p_t/D_{cy})^2 + (p_l/D_{cy})^2]^{0.5} - 1} \right\} \tag{4.5}$$

Our numerical results for the local Nusselt number based on the free stream temperature are compared with their results and presented in figure 3.10. The

local Nusselt number is plotted along the half-perimeters for the first three rows from the leading point to the trailing point in the flow direction. As may be seen from figure 3.10, the comparison shows very good agreement.

4.4.2 Without porous media

In the first validation step above, the numerical results have been checked against those of Buyruk (2002) for forced convection heat transfer from a bank of cylinders mounted in an empty channel. This investigation is performed for two geometries: three isothermal cylinders in a staggered geometry, and for four cylinders in an inline geometry, placed in very wide horizontal channel to eliminate the effect of channel blockage. Figure 3.11 depicts the physical setup of the problem. The cylinders are heated at T_w and mounted in a uniform cross-flow with velocity u_o and temperature T_o. In the present study, the cylinders are assumed to be unbounded. The longitudinal and transverse pitches between cylinders are kept constant $p_l = 2$ and $p_t = 2$, respectively. The numerical code was adjusted to accommodate the assumption of this problem for a clear convective fluid flow. Figure 3.12 shows the numerical meshes used here for both staggered and inline configurations. Far boundaries are chosen, i.e. the dimensions of the computational domains are $L = 14D_{cy}$ in length, and $H = 12D_{cy}$ in height, to satisfy their boundary conditions. The following dimensionless boundary conditions used for this case are:

$$
\begin{aligned}
&\text{at } x = 0 \quad \textbf{(Flow inlet)} : \\
&\quad u_0 = 1, v = \theta = 0 \qquad \text{for} \quad (0 < y < H) \\
&\text{at } x = L \quad \textbf{(Flow exit)} : \\
&\quad \frac{\partial \theta}{\partial x} = \frac{\partial u}{\partial x} = \frac{\partial v}{\partial x} = 0 \quad \text{for} \quad (0 < x < H) \\
&\text{at } y = 0 \text{ and } H \quad \textbf{(Free flow)} : \\
&\quad \frac{\partial u}{\partial y} = \frac{\partial \theta}{\partial y} = v = 0 \qquad \text{for} \quad (0 < x < L) \\
&\text{at} \quad \textbf{(Cylinders' surfaces)} : \\
&\quad \theta = 1, u = v = 0
\end{aligned}
\tag{4.6}
$$

The current transient numerical findings at steady state that have been ob-

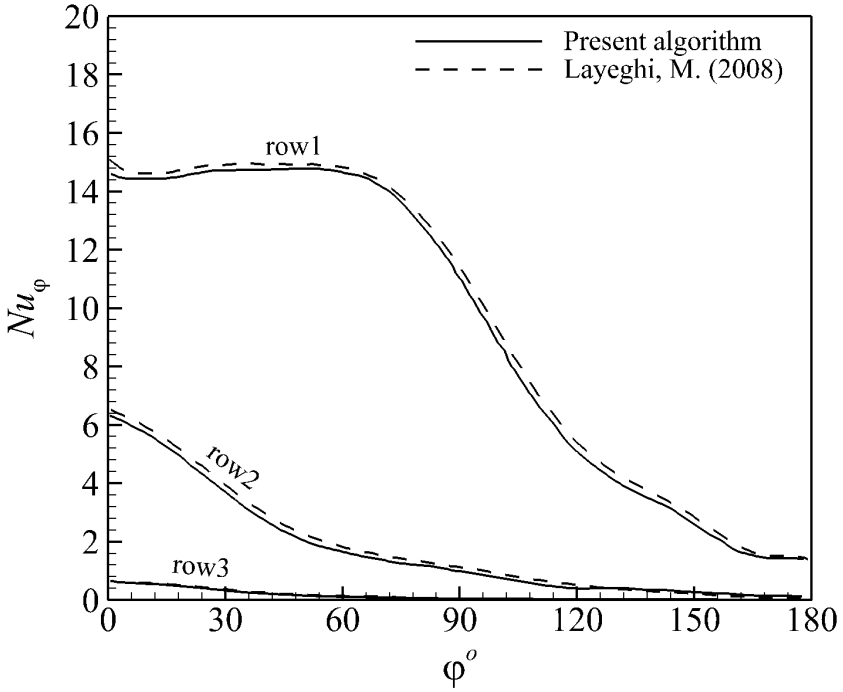

(a) At $Re_{max} = 100$

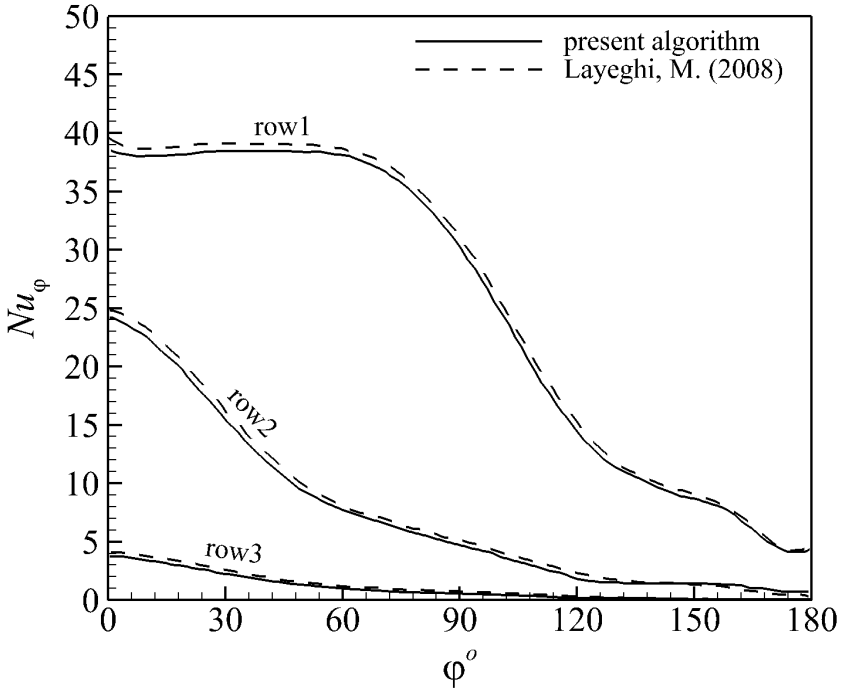

(b) At $Re_{max} = 300$

FIGURE 4.10: Comparison between two numerical models: the present model and the model used by Layeghi (2008) for local convective heat transfer from the first three rows of a staggered tube bundle embedded in a wooden porous medium $k_s/k_f = 2.5$, at maximum Reynolds number (a) $Re_{max} = 100$, and (b) 300.

tained at $Re_D = 80$ and $Pr = 0.7$, and compared with the numerical results reported by Buyruk. These are presented in figures $3.13 - 3.15$. Buyruk employed the ANSYS software program that employs the finite-volume method for predictions. Figures 3.13 and 3.14 show the comparison for the predictions of temperature contours around the three staggered cylinders and the four inline cylinders, respectively. The results show asymmetrical temperature contour distributions from the first and second rows of cylinders in both arrangements. Whereas, figure 3.15 shows comparisons for the distributions of the local Nusselt number Nu_φ along the surface of the two rows of the cylinders. An asymmetrical distribution for Nu_φ is observed for the staggered configuration, but it is not observed for the inline configuration. As can be seen from these figures that the comparisons display a satisfactory agreement between the two numerical solutions.

4.5 Validation summary

In this chapter, the numerical program has been used to produce flow and thermal predictions for a number of different problems, both experimental and numerical, that have appeared in the literature. This validation has been performed for different kinds of convective flows, e.g., mixed and forced, over a single and multiple cylinder configurations, and with and without the presence of porous media. In general very good agreement has between achieved with deviations typically 10% or much less for most of the comparisons. Since some of the input parameters, models and materials are uncertain for some of the published studies (and hence they had to be estimated), and it is unclear the resolution error associated with published numerical predictions, the match-up appears to be acceptable. Therefore, it can be concluded that the implementation is reliable to simulate the problems tackled in this thesis.

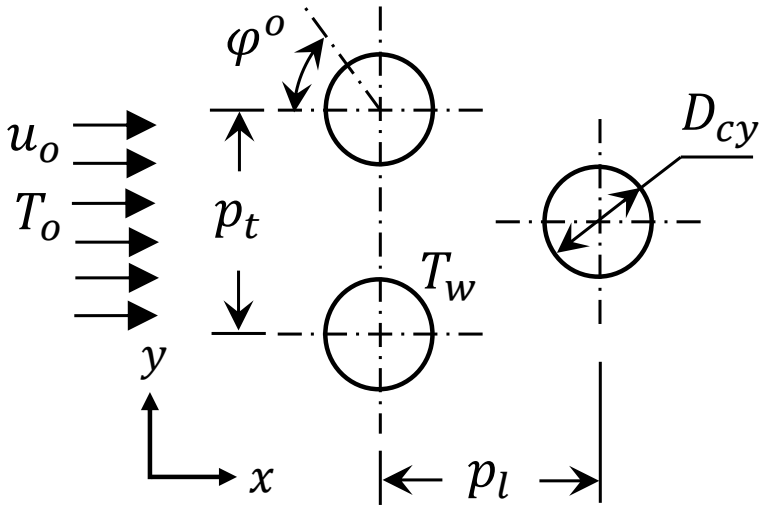

(a) Three cylinders in staggered configuration

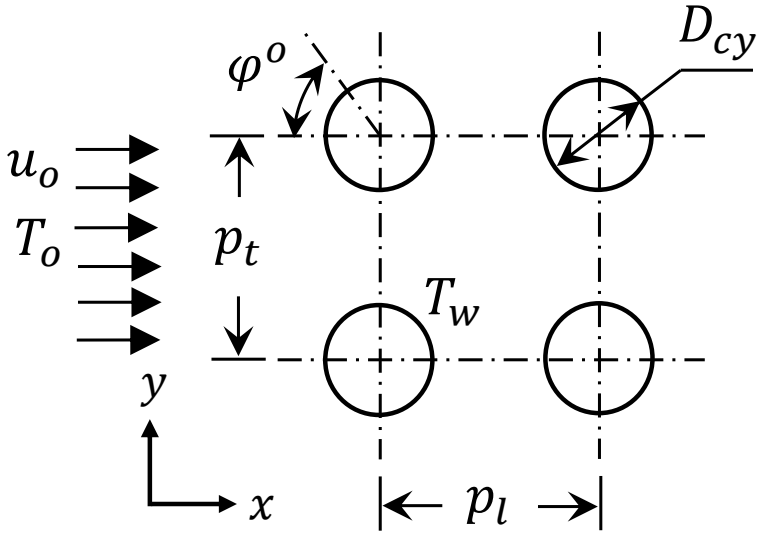

(b) Four cylinders in inline configuration

FIGURE 4.11: Physical domain used by Buyruk (2002) to investigate forced convection heat transfer from an unbounded bundle of: (a) three cylinders in staggered configuration, and (b) four cylinders in inline configuration. This case was studied in the absence of porous media.

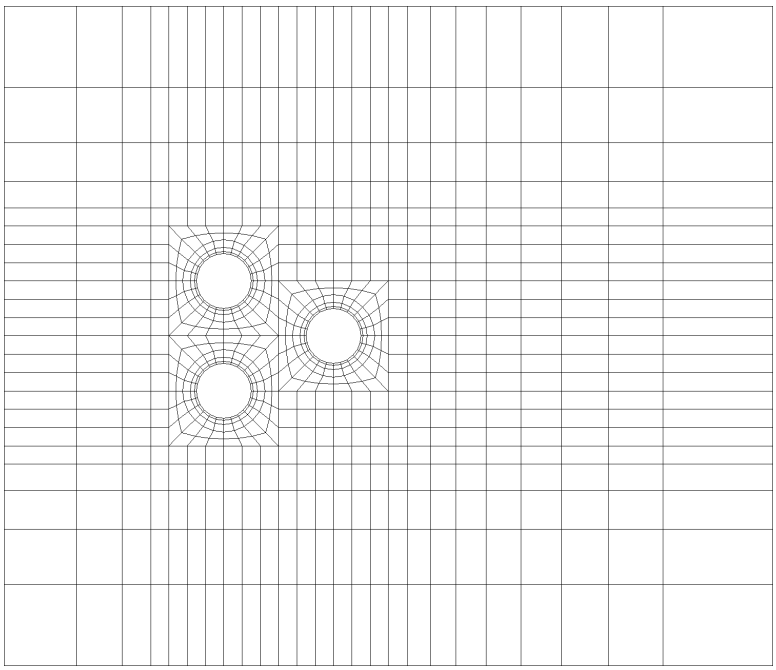

(a)

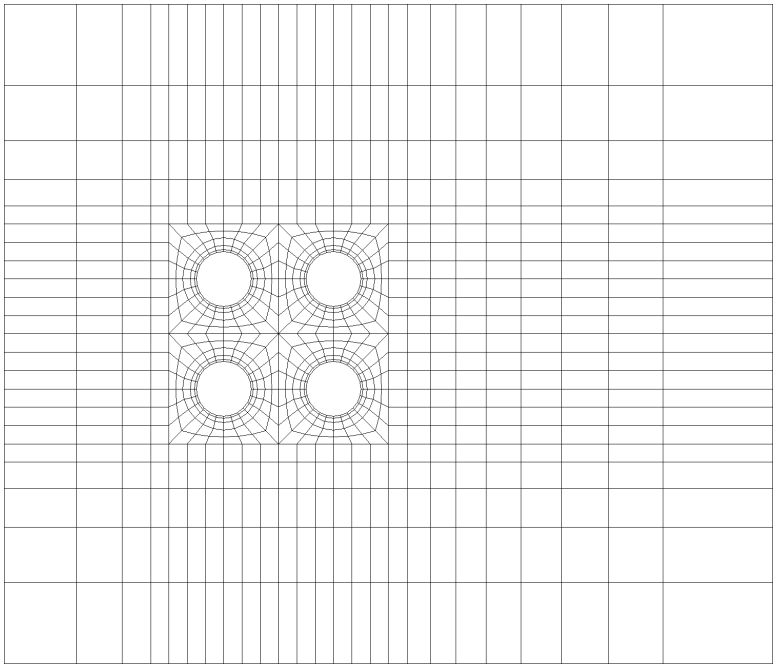

(b)

FIGURE 4.12: Computational grids used in the present study to reproduce the results of Buyruk (2002) for forced convection heat transfer from an unbounded bundle of: (a) three cylinders in staggered configuration, and (b) four cylinders in inline configuration.

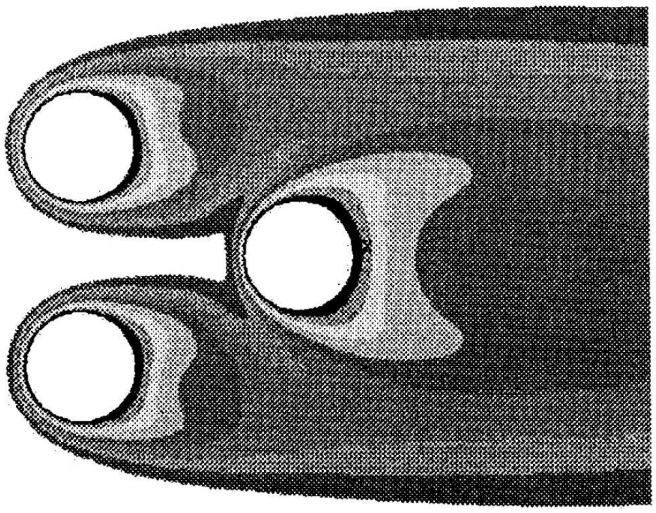

(a) Isotherms of Buyruk (2002)

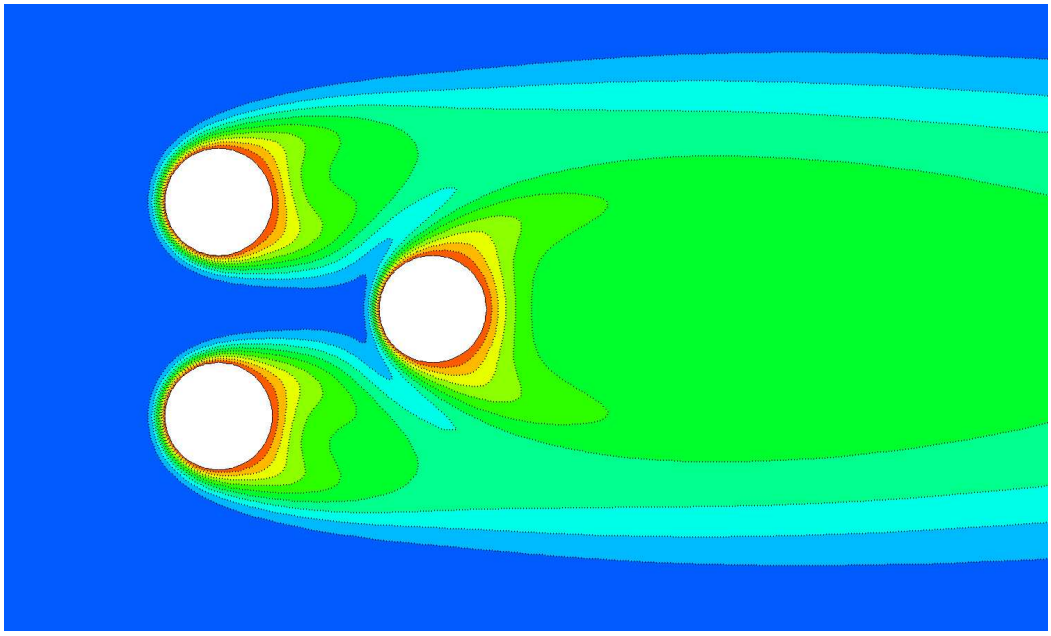

(b) Present prediction

FIGURE 4.13: Comparison between; (a) the numerical model used by Buyruk (2002), and (b) the present model, for predicting temperature contours of forced convective flow over three unbounded circular cylinders in staggered arrangement, at Reynolds number $Re_D = 80$, and at longitudinal and transverse pitches $p_l = p_t = 2$.

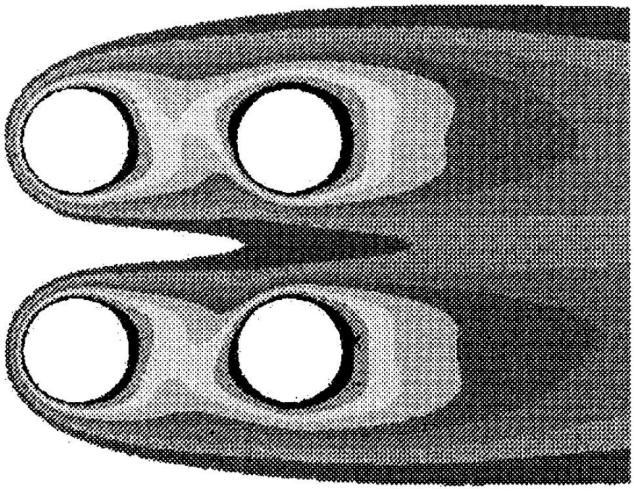

(a) Isotherms of Buyruk (2002)

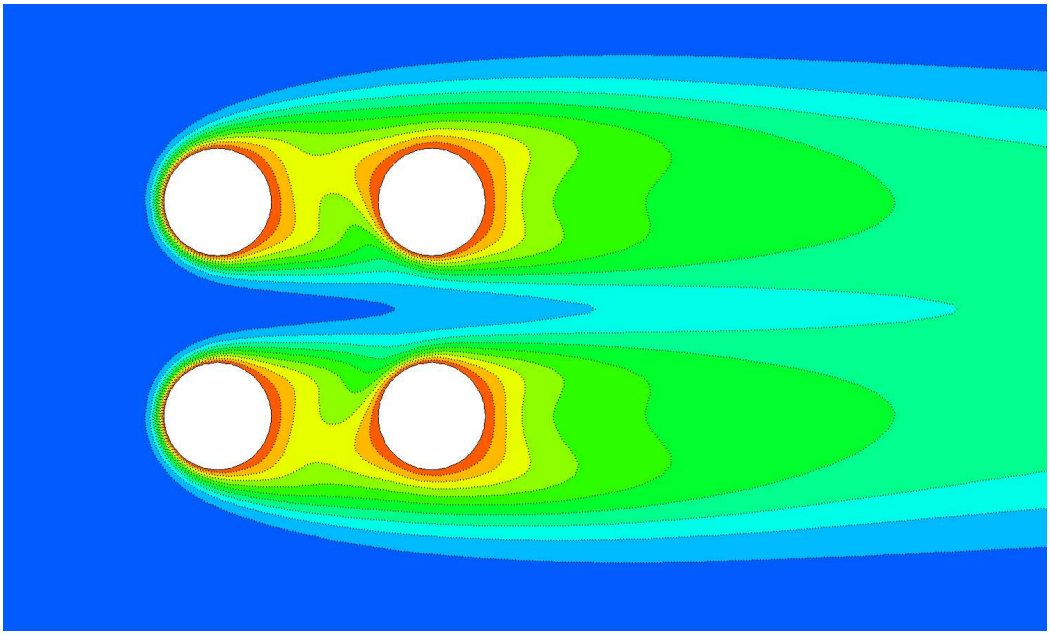

(b) Present prediction

FIGURE 4.14: Comparison between; (a) the numerical model used by Buyruk (2002), and (b) the present model, for predicting temperature contours of forced convective flow over three unbounded circular cylinders in inline arrangement, at Reynolds number $Re_D = 80$, and at longitudinal and transverse pitches $p_l = p_t = 2$.

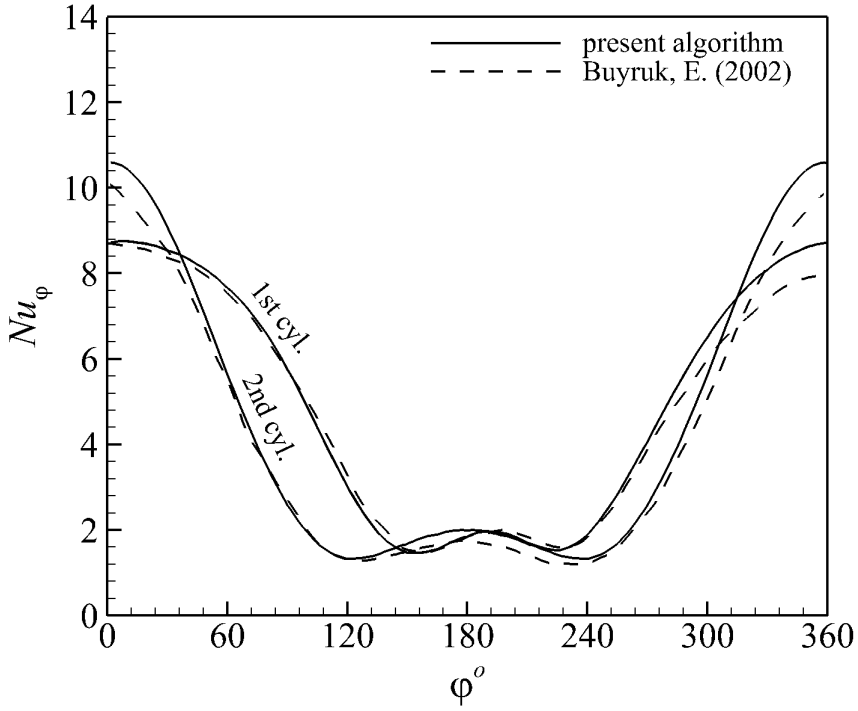

(a) For staggered cylinders configuration

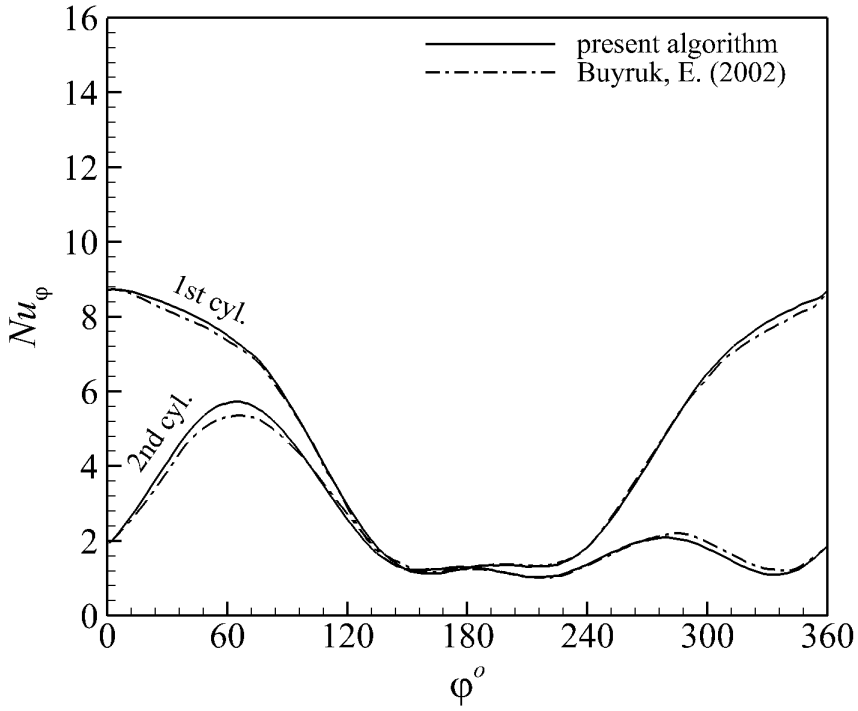

(b) For inline cylinders configuration

FIGURE 4.15: Comparison of the local Nusselt number distribution around the first and second rows of; (a) the staggered cylinders, and (b) the inline cylinders, of the present work against the numerical solution of Buyruk (2002). These plots are obtained at $Re_D = 80$ and $p_l = p_t = 2$.

Bibliography

Achenbach, E. 1995 Heat and flow characteristics of packed beds. *Experimental Thermal and Fluid Science* **10** (1), 17–27.

Aiba, S. 1990 Heat transfer around a tube in in-line tube banks near a plane wall. *Transactions of the ASME, Journal of Heat Transfer* **112**, 933–938.

Al-Nimr, M. A. & Abu-Hijleh, B. A. 2002 Validation of thermal equilibrium assumption in transient forced convection flow in porous channel. *Transport in Porous Media* **49** (2), 127–138.

Alazmi, B. & Vafai, K. 2000 Analysis of variants within the porous media transport models. *Journal of Heat Transfer* **122** (2), 303–326.

Alazmi, B. & Vafai, K. 2002 Constant wall heat flux boundary conditions in porous media under local thermal non-equilibrium conditions. *International Journal of Heat and Mass Transfer* **45** (15), 3071–3087.

Aldoss, T. K., Alkam, M. & Shatarah, M. 2004 Natural convection from a horizontal annulus partially filled with porous medium. *International Communications in Heat and Mass Transfer* **31** (3), 441–452.

Amiri, A. & Vafai, K. 1994 Analysis of dispersion effects and non-thermal equilibrium, non-darcian, variable porosity incompressible flow through porous media. *International Journal of Heat and Mass Transfer* **37** (6), 939–954.

Amiri, A. & Vafai, K. 1998 Transient analysis of incompressible flow through a packed bed. *International Journal of Heat and Mass Transfer* **41** (24), 4259–4279.

Amiri, A., Vafai, K. & Kuzay, T. M. 1995 Effects of boundary conditions on non-darcian heat transfer through porous media and experimental comparisons. *Numerical Heat Transfer; Part A* **27** (6), 651–664.

Anderson, T. B. & Jackson, R. 1967 A fluid mechanical description of fluidized beds: Equations of motion. *Industrial and Engineering Chemistry Fundamentals* **6** (4), 527–539.

Badr, H. M. & Pop, I. 1988 Combined convection from an isothermal horizontal rod buried in a porous medium. *International Journal of Heat and Mass Transfer* **31** (12), 2527–2541.

Badruddin, I. A., Zainal, Z. A., Narayana, P. A. A. & Seetharamu, K. N. 2006 Thermal non-equilibrium modeling of heat transfer through vertical annulus embedded with porous medium. *International Journal of Heat and Mass Transfer* **49** (25-26), 4955–4965.

Banu, N. & Rees, D. A. S. 2002 Onset of darcy-benard convection using a thermal non-equilibrium model. *International Journal of Heat and Mass Transfer* **45** (11), 2221–2228.

Barbosa Mota, J. P. & Saatdjian, E. 1995 Natural convection in porous cylindrical annuli. *International Journal of Numerical Methods for Heat and Fluid Flow* **5** (1), 3–12.

Barbosa Mota, J. P. & Saatdjian, E. 1997 On the reduction of natural convection heat transfer in horizontal eccentric annuli containing saturated porous media. *International Journal of Numerical Methods for Heat and Fluid Flow* **7** (4), 401–416.

Bartlett, R. F. & Viskanta, R. 1996 Enhancement of forced convection in an asymmetrically heated duct filled with high thermal conductivity porous media. *Journal of Enhhanced Heat Transfer* **3** (4), 291–299.

Bau, H. H. 1984a Convective heat losses from a pipe buried in a semi-infinite porous medium. *International Journal of Heat and Mass Transfer* **27** (11), 2047–2056.

Bau, H. H. 1984b Thermal convection in a horizontal, eccentric annulus containing a saturated porous medium - an extended perturbation expansion. *International Journal of Heat and Mass Transfer* **27** (12), 2277–2287.

Baytas, A. C. 2003 Thermal non-equilibrium natural convection in a square enclosure filled with a heat-generating solid phase, non-darcy porous medium. *International Journal of Energy Research* **27** (10), 975–988.

Baytas, A. C. & Pop, I. 2002 Free convection in a square porous cavity using a thermal nonequilibrium model. *International Journal of Thermal Sciences* **41** (9), 861–870.

Bear, J. 1972 *Dynamics of fluids in porous media*. American Elsevier, New York.

Bejan, A. 1995 The optimal spacing for cylinders in crossflow forced convection. *Transaction of the ASME, Journal of Heat Transfer* **117**, 767–770.

Bejan, A. & Kraus, A. D. 2003 *Heat Transfer Handbook.*. Wiley, New York.

Benenati, R. F. & Brosilow, C. B. 1962 Void fraction distribution in beds of spheres. *A.I.Ch.E. Journal* **8** (3), 359–361.

Bhattacharyya, S. & Singh, A. K. 2009 Augmentation of heat transfer from a solid cylinder wrapped with a porous layer. *International Journal of Heat and Mass Transfer* **52** (7-8), 1991–2001.

Brinkmann, H. C. 1949 A calculation of the viscous force exerted by a flowing fluid on a dense swarm of particles. *Applied Scientific Research* **1** (1), 27–34.

Burns, P. J. & Tien, C. L. 1979 Natural convection in porous media bounded by concentric spheres and horizontal cylinders. *International Journal of Heat and Mass Transfer* **22** (6), 929–39.

Buyruk, E. 2002 Numerical study of heat transfer characteristics on tandem cylinders, inline and staggered tube banks in cross-flow of air. *International Communications in Heat and Mass Transfer* **29** (3), 355–366.

Caltagirone, J. P. 1976 Thermoconvective instabilities in a porous medium bounded by two concentric horizontal cylinders. *Journal of Fluid Mechanics* **76** (2), 337–362.

Canuto, C. 1988 *Spectral methods in uid dynamics*. Springer-Verlag, New York.

Carbonell, R. G. & Whitaker, S. 1984 Heat and mass transfer in porous media. In *Fundamentals of transport phenomena in porous media* (ed. J. Bear & M. Y. Corapcioglu), pp. 121–198. Martinus Nijhoff, Dordrecht (Boston).

Celli, M. & Rees, D. A. S.; Barletta, A. 2010 The effect of local thermal non-equilibrium on forced convection boundary layer flow from a heated surface in porous media. *International Journal of Heat and Mass Transfer* **53**, 3533–3539, in press.

Charrier-Mojtabi, M. C., Mojtabi, A., Azaiez, M. & Labrosse, G. 1991 Numerical and experimental study of multicellular free convection flows in an annular porous layer. *International Journal of Heat and Mass Transfer* **34** (12), 3061–3074.

Chen, G. & Hadim, H. A. 1998 Numerical study of non-darcy forced convection in a packed bed saturated with a power-law fluid. *Journal of Porous Media* **1** (2), 147–157.

Chen, G. & Hadim, H. A. 1999 Numerical study of three-dimensional non-darcy forced convection in a square porous duct. *International Journal of Numerical Methods for Heat and Fluid Flow* **9** (2), 151–169.

Cheng, C. Y. 2007a A boundary layer analysis of heat transfer by free convection from permeable horizontal cylinders of elliptic cross-section in porous media using a thermal non-equilibrium model. *International Communications in Heat and Mass Transfer* **34** (5), 613–622.

Cheng, C. Y. 2007b Nonsimilar solutions for free convection from horizontal cylinders of elliptic cross section embedded in porous media using a thermal non-equilibrium model. *WSEAS Transactions on Mathematics* **6** (5), 633 – 638.

Cheng, P. 1977 Combined free and forced convection flow about inclined surfaces in porous media. *International Journal of Heat and Mass Transfer* **20** (8), 807–814.

Cheng, P. 1981 Thermal dispersion effects in non-darcian convective flows in a saturated porous medium. *Letters in Heat and Mass Transfer* **8** (4), 267–270.

Cheng, P. 1982 Mixed convection about a horizontal cylinder and a sphere in a fluid-saturated porous medium. *International Journal of Heat Mass Transfer* **25** (8), 1245–1247.

Cheng, P. 1985 Natural convection in a porous medium: External flows. In *Natural convection: Fundamentals and applications* (ed. S. Kakac, W. Aung & R. Viskanta), pp. 453–475. Martinus Nijhoff, The Hague, The Netherlands.

Cheng, P. & Vortmeyer, D. 1988 Transverse thermal dispersion and wall channelling in a packed bed with forced convective flow. *Chemical Engineering Science* **43** (9), 2523–2532.

Cho, H. W. & Hyun, J. M. 1990 Numerical solutions of pulsating flow and heat transfer characteristics in a pipe. *International Journal of Heat and Fluid Flow* **11** (4), 321–330.

Chorin, A. J. 1968 Numerical solution of the navier-stokes equations. *Mathematics of Computation* **22** (104), 745–762.

Chou, F. C. & Chung, P. Y. 1995 Effect of stagnant conductivity on non-darcian mixed convection in horizontal square packed channels. *Numerical Heat Transfer; Part A: Applications* **27** (2), 195–209.

Chrysler, G. M. & Simons, R. E. 1990 Experimental investigation of the forced convection heat transfer characteristics of fluorocarbon liquid flowing through a packed-bed for immersion cooling of microelectronic heat sources. In *Parallel and Vector Computation in Heat Transfer - Presented at AIAA/ASME Thermophysics and Heat Transfer Conference*, pp. 21–27. Seattle, WA, USA.

Cooper, W. L., Nee, V. W. & Yang, K. T. 1994 An experimental investigation of convective heat transfer from the heated floor of a rectangular duct to a low frequency, large tidal displacement oscillatory flow. *International Journal of Heat and Mass Transfer* **37** (4), 581–592.

Darcy, H. 1856 *Les Fontaines Publiques de la Ville de Dijon*. Dalmont, Paris.

David, G. L. & Cheng, P. 1991 A numerical solution of variable porosity effects on natural convection in a packed -sphere cavity. *Journal of Heat Transfer* **113**, 391–399.

Dixon, A. G. & Cresswell, D. L. 1979 Theoretical prediction of effective heat transfer parameters in packed beds. *AIChE Journal* **25** (4), 663–676.

Dullien, F. A. 1979 *Media fluid transport and pore structure*. Academic Press, New York.

Eckert, E. R. G. & Drake, R. M. 1972 *Analysis of Heat and Mass Transfer*. McGraw-Hill, New York.

Ehyaei, D., Honari, H. & Rahimian, M. 2009 Prediction of forced convection flow in a parallel plate channel filled with porous media. In *Proceedings of the 7th International Conference on Nanochannels, Microchannels, and Minichannels 2009, ICNMM2009*, , vol. 1, pp. 631–635. Pohang, South Korea.

Ergun, S. 1952 Fluid flow through packed columns. *Chemical Engineering Progress* **48** (2), 89–94.

Facas, G. N. 1994 Reducing the heat transfer from a hot pipe buried in a semi-infinite, saturated, porous medium. *Journal of Heat Transfer* **116** (2), 473–476.

Facas, G. N. 1995a Natural convection from a buried elliptic heat source. *International Journal of Heat and Fluid Flow* **16** (6), 519–526.

Facas, G. N. 1995b Natural convection from a buried pipe with external baffles. *Numerical Heat Transfer, Part A* **27**, 595–609.

Faghri, M., Javdani, K. & Faghri, A. 1979 Heat transfer with laminar pulsating flow in a pipe. *Letters in Heat and Mass Transfer* **6** (4), 259–270.

Fand, R. M. & Phan, R. T. 1987 Combined forced and natural convection heat transfer from a horizontal cylinder embedded in a porous medium. *International Journal of Heat and Mass Transfer* **30** (7), 1351 – 1358.

Fand, R. M., Steinberger, T. E. & Cheng, P. 1986 Natural convection heat transfer from a horizontal cylinder embedded in a porous medium. *International Journal of Heat and Mass Transfer* **29** (1), 119133.

Fernandez, R. T. & Schrock, V. E. 1982 Natural convection from cylinders buried in a liquid-saturated porous medium. In *Proceedings of the International Heat Transfer Conference*, , vol. 2, pp. 335–340. Munich, Germany.

Fletcher, C. A. J. 1984 *Computational Galerkin methods*. Springer-Verlag, New York.

Fletcher, C. A. J. 1991 *Computational techniques for fluid dynamics, vol. 1*. Springer-Verlag, New York.

Forchheimer, P. H. 1901 Wasserbewegung durch boden. *Zeitschrift Vereines Deutscher Ingenieure* **45** (50), 1782–1788.

Forooghi, P., Abkar, M. & Saffar-Avval, M. 2011 Steady and unsteady heat transfer in a channel partially filled with porous media under thermal non-equilibrium condition. *Transport in Porous Media* **86** (1), 177–198.

Fu, K. C., Huang, X. Y. & Liu, C. Y. 2001 An experimental study of heat transfer of a porous channel subjected to oscillating flow. *Journal of Heat Transfer* **123** (1), 162–170.

Gamson, B. W., Thodos, G. & Hougen, O. A. 1943 Heat, mass and momentum transfer in the flow of gases through granular solids. *Trans. AIChE* **39**, 1–35.

Guo, Z. & Sung, H. J. 1997 Analysis of the nusselt number in pulsating pipe flow. *International Journal of Heat and Mass Transfer* **40** (10), 2486–2489.

Haddad, O. M., Al-Nimr, M. A. & Al-Khateeb, A. N. 2004 Validation of the local thermal equilibrium assumption in natural convection from a vertical plate embedded in porous medium: Non-darcian model. *International Journal of Heat and Mass Transfer* **47** (8-9), 2037–2042.

Hadim, H. & Vafai, K. 2000 Overview of current computational studies of heat transfer in porous media and their applications-forced convection and multiphase heat transfer. *Advances in Numerical Heat Transfer* **2**, 291–329.

He, Y. L., Yang, W. W., Zhao, C. F. & Tao, W. Q. 2005 Numerical study of enhancing heat transfer by pulsating flow. *Journal of Engineering Thermophysics* **26** (3), 495–497.

Himasekhar, K. & Bau, H. H. 1986 Large rayleigh number convection in a horizontal, eccentric annulus containing saturated porous media. *International Journal of Heat and Mass Transfer* **29** (5), 703–712.

Himasekhar, K. & Bau, H. H. 1987 Thermal convection associated with hot/cold pipes buried in a semi-infinite, saturated, porous medium. *International Journal of Heat and Mass Transfer* **30** (2), 263–273.

Himasekhar, K. & Bau, H. H. 1988a Thermal convection around a heated source embedded in a box containing a saturated porous medium. *Journal of Heat Transfer* **110** (3), 649–654.

Himasekhar, K. & Bau, H. H. 1988b Two-dimensional bifurcation phenomena in thermal convection in horizontal, concentric annuli containing saturated porous media. *Journal of Fluid Mechanics* **187**, 267–300.

Horton, C. W. & Rogers, F. T. 1945 Convection currents in a porous medium. *Journal of Applied Physics* **16**, 367–370.

Hsiao, S. W., Cheng, P. & Chen, C. K. 1992 Non-uniform porosity and thermal dispersion effects on natural convection about a heated horizontal cylinder

in an enclosed porous medium. *International Journal of Heat and Mass Transfer* **35** (12), 3407–3418.

Hsu, C. T. & Cheng, P. 1990 Thermal dispersion in a porous medium. *International Journal of Heat and Mass Transfer* **33** (8), 1587–1597.

Huang, M. J., Yih, K. A., Chou, Y. L. & Chen, C. K. 1986 Mixed convection flow over a horizontal cylinder or a sphere embedded in a saturated porous medium. *Journal of Heat Transfer* **108** (2), 469–471.

Huang, P. C. & Yang, C. F. 2008 Analysis of pulsating convection from two heat sources mounted with porous blocks. *International Journal of Heat and Mass Transfer* **51** (25-26), 6294–6311.

Huang, Z. F., Nakayama, A., Yang, K., Yang, C. & Liu, W. 2010 Enhancing heat transfer in the core flow by using porous medium insert in a tube. *International Journal of Heat and Mass Transfer* **53** (5-6), 1164–1174.

Hwang, G. J. & Chao, C. H. 1994 Heat transfer measurement and analysis for sintered porous channels. *Transactions of the ASME. Journal of Heat Transfer* **116** (2), 456–464.

Ingham, D. B., Bejan, A. & Mamut, E. 2004 *Emerging Technologies and Techniques in Porous Media*. Kluwer Academic, Dordrecht.

Ingham, D. B. & Pop, I. 1987 Natural convection about a heated horizontal cylinder in a porous medium. *Journal of Fluid Mechanics* **184**, 157–181.

Ingham, D. B. & Pop, I. 1998 *Transport phenomenon in porous media*, , vol. 1. Pergamon, Oxford.

Ingham, D. B. & Pop, I. 2002 *Transport phenomenon in porous media*, , vol. 2. Pergamon, Oxford.

Iwai, H., Mambo, T., Yamamoto, N. & Suzuki, K. 2004 Laminar convective heat transfer from a circular cylinder exposed to a low frequency zero-mean velocity oscillating flow. *International Journal of Heat and Mass Transfer* **47** (21), 4659–4672.

Jeigarnik, U. A., Ivanov, F. P. & Ikranikov, N. P. 1991 Experimental data on heat transfer and hydraulic resistance in unregulated porous structures (in russian). *Teploenergetika* **21**, 33–38.

Ji, T. H., Kim, S. Y. & Hyun, J. M. 2008 Experiments on heat transfer enhancement from a heated square cylinder in a pulsating channel flow. *International Journal of Heat and Mass Transfer* **51** (5-6), 1130–1138.

Jiang, P. X., Li, M., Ma, Y. C. & Ren, Z. P. 2004a Boundary conditions and wall effect for forced convection heat transfer in sintered porous plate channels. *International Journal of Heat and Mass Transfer* **47** (10-11), 2073–2083.

Jiang, P. X. & Ren, Z. P. 2001 Numerical investigation of forced convection heat transfer in porous media using a thermal non-equilibrium model. *International Journal of Heat and Fluid Flow* **22** (1), 102–110.

Jiang, P. X., Ren, Z. P., Wang, B. X. & Wang, Z. 1996a Forced convective heat transfer in a plate channel filled with solid particles. *Journal of Thermal Science* **5** (1), 43–53.

Jiang, P. X., Si, G. S., Li, M. & Ren, Z. P. 2004b Experimental and numerical investigation of forced convection heat transfer of air in non-sintered porous media. *Experimental Thermal and Fluid Science* **28** (6), 545–555.

Jiang, P. X., Wang, B. X., Luo, D. A. & Ren, Z. P. 1996b Fluid flow and convective heat transfer in a vertical porous annulus. *Numerical Heat Transfer; Part A: Applications* **30** (3), 305–320.

Jiang, P. X., Wang, B. X. & Ren, Z. P. 1994 A numerical investigation of mixed convection in a vertical porous annulus. In *Proceedings of the 10th International Heat Transfer Conference*, pp. 303–308. Brighton, UK.

Jiang, P. X., Wang, Z., Ren, Z. P. & Wang, B. X. 1999 Experimental research of fluid flow and convection heat transfer in plate channels filled with glass or metallic particles. *Experimental Thermal and Fluid Science* **20** (1), 45–54.

Jubran, B. A., Hamdan, M. A. & Abdualh, R. M. 1993 Enhanced heat transfer, missing pin, and optimization for cylindrical pin fin arrays. *Transactions of the ASME, Journal of Heat Transfer* **115**, 576–583.

Jue, T. C. 2003 Analysis of thermal convection in a fluid-saturated porous cavity with internal heat generation. *Heat and Mass Transfer* **40** (1-2), 83–89.

Jue, T. C., Wu, H. W. & Huang, S. Y. 2001 Heat transfer predictions around three heated cylinders between two parallel plates. *Numerical Heat Transfer, Part A* **40**, 715–733.

Karniadakis, G. E., Israeli, M. & Orszag, S. A. 1991 High-order splitting methods for the incompressible navier-stokes equations. *Journal of Computational Physics* **97** (2), 414–443.

Karniadakis, G. E. & Sherwin, S. J. 2005 *Spectral/hp methods for computational fluid dynamics*. Oxford University Press, Oxford.

Kaviany, M. 1986 Non-darcian effects on natural convection in porous media confined between horizontal cylinders. *International Journal of Heat and Mass Transfer* **29** (10), 1513–1519.

Kaviany, M. 1995 *Principles of heat transfer in porous media*. Springer-Verlag, New York.

Kaviany, M. 1999 *Principles of heat transfer in porous media*. Springer-Verlag, New York.

Khashan, S. A., Al-Amiri, A. M. & Al-Nimr, M. A. 2005 Assessment of the local thermal non-equilibrium condition in developing forced convection flows through fluid-saturated porous tubes. *Applied Thermal Engineering* **25** (10), 1429–1445.

Khashan, S. A., Al-Amiri, A. M. & Pop, I. 2006 Numerical simulation of natural convection heat transfer in a porous cavity heated from below using a non-darcian and thermal non-equilibrium model. *International Journal of Heat and Mass Transfer* **49** (5-6), 1039–1049.

Khashan, S. A. & Al-Nimr, M. A. 2005 Validation of the local thermal equilibrium assumption in forced convection of non-newtonian fluids through porous channels. *Transport in Porous Media* **61** (3), 291–305.

Khodadadi, J. M. 1991 Oscillatory fluid flow through a porous medium channel bounded by two impermeable parallel plates. *Journal of Fluids Engineering, Transactions of the ASME* **113** (3), 509–511.

Kim, S. J. & Jang, S. P. 2002 Effects of the darcy number, the prandtl number, and the reynolds number on local thermal non-equilibrium. *International Journal of Heat and Mass Transfer* **45** (19), 3885–3896.

Kim, S. J., Kim, D. & Lee, D. Y. 2000 On the local thermal equilibrium in microchannel heat sinks. *International Journal of Heat and Mass Transfer* **43** (10), 1735–1748.

Kim, S. Y., Kang, B. H. & Hyun, J. M. 1993 Heat transfer in the thermally developing region of a pulsating channel flow. *International Journal of Heat and Mass Transfer* **36** (17), 4257–4266.

Kim, S. Y., Kang, B. H. & Hyun, J. M. 1994 Heat transfer from pulsating flow in a channel filled with porous media. *International Journal of Heat and Mass Transfer* **14** (37), 2025–2033.

Kimura, S. 1988 Forced convection heat transfer about an elliptic cylinder in a saturated porous medium. *International Journal of Heat and Mass Transfer* **31** (1), 197–199.

Kimura, S. 1989 Transient forced convection heat transfer from a circular cylinder in a saturated porous medium. *International Journal of Heat and Mass Transfer* **32** (1), 192–195.

Kimura, S. & Pop, I. 1991 Non-darcian effects on conjugate natural convection between horizontal concentric cylinders filled with a porous medium. *Fluid Dynamics Research* **7** (5-6), 241–253.

Kumari, M. & Nath, G. 2009 Unsteady natural convection flow over a heated cylinder buried in a fluid saturated porous medium. *Journal of Porous Media* **12** (12), 1225–1235.

Kuo, S. M. & Tien, C. L. 1988a Heat transfer augmentation in a foam-material filled duct with discrete heat sources. In *InterSociety Conference on Thermal Phenomena in the Fabrication and Operation of Electronic Components*, pp. 87–91. Los Angeles, CA, USA.

Kuo, S. M. & Tien, C. L. 1988b Transverse dispersion in packed-sphere beds. In *American Society of Mechanical Engineers (ASME)*, , vol. 96, pp. 629–634. New York, NY, USA.

Kuwahara, F., Shirota, M. & Nakayama, A. 2001 A numerical study of interfacial convective heat transfer coefficient in two-energy equation model for convection in porous media. *International Journal of Heat and Mass Transfer* **44** (6), 1153–1159.

Kuznetsov, A. V. 1997a A perturbation solution for heating a rectangular sensible heat storage packed bed with a constant temperature at the walls. *International Journal of Heat and Mass Transfer* **40** (5), 1001–1006.

Kuznetsov, A. V. 1997b Thermal nonequilibrium, non-darcian forced convection in a channel filled with a fluid saturated porous medium - a perturbation solution. *Applied Scientific Research* **57** (2), 119–131.

Kuznetsov, A. V. 1997c Thermal nonequilibrium, non-darcian forced convection in a channel filled with a fluid saturated porous medium - a perturbation solution. *Applied Scientific Research* **57** (2), 119–131.

Kuznetsov, A. V. 1998 Thermal non-equilibrium forced convection in porous media. In *Transport Phenomena in Porous Media, Ch. 5* (ed. D. B. Ingham & I. Pop), pp. 103–129. Elsevier Science, Oxford.

Kuznetsov, A. V. & Nield, D. A. 2006 Forced convection with laminar pulsating flow in a saturated porous channel or tube. *Transport in Porous Media* **65** (3), 505–523.

Kwendakwema, N. J. & Boehm, R. F. 1991 Parametric study of mixed convection in a porous medium between vertical concentric cylinders. *Journal of Heat Transfer* **113** (1), 128–134.

Lai, F. C., Choi, C. Y. & Kulacki, F. A. 1990 Free and mixed convection in horizontal porous layers with multiple heat sources. *Journal of Thermophysics and Heat Transfer* **4** (2), 221–227.

Lai, F. C. & Kulacki, F. A. 1988 Transient mixed convection in horizontal porous layers locally heated from below. In *Proceedings of the National Heat Transfer Conference*, , vol. 96, pp. 353–364. American Society of Mechanical Engineers, Heat Transfer Division, (Publication) HTD.

Lai, F. C. & Kulacki, F. A. 1991 Oscillatory mixed convection in horizontal porous layers locally heated from below. *International Journal of Heat and Mass Transfer* **34** (3), 887–890.

Lapwood, E. R. 1948 Convection of a fluid in a porous medium. In *Proceedings of the Cambridge Philosophical Society*, , vol. 44, pp. 508–521. UK.

Layeghi, M. 2008 Numerical analysis of wooden porous media effects on heat transfer from a staggered tube bundle. *Transactions of the ASME, Journal of Heat Transfer* **130**, 014501.1–014501.6.

Layeghi, M. & Nouri-Borujerdi, A. 2004 Fluid flow and heat transfer around circular cylinders in the presence and no-presence of porous media. *Journal of Porous Media* **7** (3), 239–247.

Layeghi, M. & Nouri-Borujerdi, A. 2006 Darcy model for the study of the fluid flow and heat transfer around a cylinder embedded in porous media. *International Journal of Computational Methods in Engineering Science and Mechanics* **7** (5), 323–329.

Lee, D. Y. & Vafai, K. 1999 Analytical characterization and conceptual assessment of solid and fluid temperature differentials in porous media. *International Journal of Heat and Mass Transfer* **42** (3), 423–435.

Leong, K. C. & Jin, L. W. 2004 Heat transfer of oscillating and steady flows in a channel filled with porous media. *International Communications in Heat and Mass Transfer* **31** (1), 63–72.

Leong, K. C. & Jin, L. W. 2005 An experimental study of heat transfer in oscillating flow through a channel filled with an aluminum foam. *International Journal of Heat and Mass Transfer* **48** (2), 243–253.

Levec, J. & Carbonell, R. G. 1985 Longitudinal and lateral thermal dispersion in packed beds. part ii: Comparison between theory and experiment. *AIChE Journal* **31** (4), 591–602.

Marafie, A. & Vafai, K. 2001 Analysis of non-darcian effects on temperature differentials in porous media. *International Journal of Heat and Mass Transfer* **44** (23), 4401–4411.

Merkin, J. H. 1979 Free convection boundary layers on axi-symmetric and two-dimensional bodies of arbitrary shape in a saturated porous medium. *International Journal of Heat and Mass Transfer* **22** (10), 14611462.

Minkowycz, W. J., Cheng, P. & Chang, C. H. 1985 Mixed convection about a nonisothermal cylinder and sphere in a porous medium. *Numerical Heat Transfer* **8** (3), 349–359.

Minkowycz, W. J., Haji-Sheikh, A. & Vafai, K. 1999 On departure from local thermal equilibrium in porous media due to a rapidly changing heat source: The sparrow number. *International Journal of Heat and Mass Transfer* **42** (18), 3373–3385.

Moghari, M. 2008 A numerical study of non-equilibrium convective heat transfer in porous media. *Journal of Enhanced Heat Transfer* **15** (1), 81–99.

Mohamad, A. A. 2000 Nonequilibrium natural convection in a differentially heated cavity filled with a saturated porous matrix. *Journal of Heat Transfer* **122** (2), 380–384.

Mohamad, A. A. 2001 Natural convection from a vertical plate in a saturated porous medium: Nonequilibrium theory. *Journal of Porous Media* **4** (2), 181–186.

Murty, V. D., Camden, M. P., Clay, C. L. & Paul, D. B. 1990 A study of non-darcian effects on forced convection heat transfer over a cylinder embedded in a porous medium. In *Proceedings of the International Heat Transfer Conference*, pp. 201–206. New York, USA.

Muskat, M. 1937 *The flow of homogeneous fluids through porous media*. McGraw-Hill, New York.

Nasr, K., Ramadhyani, S. & Viskanta, R. 1994 Experimental investigation on forced convection heat transfer from a cylinder embedded in a packed bed. *Journal of Heat Transfer* **116** (1), 73–80.

Nield, D. A. 1998 Effects of local thermal non-equilibrium in steady convective processes in a saturated porous medium: Forced convection in a channel. *Journal of Porous Media* **1** (2), 181–186.

Nield, D. A. & Bejan, A. 2006 *Convection in porous media*. Third edition, Springer Science+Business Media, New York, NY, USA.

Nield, D. A. & Kuznetsov, A. V. 1999 Local thermal non-equilibrium effects in forced convection in a porous medium channel: A conjugate problem. *International Journal of Heat and Mass Transfer* **42** (17), 3245–3252.

Oosthuizen, P. H. 1987 Mixed convection heat transfer from a cylinder in a porous medium near an impermeable surface. In *Mixed convection heat transfer*, , vol. 84, pp. 75–82. American Society of Mechanical Engineers, Heat Transfer Division, (Publication) HTD.

Oosthuizen, P. H. & Naylor, D. 1996 Natural convective heat transfer from a cylinder in an enclosure partly filled with a porous medium. *International Journal of Numerical Methods for Heat and Fluid Flow* **6** (6), 51–63.

Paek, J. W., Kang, B. H. & Hyun, J. M. 1999 Transient cool-down of a porous medium in pulsating flow. *International Journal of Heat and Mass transfer* **42** (18), 3523–3527.

Pavel, B. I. & Mohamad, A. A. 2004a An experimental and numerical study on heat transfer enhancement for gas heat exchangers fitted with porous media. *International Journal of Heat and Mass Transfer* **47** (23), 4939–4952.

Pavel, B. I. & Mohamad, A. A. 2004b Experimental investigation of the potential of metallic porous inserts in enhancing forced convective heat transfer. *Journal of Heat Transfer* **126** (4), 540–545.

Phanikumar, M. S. & Mahajan, R. L. 2002 Non-darcy natural convection in high porosity metal foams. *International Journal of Heat and Mass Transfer* **45** (18), 3781–3793.

Pop, I. & Cheng, P. 1992 Flow past a circular cylinder embedded in a porous medium based on the brinkman model. *International Journal of Engineering Science* **30** (2), 257–262.

Pop, I. & Ingham, D. B. 2001 *Convective heat transfer: Mathematical and computational modeling of viscous fluids and porous media.*. Pergamon, Oxford.

Pop, I., Kumari, M. & Nath, G. 1992 Free convection about cylinders of elliptic cross section embedded in a porous medium. *International Journal of Engineering Science* **30** (1), 35–45.

Pop, I. & Yan, B. 1998 Forced convection flow past a circular cylinder and a sphere in a darcian fluid at large peclet numbers. *International Communications in Heat and Mass Transfer* **25** (2), 261–267.

Quintard, M. 1998 Modeling local non-equilibrium heat transfer in porous media. In *Proceedings of the 11th International Heat Transfer Conference*, , vol. 1, pp. 279–285. Kyongju, South Korea.

Quintard, M., Kaviany, M. & Whitaker, S. 1997 Two-medium treatment of heat transfer in porous media: numerical results for effective properties. *Advances in Water Resources* **20** (2-3 SPEC. ISS.), 77–94.

Quintard, M. & Whitaker, S. 1993 One- and two-equation models for transient diffusion processes in two-phase systems. *Advances in Heat Transfer* **23** (C), 369–464.

Quintard, M. & Whitaker, S. 1995 Local thermal equilibrium for transient heat conduction: theory and comparison with numerical experiments. *International Journal of Heat and Mass Transfer* **38** (15), 2779–2796.

Quintard, M. & Whitaker, S. 2000 Theoretical analysis of transport in porous media. In *Handbook of heat transfer in porous Media* (ed. K. Vafai), pp. 1–50. Marcel Dekker, New York.

Rao, Y. F., Fukuda, K. & Hasegawa, S. 1988 A numerical study of three-dimensional natural convection in a horizontal porous annulus with galerkin method. *International Journal of Heat and Mass Transfer* **31** (4), 695–707.

Rees, D. A., Bassom, A. P. & Pop, I. 2003 Forced convection past a heated cylinder in a porous medium using a thermal nonequilibrium model: boundary layer analysis. *European Journal of Mechanics, B/Fluids* **22** (5), 473–486.

Rees, D. A. S. & Pop, I. 2000 Vertical free convective boundary-layer flow in a porous medium using a thermal nonequilibrium model. *Journal of Porous Media* **3** (1), 31–44.

Roblee, L. H. S., Baird, R. M. & Tierney, J. W. 1958 Radial porosity variations in packed beds. *A.I.Ch.E. Journal* **4** (4), 460–464.

Roychowdhury, D. G., Das, S. K. & Sundararajan, T. 2002 Numerical simulation of laminar flow and heat transfer over banks of staggered cylinders. *International Journal for Numerical Methods in Fluids* **39**, 23–40.

Saada, M. A., Chikh, S. & Campo, A. 2007 Natural convection around a horizontal solid cylinder wrapped with a layer of fibrous or porous material. *International Journal of Heat and Fluid Flow* **28** (3), 483495.

Saeid, N. H. 2006 Analysis of free convection about a horizontal cylinder in a porous media using a thermal non-equilibrium model. *International Communications in Heat and Mass Transfer* **33** (2), 158–165.

Saeid, N. H. 2007 Maximum density effects on natural convection in a porous cavity under thermal non-equilibrium conditions. *Acta Mechanica* **188** (1-2), 55–68.

Saeid, N. H. & Pop, I. 2004 Transient free convection in a square cavity filled with a porous medium. *International Journal of Heat and Mass Transfer* **47** (8-9), 1917–1924.

Saito, M. B. & Lemos, M. J. S. 2009 Laminar heat transfer in a porous channel simulated with a two-energy equation model. *International Communications in Heat and Mass Transfer* **36** (10), 1002–1007.

Sano, T. 1980 Unsteady heat transfer from a circular cylinder immersed in a darcy flow. *Journal of Engineering Mathematics* **14** (3), 177–190.

Scheidegger, A. E. 1960 *The physics of flow through porous media*. 2nd edition, University of Toronto Press, Toronto.

Scheidegger, A. E. 1974 *The physics of flow through porous media*. Third Edition, University of Toronto, Toronto.

Schumann, T. E. W. 1929 Heat transfer: A liquid flowing through a porous prism. *Journal of the Franklin Institute* **208** (3), 405–416.

Sert, C. & Beskok, A. 2003 Numerical simulation of reciprocating flow forced convection in two-dimensional channels. *Journal of Heat Transfer* **125** (3), 403–412.

Siegel, R. & Perlmutter, M. 1962 Heat transfer for pulsating laminar duct flow. *Transaction of the ASME, Journal of Heat Transfer* pp. 111–123.

Slattery, J. C. 1967 Flow of viscoelastic fluids through porous media. *A.I.Ch.E. Journal* **13** (6), 1066–1071.

Sözen, M. & Vafai, K. 1991 Analysis of oscillating compressible flow through a packed bed. *International Journal of Heat and Fluid Flow* **130-136** (2), 12.

Thevenin, J. 1995 Transient forced convection heat transfer from a circular cylinder embedded in a porous medium. *International Communications in Heat and Mass Transfer* **22** (4), 507–516.

Thevenin, J. & Sadaoui, D. 1995 About enhancement of heat transfer over a circular cylinder embedded in a porous medium. *International Communications in Heat and Mass Transfer* **22** (2), 295–304.

Thiyagarajan, R. & Yovanovich, M. M. 1974 Thermal resistance of a buried cylinder with constant flux boundary condition. *Journal of Heat Transfer* **96**, 249–250.

Thom, A. & Apelt, C. J. 1961 *Field computations in engineering and physics*. Van Nostrand, London.

Thompson, M. C., Hourigan, K., Cheung, A. & Leweke, T. 2006 Hydrodynamics of a particle impact on a wall. *Applied Mathematical Modelling* **30** (11), 1356–1369.

Uchida, S. 1956 The pulsating viscous flow superposed on the steady laminar motion of incompressible fluid in a circular pipe. *Zeitschrift fr Angewandte Mathematik und Physik (ZAMP)* **7** (5), 403–422.

Vafai, K. 1984 Convective flow and heat transfer in variable-porosity media. *Journal of Fluid Mechanics* **147**, 233–259.

Vafai, K. 2000 *Handbook of Porous Media.*. Marcel dekker, New York.

Vafai, K. & Hadim, H. 2000 Overview of current computational studies of heat transfer in porous media and their applications-natural and mixed convection and multiphase heat transfer. *Advances in Numerical Heat Transfer* **2**, 331–369.

Vafai, K. & Sözen, M. 1990a Analysis of energy and momentum transport for fluid flow through a porous bed. *Transactions of the ASME. Journal of Heat Transfer* **112** (3), 390–399.

Vafai, K. & Sözen, M. 1990b An investigation of a latent heat storage porous bed and condensing flow through it. *Transactions of the ASME. Journal of Heat Transfer* **112** (4), 1014–1022.

Vafai, K. & Tien, C. L. 1981 Boundary and inertia effects on flow and heat transfer in porous media. *International Journal of Heat and Mass Transfer* **195-203** (24), 2.

Wakao, N. & Kaguei, S. 1982 *Heat and Mass Transfer in Packed Beds*. Gordon and Breach, New York.

Wakao, N., Kaguei, S. & Funazkri, T. 1979 Effect of fluid dispersion coefficients on particle-to-fluid heat transfer coefficients in packed beds- correlation of nusselt numbers. *Chemical Engineering Science* **34** (3), 325–336.

Wang, B. X. & Du, J. H. 1993 Forced convective heat transfer in a vertical annulus filled with porous media. *International Journal of Heat and Mass Transfer* **36** (17), 4207–4213.

Wang, J. H. & Wang, H. N. 2006 A discussion of transpiration cooling problems through an analytical solution of local thermal nonequilibrium model. *Journal of Heat Transfer* **128** (10), 1093–1098.

Wang, Y. Q., Penner, L. A. & Ormiston, S. J. 2000 Analysis of laminar forced convection of air for crossflow in banks of staggered tubes. *Numerical Heat Transfer, Part A* **38**, 819–845.

Whitaker, S. 1967 Diffusion and dispersion in porous media. *A.I.Ch.E. Journal* **13** (3), 420–427.

Whitaker, S. 1991 Improved constraints for the principle of local thermal equilibrium. *Industrial and Engineering Chemistry Research* **30** (5), 983–997.

Wong, K. C. & Saeid, N. H. 2009 Numerical study of mixed convection on jet impingement cooling in a horizontal porous layer under local thermal non-equilibrium conditions. *International Journal of Thermal Sciences* **48** (5), 860–870.

Wong, W. S., Rees, D. A. & Pop, I. 2004 Forced convection past a heated cylinder in a porous medium using a thermal nonequilibrium model: Finite peclet number effects. *International Journal of Thermal Sciences* **43** (3), 213–220.

Wooding, R. A. 1960 Rayleigh instability of a thermal boundary layer in flow through a porous medium. *Journal of Fluid Mechanics* **9**, 183–192.

Wooding, R. A. 1963 Convection in a saturated porous medium at large rayleigh number of pećlet number. *Journal of Fluid Mechanics* **15**, 527–544.

Yagi, S. & Kunii, D. 1957 Studies on effective thermal conductivities in packed beds. *Chemical Engineering Progress* **3** (3), 373–381.

Yagi, S., Kunii, D. & Wakao, N. 1960 Studies on axial effective thermal conductivities in packed beds. *AIChE Journal* **6** (4), 543–546.

Yagi, S. & Wakao, N. 1959 Heat and mass transfer from wall to fluid in packed beds. *AIChE Journal* **5** (1), 79–85.

Yang, C., Ando, K. & Nakayama, A. 2011 A local thermal non-equilibrium analysis of fully developed forced convective flow in a tube filled with a porous medium. *Transport in Porous Media* pp. 1–13, in press.

Younis, L. B. 2010 Cross flowheat exchanger embedded within a porous medium. *Journal of Porous Media* **13** (11), 981–988.

Zdravkovic, M. M. 1994 *Flow around circular cylinders*. Volume 1, Oxford University Press.

Zehner, P. & Schluender, E. U. 1970 Thermal conductivity of granular materials at moderate temperatures. *Chemie-Ingenieur-Technik* **42** (14), 933–941.

Zhang, X. & Liu, W. 2008 New criterion for local thermal equilibrium in porous media. *Journal of Thermophysics and Heat Transfer* **22** (4), 649–653.

Zhao, T. S. & Cheng, P. 1995 A numerical solution of laminar forced convection in a heated pipe subjected to a reciprocating flow. *International Journal of Heat and Mass Transfer* **38** (16), 3011–3022.

Zhao, T. S. & Cheng, P. 1996 Oscillatory heat transfer in a pipe subjected to a laminar reciprocating flow. *Journal of Heat Transfer* **118** (3), 592–597.

Zhou, M. J. & Lai, R. C. 2002 Aiding and opposing mixed convection from a cylinder in a saturated porous medium. *Journal of Porous Media* **5** (2), 103–111.

Zhou, Y. & Yiu, M. W. 2006 Flow structure, momentum and heat transport in a two-tandem-cylinder wake. *Journal of Fluid Mechanics* **548**, 17–48.

Zhukauskas, A. 1972 Heat transfer from tubes in cross flow. *Advances in Heat Transfer* **8**, 93–160.